UNIVERSITÀ DEGLI STUDI DI PARMA

Dottorato di Ricerca in Tecnologie dell'Informazione

XXV Ciclo

SPECTRALLY EFFICIENT SYSTEMS FOR SATELLITE COMMUNICATIONS

Coordinatore:

Chiar.mo Prof. Marco Locatelli

Tutor:

Chiar.mo Prof. Giulio Colavolpe

Dottorando: *Nicolò Mazzali*

Gennaio 2013

alla mia famiglia
ed ai miei amici

Contents

List of Figures

List of Tables

Acronyms

AIS Automatic Identification Service

AWGN Additive White Gaussian Noise

BCJR Bahl Cocke Jelinek Raviv

BER Bit Error Rate

BPSK Binary Phase-Shift Keying

CDMA Code Division Multiple Access

CPCM Continuous Phase Chip Modulation

CPFSK Continuous Phase Frequency Shift Keying

CRB Cramér-Rao Bound

DA Data Aided

DS Direct Sequence

DTH Direct To Home

DVB Digital Video Broadcasting

DVB-RCS Digital Video Broadcasting - Return Channel Satellite

DVB-S2 Digital Video Broadcast - Satellite - 2nd generation

FDM Frequency Division Multiplexing

FH Frequency Hopping

FSK Frequency Shift Keying

FSM Finite-State Machine

GenMSK Generalized Minimum Shift Keying

HIC Hard Interference Cancellation

ICI Inter-Channel Interference

ISI Inter-Symbol Interference

LDPC Low-Density Parity-Check

LLR Log-Likelihood Ratio

LUT Look-Up Table

MAI Multiple Access Interference

MAP Maximum A posteriori Probability

MSS Mobile Satellite Service

MSV Mean Squared Value

MUD Multi-User Detector

PAM Pulse Amplitude Modulation

PAPR Peak-to-Average-Power Ratio

PDF Probability Density Function

PMF Probability Mass Function

PSD Power Spectral Density

PSS Phase Spreading Sequence

RRC Root Raised Cosine

RV Random Variable

SE Spectral Efficiency

SIC Soft Interference Cancellation

SISO Soft-Input Soft-Output

SNR Signal-to-Noise Ratio

SS Spread Spectrum

SSMH Spread Spectrum Multi-*h*

SUD Single-User Detector

Introduction

Satellite communications are one of the most growing fields in communication industry, and in the last decade a remarkable number of networks, providing many different services, has been deployed. A general class of mobile satellite services (MSSs) is supplied in aeronautical, land, and maritime scenarios. For example, systems such as Thuraya, Telesat, Inmarsat, and Iridium (just to cite few of them) provide a telephone connection similar to a cellular telephone link, except that the repeaters are in orbit around the Earth. Moreover, MSSs include railway applications, security issues (e.g., the Automatic Identification Service, AIS, which supplies identification and localization information to vessels and shore stations), traffic monitoring, disaster management, e-health applications, digital video transmission, and many more. We will focus on digital video services, which range from custom services (such as interactive applications) to professional and TV broadcasting services (e.g., the Direct-to-Home, DTH). In particular, we will consider the Digital Video Broadcasting (DVB) service and its two standards: the second generation of DVB-Satellite (DVB-S2), which describes the forward link (i.e., the connection between a gateway and the user terminal through a satellite repeater) [1], and the DVB-Return Channel Satellite (DVB-RCS) that defines the return link [2]. In all standards the spectrum allocation is critical since the band occupation is severely regulated and the available bandwidth is becoming more and more scarce with the growing of the satellite market. Therefore, the need for maximizing the broadcast information compels the adoption of spectrally efficient transmission techniques.

After the introduction of some technical backgrounds in Chapter 1, in this The-

sis we will propose three different solutions to the spectral efficiency issue. First, in Chapter 2 we will consider a multi-user scenario with frequency multiplexing, that is one of the scenarios included in the DVB-RCS standard. We will adopt continuous phase modulations (CPMs) serially concatenated with an outer code through an interleaver, and iterative detection/decoding. The choice of the modulation formats is justified by the intrinsic high spectral efficiency of CPMs, which can be further increased exploiting the frequency packing technique. Such an improvement does not come for free, in fact an accurate synchronization has to be guaranteed to allow the detector to work properly. To this purpose, new iterative frequency and phase estimators will be derived and the synchronization accuracy tested.

Then, in Chapter 3 we will focus on code division multiple access (CDMA) systems employing CPMs. A brand new spectral spreading technique, especially tailored to CPMs, will be presented. We will show how to easily obtain a large, flat, and smooth power spectral density, without resorting to spreading sequences and then getting rid of all the design problems that come with. Moreover, we will derive some suboptimal multi-user detectors that will be employed to show that the proposed system outperforms all the other considered systems, found in the literature, in terms of bit error rate and spectral efficiency.

Finally, considering the DVB-S2 scenario, in Chapter 4 we will propose to increase the spectral efficiency through time and frequency packing. This technique will cause intersymbol and interchannel interferences to arise, requiring a significant increase in the number of pilots used to carry out frequency and phase synchronization. Therefore, new pilot designs will be introduced, and suited optimal and suboptimal reduced-complexity algorithms derived. We will show that the proposed systems may outperform the DVB-S2 standard in terms of bit error rate and spectral efficiency.

At last, we will draw some conclusions and sketch some possible future investigations.

Chapter 1

Backgrounds

In this Chapter we give the basic frameworks, algorithms, and definitions extensively used in this Thesis. First, the continuous phase modulations (CPMs) are defined and their characteristics described. They will be employed in the first two Chapters of this Thesis in two different scenarios. Then, maximum a posteriori probability (MAP) symbol detection strategy and the factor graph/sum-product algorithm (FG/SPA) framework, pervasively adopted in every chapter, are illustrated. Finally, we sketch the iterative joint detection/decoding procedure and the simulation-based algorithm employed for the computation of the information rate.

1.1 Continuous phase modulations

CPMs are constant envelope modulations, hence low cost amplifiers can be used in heavy saturation. Since the phase is continuous, these modulations result to be highly spectral and power efficient [3].

Phase continuity introduces a memory in the modulated signal. The complex envelope of a CPM signal is therefore

$$s(t;\alpha) = \sqrt{\frac{2E_s}{T}} \exp\left\{ 2\pi h \sum_i \alpha_i q(t - iT) + \theta \right\}$$

where E_s is the energy per symbol, T the symbol period, h a constant called *modulation index*, $\{\alpha_k\}$ are the information symbols belonging to the alphabet $\{\pm 1, ..., \pm(M-1)\}$, $q(t)$ is the *phase smoothing response* defined as

$$q(t) = \begin{cases} 0 & \text{when } t < 0 \\ \frac{1}{2} & \text{when } t > LT \end{cases}$$

and θ is the initial phase offset. Parameter L is the *correlation length* of the CPM signal. The phase smoothing function can be expressed as integral of the *frequency pulse*

$$g(t) = \frac{\mathrm{d}q(t)}{\mathrm{d}t}$$

whose duration is at most LT. Since the frequency pulse is different from zero only in the interval $[0, LT]$, the phase of the signal can be expressed as the sum of three terms (in addition to the initial phase θ). Considering a finite-duration transmission, we have

$$\begin{aligned} \phi(t;\alpha_k,\sigma_k) = {} & 2\pi h \sum_{i=0}^{k-L} \alpha_i \frac{1}{2} + \\ & + 2\pi h \sum_{i=k-L+1}^{k-1} \alpha_i q(t-iT) + \\ & + 2\pi h \alpha_k q(t-kT) \qquad\qquad kT \le t < (k+1)T\,. \end{aligned}$$

The first of these terms depends on the "old" symbols whose response $q(t)$ has reached its final value $1/2$ and is called *phase state*

$$\varphi_k = \left(\pi h \sum_{i=0}^{k-L} \alpha_i \right) \bmod 2\pi\,.$$

The second term depends on the $L-1$ most recent symbols $\alpha_{k-L+1}, \ldots, \alpha_{k-1}$. This group of symbols defines the *correlative state* and, together with the phase state, contributes to the definition of the *modulator state* at time kT, that is

$$\sigma_k = (\alpha_{k-1}, \ldots, \alpha_{k-L+1}; \varphi_k)\,.$$

Given the symbol and the state at time kT, the phase $\phi(t;\alpha_k,\sigma_k)$—and hence the CPM signal—results determined.

At time $t=(k+1)T$, the next modulator state becomes

$$\sigma_{k+1}=(\alpha_k,\ldots,\alpha_{k-L+2};\varphi_{k+1})$$

where the new correlative state is obtained just right-shifting the old one, and the new phase state is

$$\varphi_{k+1}=(\varphi_k+\pi h\alpha_{k-L+1}) \bmod 2\pi .$$

To evaluate the number of states of the modulator we observe that the number of correlative states is M^{L-1}. Theoretically, the number of phase states may be infinite. Fortunately, it results to be finite if the modulation index is a rational number [3]

$$h=\frac{n}{p}$$

where n and p are relatively prime. If n is even, there are p distinct phase states, otherwise there are $2p$ possible phase states. Among these $2p$ values, only p can be taken on in the even time epochs, while in the odd time epochs only the other p values can be taken on. Hence, the total number of states of a CPM modulator is always pM^{L-1}. If n and p are not relatively prime, the index definition is still valid but the trellis is redundant and can be reduced.

An integer representation of the phase state and the information symbols allows to work with a new phase state whose alphabet results to be time-invariant [4]. Defining

$$\alpha_k=2\bar{\alpha}_k-(M-1)$$
$$\varphi_k=2\pi h\bar{\varphi}_k-\pi h(M-1)k$$

we have that $\bar{\alpha}_k\in\{0,1,\ldots,M-1\}$ and $\bar{\varphi}_k\in\{0,1,\ldots,p-1\}$, and the new update law becomes

$$\bar{\varphi}_{k+1}=(\bar{\varphi}_k+\bar{\alpha}_{k-L+1}) \bmod p$$

where $\bar{\varphi}_{k+1}$ takes on values in the same alphabet of $\bar{\varphi}_k$ independently of the time k (even or odd).

CPMs are grouped in two classes according to the correlation length. Namely, they are said to be *full response* CPMs if $L=1$, or *partial response* CPMs if $L>1$.

1.2 MAP symbol detection strategy and BCJR algorithm

Given a sequence of transmitted symbols $\{a_n\}$ collected into vector $\mathbf{a}$, where $\mathbf{a} = (a_0, \ldots, a_{K-1})$, and a channel with memory, we denote by vector $\mathbf{r}$ the sufficient statistics of the received signal $r(t)$, extracted by the receiver. In particular, the n-th element of vector $\mathbf{r}$ can be a vector, denoted in the following $\mathbf{r}_n$, since in general, at each time epoch n, the number of sufficient statistics can be greater than one. Thus, the MAP symbol detection strategy minimizing the average symbol error probability is

$$\hat{a}_n = \underset{a_n}{\operatorname{argmax}} P(a_n|\mathbf{r}) \tag{1.1}$$

where $P(.)$ denotes a probability mass function (PMF). We adopt this strategy because it provides soft-output decisions and, as a by-product, the a posteriori probabilities (APPs) $\{P(a_n|\mathbf{r})\}$, which can be considered as reliability estimates on the chosen symbols $\{\hat{a}_n\}$. These estimates allow us to derive soft-input soft-output (SISO) detection (or decoding) algorithms, necessary to implement iterative joint detection/decoding schemes [5].

In particular, by employing the Bayes rules, we can express the MAP symbol strategy in (1.1) as

$$\hat{a}_n = \underset{a_n}{\operatorname{argmax}}\, p(\mathbf{r}|a_n)P(a_n) \tag{1.2}$$

where $\{P(a_n)\}$ are the a priori probabilities of symbols $\{a_n\}$ and $p(.)$ denotes a probability density function (PDF). Thus, in order to accomplish the proposed maximization, we need to compute the PDF $p(\mathbf{r}|a_n)$. Considering a channel with memory described as a finite-state machine (FSM), whose state is denoted by σ_n, we can solve the MAP symbol problem by the Bahl, Cocke, Jelinek, Raviv (BCJR) algorithm [6] based on a probabilistic derivation. In particular, $p(\mathbf{r}|a_n)$ expression is given by

$$p(\mathbf{r}|a_n) = \sum_{\sigma_n} \alpha_n(\sigma_n)\beta_{n+1}(\sigma_{n+1})p(\mathbf{r}_n|a_n, \sigma_n) \tag{1.3}$$

where

- $\alpha_n(\sigma_n)$ is the forward metric defined as

$$\alpha_n(\sigma_n) = p(\mathbf{r}_0^{n-1}|\sigma_n)P(\sigma_n)$$

where we denote by $\mathbf{r}_{n_1}^{n_2}$ the vector collecting all the sufficient statistics $\mathbf{r}_n$ from $n = n_1$ to $n = n_2$;

- $\beta_{n+1}(\sigma_{n+1})$ is the backward metric and reads

$$\beta_{n+1}(\sigma_{n+1}) = p(\mathbf{r}_{n+1}^{K-1}|\sigma_{n+1}).$$

Forward and backward metrics can be recursively computed through the following forward and backward recursions

$$\alpha_{n+1}(\sigma_{n+1}) = \sum_{a_n,\sigma_n} \alpha_n(\sigma_n) p(\mathbf{r}_n|a_n,\sigma_n) P(a_n) \tag{1.4}$$

$$\beta_n(\sigma_n) = \sum_{a_n,\sigma_{n+1}} \beta_{n+1}(\sigma_{n+1}) p(\mathbf{r}_n|a_n,\sigma_n) P(a_n). \tag{1.5}$$

Hence the BCJR algorithm works as follows:

- forward and backward metrics are computed by means of (1.4) and (1.5) for each time epoch n and each state value σ_n;
- the PDF $p(\mathbf{r}|a_n)$ is derived by (1.3) exploiting $\alpha_n(\sigma_n), \beta_{n+1}(\sigma_{n+1})$, and $p(\mathbf{r}_n|a_n,\sigma_n)$;
- finally, the MAP strategy (1.2) can be implemented and APPs $\{P(a_n|\mathbf{r})\}$ obtained.

However, this algorithm is usually unsuitable for direct implementation because of the difficulties in numerically representing probabilities, nonlinear functions, and basic arithmetical operations (multiplication and sum) involving these values. Therefore, a perfectly equivalent algorithm, working in the logarithmic domain, is usually adopted since it does not present these problems of implementation [7]. In the logarithmic domain, Equations (1.3), (1.4), and (1.5) are all in the form

$$\ln f(\delta_1,\ldots,\delta_n) = \ln\left(e^{\delta_1} + \ldots + e^{\delta_n}\right)$$

which can be recursively calculated resorting to the Jacobian logarithm, i.e.

$$\ln\left(e^{\delta_1} + e^{\delta_2}\right) = \max\{\delta_1,\delta_2\} + \ln\left(1 + e^{-|\delta_1-\delta_2|}\right).$$

Typically, when symbols $\{a_n\}$ are generated from an M-ary alphabet, we choose the set $\{\ell_{a,n}\}$ of $M-1$ logarithmic ratios of APPs $\{P(a_n|\mathbf{r})\}$ as reliability estimates of decisions on symbols $\{a_n\}$. The log-likelihood ratio (LLR) $\ell_{a,n}$ is hence defined as

$$\ell_{a,n} = \ln \frac{P(a_n = a|\mathbf{r})}{P(a_n = 0|\mathbf{r})} \tag{1.6}$$

where $a \in \{1, \ldots, M-1\}$.

1.3 Factor graphs and sum-product algorithm

An alternative derivation of the BCJR algorithm can be obtained by means of the factor graphs (FGs) and the sum-product algorithm (SPA) presented in [8]. These tools are particularly suited to find the marginals of a joint PMF that can be expressed as product of "local" functions, each of which depends on a subset of the variables. This factorization can be visualized with a FG, which is a bipartite graph that indicates which variables are argument of each local function. The SPA works on the FG and computes the marginal functions derived from the global function.

Let $\mathbf{x} = (x_1, \ldots, x_n)$ be a collection of variables, where x_i takes on values on some (usually finite) domain $\mathcal{A}_i$, and let $f(\mathbf{x})$ be a multivariate function. Suppose that $f(\mathbf{x})$ factors into a product of several local functions f_j, each having a subset $\mathbf{x}_j$ of $\mathbf{x}$ as argument:

$$f(\mathbf{x}) = \prod_{j \in J} f_j(\mathbf{x}_j)$$

where J is a discrete index set. A FG is a bipartite graph which has a variable node for each variable x_i, a factor node for each function f_j, and an edge connecting variable node x_i to function node f_j if and only if x_i is an argument of f_j. The SPA is defined by the computation rules at variable and factor nodes, and by a suitable node activation schedule. Denoting by $\mu_{x_i \to f_j}(x_i)$ a message sent from the variable node x_i to the factor node f_j, by $\mu_{f_j \to x_i}(x_i)$ a message in the opposite direction, and by $\mathcal{B}_i$ the set of functions f_j having x_i as argument, the message computations performed at variable

and factor nodes are, respectively [8]

$$\mu_{x_i \to f_j}(x_i) = \prod_{h \in \mathcal{B}_i \setminus \{f_j\}} \mu_{h \to x_i}(x_i) \tag{1.7}$$

$$\mu_{f_j \to x_i}(x_i) = \sum_{\sim\{x_i\}} \left[f_j(\{y \in C_j\}) \prod_{y \in C_j \setminus \{x_i\}} \mu_{y \to f_j}(y) \right] \tag{1.8}$$

where C_j is the set of variables argument of f_j and $\sum_{\sim\{x_i\}}$ is the *summary* operator, i.e., a sum over all the variables in C_j excluding x_i.

Thus, we can factor the PMF $P(\mathbf{a}|\mathbf{r})$ in order to find, through the SPA, the marginal APPs $\{P(a_n|\mathbf{r})\}$ required by the MAP symbol strategy (1.1). If the FG has cycles, the SPA is inherently iterative and the convergence to the exact marginal PMFs is not guaranteed. Nevertheless, for many relevant problems characterized by FGs with cycles, the SPA was found to provide very good results and therefore it represents a viable solution to the approximated marginalization of multivariate PMFs when exact calculation is not feasible because of complexity.

Finally, we define the message-passing schedule in the SPA as the specification of the order in which messages are updated. In general, especially for graphs with cycles, the so-called flooding schedule is adopted [9]: in each iteration, all variable nodes and subsequently all factor nodes pass new messages to their neighbors.

1.4 Iterative joint detection/decoding

When we consider a communication system characterized by an error correcting code and a channel with memory, the set of possible states of the overall system can have a very large cardinality. Hence, the optimal MAP symbol (or sequence) detection strategy at the receiver may become infeasible. In these cases, we can resort to a suboptimal iterative joint detection/decoding scheme which exhibits a computational complexity much lower than the complexity of the optimal scheme, but whose performance approaches that of the optimal one (as verified by numerical results) [10]. In particular, here we describe the operations of a serially concatenated scheme, which is the scheme adopted in all the following Chapters for the detection of the transmit-

ted signal (a CPM or a linearly modulated signal) in the presence of an outer error correcting code.

In an iterative concatenated joint detection/decoding scheme, each component block (i.e., the detector and the decoder) works separately by implementing the MAP symbol strategy optimal for the single block, assuming that no other memory sources are present in the system. They employ a detection (respectively, decoding) algorithm based on the MAP symbol rule which provides reliability estimates on the algorithm decisions. In general, an iterative concatenated scheme is based on the following basic concept: each component block exploits the suggestions provided by the other component block, in order to derive decisions which become more reliable with the iterations. In detail, a serially concatenated scheme works as follows. First of all, the detector performs an instance of the detection algorithm, operating on the channel sufficient statistics $\mathbf{r}$. Then, the soft decisions produced on each symbol a_n are forwarded to the decoder, which employs the detector APPs as a priori probabilities on symbols $\{a_n\}$ while performing decoding. Thus, a new set of soft decisions on the symbols are produced and passed to the detector. The detector exploits these reliability estimates as a priori probabilities on $\{a_n\}$ and starts a new iteration of the serially concatenated scheme. The joint detection/decoding process continues for a fixed number of iterations, then hard final decisions on symbols $\{a_n\}$ are made.

In order to accelerate the convergence of the iterative detection/decoding process, each component block must receive as input an information that is not self-produced. With this purpose, in [11] and [12] the concept of *extrinsic information* is introduced, which identifies the reliability information produced by a component block which does not depend on the information received as input. If we denote by $\ell_{a,n}^{\text{out}}$ the LLR defined in (1.6) and produced by a block, representing the reliability measure of a MAP symbol algorithm on the decision on the symbol a_n, the extrinsic information $\ell_{a,n}^{\text{e,out}}$ generated by such block is given by

$$\ell_{a,n}^{\text{e,out}} = \ell_{a,n}^{\text{out}} - \ell_{a,n}^{\text{e,in}} .$$

The FG/SPA tool intrinsically propagates extrinsic information, as described by (1.7) and (1.8).

The turbo principle, i.e., the exchange of information between two soft blocks, can be employed also in iterative decoding applied to low-density parity-check (LDPC) codes and turbo codes [13].

1.5 Information rate for channels with memory

The *information rate* $I(\mathbf{x};\mathbf{y})$ quantifies the amount of information that can be transmitted over a channel with input random process $\mathcal{X}$ and output random process $\mathcal{Y}$, and is expressed in bits per channel use. In the following we will focus on the case where both $\mathcal{X}$ and $\mathcal{Y}$ are stationary processes. From them we extract the discrete-time stationary random sequences $\mathbf{x}$ and $\mathbf{y}$ respectively, in general not of the same length. From information theory results [14], we know that for every channel $I(\mathbf{x};\mathbf{y})$ can be expressed as

$$I(\mathbf{x};\mathbf{y}) = h(\mathbf{x}) - h(\mathbf{x}|\mathbf{y}) \quad \left(\frac{\text{bit}}{\text{ch.use}}\right) \tag{1.9}$$

where $h(\mathbf{x})$ is the *differential entropy rate* of the input sequence $\mathbf{x}$

$$h(\mathbf{x}) = -\mathrm{E}\{\log_2 p(\mathbf{x})\} = \int_{-\infty}^{+\infty} p(\mathbf{x}) \log_2 \frac{1}{p(\mathbf{x})} \mathrm{d}\mathbf{x}$$

and $h(\mathbf{x}|\mathbf{y})$ is the *conditional* differential entropy rate of the input sequence $\mathbf{x}$ given the channel output sequence $\mathbf{y}$

$$h(\mathbf{x}|\mathbf{y}) = -\mathrm{E}\{\log_2 p(\mathbf{x}|\mathbf{y})\} = \int_{-\infty}^{+\infty} p(\mathbf{x},\mathbf{y}) \log_2 \frac{1}{p(\mathbf{x}|\mathbf{y})} \mathrm{d}\mathbf{x}\mathrm{d}\mathbf{y}$$

which depends only on the channel characteristics. It can be shown that (1.9) is equivalent to

$$I(\mathbf{x};\mathbf{y}) = h(\mathbf{y}) - h(\mathbf{y}|\mathbf{x}) \quad \left(\frac{\text{bit}}{\text{ch.use}}\right). \tag{1.10}$$

A method to compute the information rate of a finite-state hidden Markov model is described in [15], and employs the forward recursion of the BCJR algorithm. This method can be extended to all channel models with an infinite number of states (for example additive white Gaussian noise channels affected by phase noise) finding an auxiliary finite-state channel that approximates the actual channel. In this case, the

algorithm allows to compute a lower bound of the actual information rate—the better the channel approximation, the tighter the bound.

The method is the following. Given a certain channel input sequence $\mathbf{x}_1^N = (x_1, \ldots, x_N)$ and the corresponding output sequence of the same length $\mathbf{y}_1^N = (y_1, \ldots, y_N)$, the computation of the differential entropy rate $h(\mathbf{y})$ and of the conditional differential entropy rate $h(\mathbf{y}|\mathbf{x})$ can be carried out thanks to the Shannon-McMillian-Breimann theorem [14] which ensures the convergence, with probability equal to one, of

$$h(\mathbf{y}) = -\lim_{N\to+\infty} \frac{1}{N} \mathrm{E}\left\{\log_2 p(\mathbf{y}_1^N)\right\} \tag{1.11}$$

$$h(\mathbf{y}|\mathbf{x}) = -\lim_{N\to+\infty} \frac{1}{N} \mathrm{E}\left\{\log_2 p(\mathbf{y}_1^N|\mathbf{x}_1^N)\right\} \tag{1.12}$$

if $\mathbf{x}_1^N$ and $\mathbf{y}_1^N$ are realizations of stationary ergodic finite-state hidden Markov processes. Replacing (1.11) and (1.12) in (1.10), we get

$$I(\mathbf{x};\mathbf{y}) = \lim_{N\to+\infty} \frac{1}{N} \mathrm{E}\left\{\log_2 \frac{p(\mathbf{y}_1^N|\mathbf{x}_1^N)}{p(\mathbf{y}_1^N)}\right\}. \tag{1.13}$$

Hence, to compute the information rate we just need to evaluate the PDFs $p(\mathbf{y}_1^N)$ and $p(\mathbf{y}_1^N|\mathbf{x}_1^N)$. These values can be effectively obtained by the forward recursion of the BCJR algorithm implementing the MAP symbol detection strategy. Finally, to evaluate the expectation in (1.13) the Montecarlo method is adopted.

Chapter 2

Synchronization for FDM-CPM systems

Spectral efficiency (SE) of frequency division multiplexed (FDM) systems can be increased by reducing the spacing between two adjacent channels, thus allowing overlap in frequency and hence admitting a certain amount of interference [16][17]. This aspect has been investigated from an information-theoretic point of view for linear [18] as well as continuous phase modulations (CPMs) [19][20], showing that a significant improvement can be obtained through packing even when at the receiver side a single-user detector is employed. When a multi-user receiver is adopted, the benefits in terms of SE can be even larger and the signals can be packed denser and denser [16]–[21].

Since, as known, the complexity of the optimal multi-user detector increases exponentially with the number of channels, suboptimal detection schemes are required. In the case of a satellite FDM system using linear modulations, the adoption of reduced-complexity multi-user detection (MUD) algorithms borrowed from the literature on code division multiple access (CDMA) is investigated in [16]–[18] showing that these techniques work well also in this scenario. Although this is, in principle, possible for CPM systems as well, a new reduced-complexity MUD algorithm for an additive white Gaussian noise (AWGN) channel is derived in [22] based on factor

graphs (FGs) and the sum-product algorithm (SPA) [8]. This latter framework, often used in the past to reinterpret known algorithms, is very useful for deriving new detection schemes with an unprecedented complexity/performance trade-off [23]–[27] or for applications where traditional probabilistic methods fail [28]. In this case, the new algorithm designed in [22] by using this framework outperforms all other suboptimal MUD algorithms both from performance and complexity points of view [20]. But a denser packing has an impact not only on the detection algorithm. In fact, once satisfactorily suboptimal MUD algorithms are available, other subsystems become critical. In particular, carrier synchronization schemes able to cope with the increased interference must be adopted.

In this Chapter, we will focus on CPMs, since they are often employed in satellite communications and they have been recently included in the 2nd-generation Digital Video Broadcasting - Return Channel Satellite (DVB-RCS2) standard [2]. CPM signals are appealing for satellite systems for their robustness to nonlinearities, stemming from the constant envelope, their claimed power and spectral efficiency, and their recursive nature which allows to employ them in serially concatenated schemes [29][30].

2.1 System model

We assume that the channel is shared by U independent users. Without loss of generality, we consider synchronous users, all employing the same modulation format, equally spaced in the frequency domain, transmitting at the same power, and a return link satellite channel. The extension to the case of asynchronous users, possibly with different power and modulation formats can be pursued as described in [22]. The adoption of CPMs allows to use cheaper nonlinear amplifiers at the transmitters, which can be driven in saturation and whose effect can be neglected in our analysis. On the other hand, we assume that the on-board satellite amplifier works far from the saturation to avoid distortions on the composite signal—this is a common

operating choice for this kind of systems[1]. We assume that each user transmits N symbols and we denote by $\alpha_n^{(u)}$ the symbol transmitted by user u at discrete-time n, which takes on values in the M-ary alphabet $\{\pm 1, \pm 3 \cdots \pm (M-1)\}$. Moreover, $\boldsymbol{\alpha}^{(u)} = (\alpha_0^{(u)}, \ldots, \alpha_{N-1}^{(u)})^T$ is the vector of the N symbols transmitted by user u and we also denote $\boldsymbol{\alpha}_n = (\alpha_n^{(1)}, \ldots, \alpha_n^{(U)})^T$ and $\boldsymbol{\alpha} = (\boldsymbol{\alpha}_0^T, \ldots, \boldsymbol{\alpha}_{N-1}^T)^T$. In the following, $(\cdot)^T$ denotes transpose and $(\cdot)^H$ transpose conjugate. The complex envelope of the received signal can be written as

$$r(t) = \sum_{u=1}^{U} s^{(u)}(t, \boldsymbol{\alpha}^{(u)}) e^{\theta^{(u)}(t)} + w(t) \tag{2.1}$$

where $w(t)$ is a zero-mean circularly symmetric white Gaussian noise process with power spectral density (PSD) $2N_0$ (N_0 assumed perfectly known at the receiver), $\theta^{(u)}(t)$ is the phase noise (PN) affecting user u ($\theta^{(u)}(t)$ and $\theta^{(v)}(t)$ are assumed independent for $u \neq v$), and $s^{(u)}(t, \boldsymbol{\alpha}^{(u)})$ is the CPM information-bearing signal of user u which reads

$$s^{(u)}(t, \boldsymbol{\alpha}^{(u)}) = \sqrt{\frac{2E_S}{T}} \exp\left\{ 2\pi f^{(u)} t + h \sum_{n=0}^{N-1} \alpha_n^{(u)} q(t - nT) \right\}. \tag{2.2}$$

In the generic time interval $[nT, nT+T)$, the CPM signal of user u is completely defined by symbol $\alpha_n^{(u)}$ and state $\sigma_n^{(u)} = (\omega_n, \phi_n)$, where

$$\omega_n^{(u)} = (\alpha_{n-1}^{(u)}, \ldots, \alpha_{n-L+1}^{(u)})$$

is the correlative state and ϕ_n, which takes on p values, is the phase state. In the following, we define $\boldsymbol{\sigma}_n = (\sigma_n^{(1)}, \ldots, \sigma_n^{(U)})^T$ and $\boldsymbol{\sigma} = (\boldsymbol{\sigma}_0^T, \ldots, \boldsymbol{\sigma}_N^T)^T$.

An approximated set of sufficient statistics can be obtained by extracting η samples per symbol interval from the received signal prefiltered by means of an analog low-pass filter which leaves unmodified the useful signal and has a vestigial symmetry around $\eta/2T$. The condition on the vestigial symmetry of the analog prefilter

[1] We are dealing with a multiple carrier per transponder scenario, which is common in the return link of satellite systems.

ensures that the noise samples are independent and identically distributed (i.i.d.) complex Gaussian random variables with independent components, each with mean zero and variance $\Xi^2 = N_0\eta/T$ [22]. We will denote by $r_{n,m}$ the m-th received sample ($m = 0, 1, \ldots, \eta - 1$) of the n-th symbol interval. Assuming $\theta^{(u)}(t)$ constant over an interval of length T, this sample can be expressed as

$$r_{n,m} = \sum_{u=1}^{U} s_{n,m}^{(u)}(\alpha_n^{(u)}, \sigma_n^{(u)}) e^{\theta_n^{(u)}} + w_{n,m} \tag{2.3}$$

where $\theta_n^{(u)} = \theta^{(u)}(nT)$, $\{w_{n,m}\}$ are i.i.d. complex Gaussian noise samples, and $s_{n,m}^{(u)}(\alpha^{(u)}, \sigma^{(u)})$ (whose dependence on $\alpha^{(u)}$ and $\sigma^{(u)}$ will be omitted in the following when unnecessary) is the contribution of user u to the useful signal component. The random process $\{\theta_n^{(u)}\}$ is modeled according to a discrete-time Wiener process, whose incremental standard deviation over a symbol interval σ_Δ is known at the receiver [27]. In the following, we will define $\mathbf{r}_n = (r_{n,0}, r_{n,1}, \ldots, r_{n,\eta-1})^T$, $\mathbf{r} = (\mathbf{r}_0^T, \mathbf{r}_1^T, \ldots, \mathbf{r}_{N-1}^T)^T$ and $\mathbf{s}_n^{(u)} = (s_{n,0}^{(u)}, s_{n,1}^{(u)}, \ldots, s_{n,\eta-1}^{(u)})^T$.

2.2 Carrier synchronization algorithms

2.2.1 Multi-user joint detection and phase synchronization

In the presence of PN, phase synchronization must be performed jointly with detection [23], [27]. We describe the extension of the reduced-complexity MUD scheme in [22] to the case of channels affected by PN. This algorithm is obtained by means of some graphical manipulations on the FG representing the joint distribution of the transmitted symbols and the channel phase. We follow the Bayesian approach employed in [27] to design single-user detectors for the PN channel.

We can rewrite the signal of user u highlighting the component that depends on the CPM phase state:

$$s_{n,m}^{(u)}(\alpha_n^{(u)}, \sigma_n^{(u)}) = \overline{s}_{n,m}^{(u)}(\alpha_n^{(u)}, \omega_n^{(u)}) e^{\phi_n^{(u)}}$$

Defining $\psi_n^{(u)} = [\phi_n^{(u)} + \theta_n^{(u)}]_{2\pi}$, where $[.]_{2\pi}$ denotes the modulus 2π operator, the received signal (2.3) can be expressed as

$$r_{n,m} = \sum_{u=1}^{U} \overline{s}_{n,m}^{(u)}(\alpha_n^{(u)}, \omega_n^{(u)}) e^{\psi_n^{(u)}} + w_{n,m}\,. \tag{2.4}$$

Let us now define $\boldsymbol{\omega}_n = (\omega_n^{(1)}, \ldots, \omega_n^{(U)})^T$, $\boldsymbol{\omega} = (\boldsymbol{\omega}_0^T, \ldots, \boldsymbol{\omega}_N^T)^T$, $\boldsymbol{\psi}_n = (\psi_n^{(1)}, \ldots, \psi_n^{(U)})^T$, $\boldsymbol{\psi} = (\boldsymbol{\psi}_0^T, \ldots, \boldsymbol{\psi}_N^T)^T$, and $\overline{\mathbf{s}}_n^{(u)} = (\overline{s}_{n,0}^{(u)}, \overline{s}_{n,1}^{(u)}, \ldots, \overline{s}_{n,\eta-1}^{(u)})^T$. Discarding the terms independent of symbols and states and taking into account that a CPM signal has a constant envelope, the joint distribution $p(\boldsymbol{\alpha}, \boldsymbol{\omega}, \boldsymbol{\psi}|\mathbf{r})$ can be factored as

$$\begin{aligned} p(\boldsymbol{\alpha}, \boldsymbol{\omega}, \boldsymbol{\psi}|\mathbf{r}) \propto & \left[\prod_{u=1}^{U} P(\omega_0^{(u)}) P(\psi_0^{(u)})\right] \prod_{n=0}^{N-1} E_n(\boldsymbol{\alpha}_n, \boldsymbol{\omega}_n, \boldsymbol{\psi}_n) \cdot \\ & \cdot \prod_{u=1}^{U} T_n^{(u)}(\alpha_n^{(u)}, \omega_n^{(u)}, \psi_n^{(u)}) G_n^{(u)}(\psi_{n+1}^{(u)}, \psi_n^{(u)}, \omega_n^{(u)}) I_n^{(u)}(\omega_{n+1}^{(u)}, \omega_n^{(u)}, \alpha_n^{(u)}) P(\alpha_n^{(u)}) \end{aligned} \tag{2.5}$$

where

$$\begin{aligned} I_n^{(u)}(\omega_{n+1}^{(u)}, \omega_n^{(u)}, \alpha_n^{(u)}) &= P(\omega_{n+1}^{(u)}|\omega_n^{(u)}, \alpha_n^{(u)}) \\ G_n^{(u)}(\psi_{n+1}^{(u)}, \psi_n^{(u)}, \omega_n^{(u)}) &= p(\psi_{n+1}^{(u)}|\psi_n^{(u)}, \omega_n^{(u)}) \\ T_n^{(u)}(\alpha_n^{(u)}, \omega_n^{(u)}, \psi_n^{(u)}) &= \exp\left\{\frac{1}{\Xi^2}\Re\left[\mathbf{r}_n^H \overline{\mathbf{s}}_n^{(u)} e^{\psi_n^{(u)}}\right]\right\} \\ E_n(\boldsymbol{\alpha}_n, \boldsymbol{\omega}_n, \boldsymbol{\psi}_n) &= \prod_{i=1}^{U-1} \prod_{k=i+1}^{U} \exp\left\{-\frac{1}{\Xi^2}\Re\left[\overline{\mathbf{s}}_n^{(i)H} \overline{\mathbf{s}}_n^{(k)} e^{-(\psi_n^{(i)} - \psi_n^{(k)})}\right]\right\} \end{aligned} \tag{2.6}$$

Notice that $P(\omega_{n+1}^{(u)}|\omega_n^{(u)}, \alpha_n^{(u)})$ is an indicator function, equal to one if $\alpha_n^{(u)}$, $\omega_n^{(u)}$, and $\omega_{n+1}^{(u)}$ are compatible and to zero otherwise, and $p(\psi_{n+1}^{(u)}|\psi_n^{(u)}, \omega_n^{(u)}) = p(\psi_{n+1}^{(u)}|\psi_n^{(u)}, \alpha_{n-L+1}^{(u)})$ is a Gaussian PDF in $\psi_{n+1}^{(u)}$ with mean $[\psi_n^{(u)} + \pi h \alpha_{n-L+1}]_{2\pi}$ and standard deviation σ_Δ. The FG corresponding to (2.5) has cycles of length four, that make unlikely the convergence of the SPA, since they are too short. We remove these short cycles by clustering the variables $\omega_n^{(u)}$ and $\psi_n^{(u)}$ and then stretching them in $(\alpha_n^{(u)}, \omega_n^{(u)}, \psi_n^{(u)})$ [8], obtaining a graph with shortest cycles of length twelve. Assuming as in [22] that the

interference among non-adjacent users is negligible, we approximate (2.6) as

$$E_n(\boldsymbol{\alpha}_n,\boldsymbol{\omega}_n,\boldsymbol{\psi}_n) \simeq \prod_{i=1}^{U-1} E_n^{(i,i+1)}(\alpha_n^{(i)},\omega_n^{(i)},\psi_n^{(i)},\alpha_n^{(i+1)},\omega_n^{(i+1)},\psi_n^{(i+1)}) \tag{2.7}$$

where

$$E_n^{(i,i+1)}(\alpha_n^{(i)},\omega_n^{(i)},\psi_n^{(i)},\alpha_n^{(i+1)},\omega_n^{(i+1)},\psi_n^{(i+1)}) = \exp\left\{-\frac{1}{\Xi^2}\Re\left[\bar{\mathbf{s}}_n^{(i)H}\bar{\mathbf{s}}_n^{(i+1)}e^{-(\psi_n^{(i)}-\psi_n^{(i+1)})}\right]\right\}.$$

This FG is shown in Fig. 2.1 and is similar to that for the AWGN channel [22]. A major difference is represented here by the fact that continuous variables $\psi_n^{(u)}$ are now represented in the graph. Hence, the application of the SPA involves the computation of continuous PDFs and is not suited for a practical implementation. To overcome this problem, we may resort, as in [27], to the canonical distribution approach. Examples of commonly used canonical distributions for this channel can be found in [27]. In the numerical results, we will consider a canonical distribution composed of a weighted sum of impulses. In other words, each phase $\psi_n^{(u)}$ is quantized to D equally spaced values. Although the algorithm has been obtained by assuming a Wiener PN with known incremental variance over a symbol variance, it can be employed even when the PN follows a different model. In this case, the value of σ_Δ^2 assumed at the receiver must be optimized by simulation for the PN at hand. In any case, there is in general a benefit from using at the receiver a value of thermal noise variance σ^2 larger than the actual one. The rationale of this trick is the following: since there is an overconfidence in the computed messages, we can make the algorithm less confident simply by describing the channel as if it added more noise than it really does [31].

2.2.2 Data-aided multi-user fine frequency synchronization

The MUD algorithm requires the knowledge of the amplitude $\sqrt{2E_S/T}$ (possibly different in case of users with different powers) and frequency values $f^{(u)}$ for each user. For them, we resort to data-aided (DA) estimation algorithms based on known data fields usually inserted in the frame. Amplitude estimation is not an issue. In fact, the application of U occurrences of a DA maximum-likelihood single-user estimation

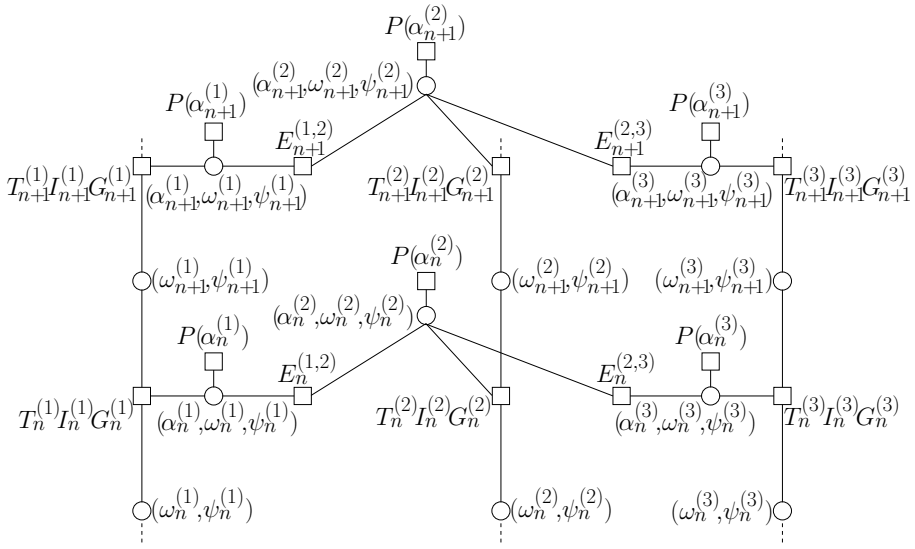

Figure 2.1: FG resulting from the approximation (2.7) and for $U = 3$.

algorithm provides amplitude estimates with a good accuracy for typical preamble lengths. Instead, DA single-user frequency estimation algorithms do not provide the required accuracy. This is obviously due to the interference of adjacent channels. For this reason, we employ interference cancellation to refine the estimates.

A first set of estimates of the frequency values $f^{(u)}$ is obtained by applying the DA algorithm in [32] to the preamble of each user. This algorithm does not require the knowledge of the channel phase for each user. These estimates are then iteratively refined still using the same single-user algorithm to the received signal after the contribution of the adjacent signals has been removed. To perform interference cancellation we need to employ not only the already estimated amplitude values and the frequency values of the previous iteration, but also the instantaneous (in case of a time-varying channel phase) values of the channel phase for each user. These are obtained by using the DA multi-user carrier phase estimation algorithm described in the next paragraph, and refined every time a new set of frequency estimates becomes available.

In summary, the algorithm proceeds as follows. The amplitude of each user is

estimated first. Then, at each iteration a new set of frequency estimates is derived by using the single-user DA algorithm in [32] after the contribution of adjacent users has been removed. This set of frequency estimates is employed to perform DA multi-user carrier phase estimation whose output will be employed for interference cancellation at the next iteration. A few iterations are in general sufficient, provided the known data fields of all users have been properly optimized.

2.2.3 Data-aided multi-user carrier phase estimation

We now describe a DA multi-user carrier phase estimation algorithm that requires the knowledge of frequency and amplitude values of each user, estimated as described in the previous paragraph. As mentioned, phase estimates are used for interference cancellation necessary to improve frequency estimates.

Let us assume a known data field of P symbols ($K = \eta P$ samples). Defining $z_k = r_{n,m}$, $x_k^{(u)} = s_{n,m}^{(u)}$, and $\zeta_k = w_{n,m}$, with $k = n\eta + m$, we will assume that the known data field corresponds to values $k = 0, 1, \ldots, K-1$. We also remove the hypothesis that the PN is constant over a symbol interval and define $\varphi_k^{(u)} = \theta^{(u)}(kT/\eta)$. Hence, we may express

$$z_k = \sum_{u=1}^{U} x_k^{(u)} e^{\varphi_k^{(u)}} + \zeta_k \,. \tag{2.8}$$

Let us define $\boldsymbol{\varphi}_k = (\varphi_k^{(1)}, \ldots, \varphi_k^{(U)})^T$, $\boldsymbol{\varphi} = (\boldsymbol{\varphi}_0^T, \ldots, \boldsymbol{\varphi}_{K-1}^T)^T$ and $\mathbf{z} = (z_0, \ldots, z_{K-1})^T$. As before, we model the PN as a discrete-time Wiener process with incremental standard deviation over a symbol interval σ_Δ. We derive the MAP DA phase estimator as

$$\hat{\varphi}_k^{(u)} = \underset{\varphi_k^{(u)}}{\operatorname{argmax}}\, p(\varphi_k^{(u)}|\mathbf{z}) \qquad u = 1, \ldots, U, \quad k = 0, \ldots, K-1 \,.$$

PDFs $\{p(\varphi_k^{(u)}|\mathbf{z})\}$ are obtained from $p(\boldsymbol{\varphi}|\mathbf{z})$ by using the FG/SPA framework. From

(2.8), we may express

$$p(\boldsymbol{\varphi}|\mathbf{z}) \propto p(\mathbf{z}|\boldsymbol{\varphi})p(\boldsymbol{\varphi}) = \prod_{k=0}^{K-1}\left[p(z_k|\boldsymbol{\varphi}_k)\prod_{u=1}^{U}p(\varphi_k^{(u)}|\varphi_{k-1}^{(u)})\right]$$
$$= \prod_{k=0}^{K-1}\left[p(z_k|\boldsymbol{\varphi}_k)\prod_{u=1}^{U}D_{k,k-1}^{(u)}(\varphi_k^{(u)}-\varphi_{k-1}^{(u)})\right] \tag{2.9}$$

where $D_{k,k-1}^{(u)}(\varphi_k^{(u)}-\varphi_{k-1}^{(u)}) = p(\varphi_k^{(u)}|\varphi_{k-1}^{(u)})$ is a Gaussian PDF with mean $\varphi_{k-1}^{(u)}$ and standard deviation $\sigma_\Delta/\sqrt{\eta}$, according to the Wiener model. Neglecting irrelevant multiplicative terms, we can further factor

$$p(z_k|\boldsymbol{\varphi}_k) \propto \exp\left\{-\frac{1}{2\Xi^2}\left|z_k-\sum_{u=1}^{U}x_k^{(u)}e^{\varphi_k^{(u)}}\right|^2\right\}$$
$$\propto \prod_{u=1}^{U}B_k^{(u)}(\varphi_k^{(u)})\prod_{u=1}^{U-1}\prod_{v=u+1}^{U}C_k^{(u,v)}(\varphi_k^{(u)},\varphi_k^{(v)}) \tag{2.10}$$

having defined

$$B_k^{(u)}(\varphi_k^{(u)}) = \exp\left\{\frac{1}{\Xi^2}\Re\left[z_k x_k^{(u)*}e^{-\varphi_k^{(u)}}\right]\right\}$$
$$C_k^{(u,v)}(\varphi_k^{(u)},\varphi_k^{(v)}) = \exp\left\{\frac{1}{\Xi^2}\Re\left[x_k^{(u)}x_k^{(v)*}e^{(\varphi_k^{(u)}-\varphi_k^{(v)})}\right]\right\}.$$

From (2.9) and (2.10), we finally obtain the relevant factorization of $p(\boldsymbol{\varphi}|\mathbf{z})$. Node $C_k^{(u,v)}$ in the resulting FG connects variable nodes $\varphi_k^{(u)}$ and $\varphi_k^{(v)}$. Since the interference between two non-adjacent users is much smaller than the interference between adjacent users, we consider only functions connecting adjacent variable nodes, i.e. functions $C_k^{(u,u+1)}$. The simplified FG is shown in Fig. 2.2.

Due to the presence of cycles in the FG of Fig. 2.2, the application of the SPA gives an iterative algorithm which provides proper approximations of PDFs $\{p(\varphi_k^{(u)}|\mathbf{z})\}$. We adopt the canonical distribution approach and, as in [23], we model the messages

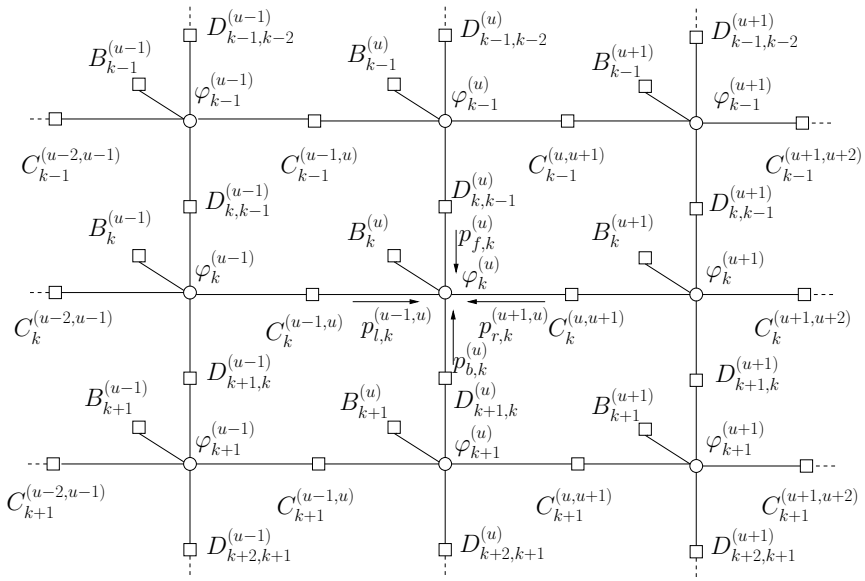

Figure 2.2: FG for the multi-user DA phase estimator.

represented in Fig. 2.2 as Tikhonov PDFs, i.e.

$$p^{(u)}_{f,k}(\varphi^{(u)}_k) = t(a^{(u)}_{f,k};\varphi^{(u)}_k)$$
$$p^{(u)}_{b,k}(\varphi^{(u)}_k) = t(a^{(u)}_{b,k};\varphi^{(u)}_k)$$
$$p^{(u-1,u)}_{l,k}(\varphi^{(u)}_k) = t(a^{(u-1,u)}_{l,k};\varphi^{(u)}_k)$$
$$p^{(u+1,u)}_{r,k}(\varphi^{(u)}_k) = t(a^{(u+1,u)}_{r,k};\varphi^{(u)}_k)$$

where $t(\xi;x)$ is a Tikhonov distribution in the random variable (RV) x characterized by the complex parameter ξ:

$$t(\xi;x) = \frac{1}{2\pi \mathrm{I}_0(|\xi|)} \exp\left\{\Re\left[\xi e^{-jx}\right]\right\}$$

being $\mathrm{I}_0(\cdot)$ the zeroth-order modified Bessel function of the first kind. Hence, we simply have to update and propagate the complex parameters describing the Tikhonov PDFs. Let us first consider the update of parameter $a^{(u)}_{f,k}$. By generalizing the results

in [23], we have

$$a_{f,k+1}^{(u)} = \gamma\left(a_{f,k}^{(u)} + \frac{z_k x_k^{(u)*}}{\Xi^2} + a_{l,k}^{(u-1,u)} + a_{r,k}^{(u+1,u)}, \frac{\sigma_\Delta}{\sqrt{\eta}}\right) \tag{2.11}$$

having defined

$$\gamma(\epsilon,\zeta) = \frac{\epsilon}{1+|\epsilon|\zeta^2}\,.$$

Similarly,

$$a_{b,k-1}^{(u)} = \gamma\left(a_{b,k}^{(u)} + \frac{z_k x_k^{(u)*}}{\Xi^2} + a_{l,k}^{(u-1,u)} + a_{r,k}^{(u+1,u)}, \frac{\sigma_\Delta}{\sqrt{\eta}}\right). \tag{2.12}$$

Regarding parameters $a_{l,k}^{(u-1,u)}$ and $a_{r,k}^{(u+1,u)}$ we have

$$a_{l,k}^{(u,u+1)} = \delta\left(a_{f,k}^{(u)} + a_{b,k}^{(u)} + \frac{z_k x_k^{(u)*}}{\Xi^2} + a_{l,k}^{(u-1,u)}, \frac{x_k^{(u)} x_k^{(u+1)*}}{\Xi^2}\right) \tag{2.13}$$

and

$$a_{r,k}^{(u,u-1)} = \delta\left(a_{f,k}^{(u)} + a_{b,k}^{(u)} + \frac{z_k x_k^{(u)*}}{\Xi^2} + a_{r,k}^{(u+1,u)}, \frac{x_k^{(u-1)} x_k^{(u)*}}{\Xi^2}\right) \tag{2.14}$$

where

$$\delta(\epsilon,\zeta) = \frac{\epsilon\zeta}{\sqrt{|\epsilon|^2+|\zeta|^2}}\,.$$

In order to obtain (2.13) and (2.14), two approximations have been employed: $\mathrm{I}_0(|x|) \simeq e^{|x|}$ and $\sqrt{1+x} \simeq 1 + x/2$. The following schedule is adopted: messages $a_{f,k}^{(u)}$ and $a_{b,k}^{(u)}$ are first updated, for $k = 0,\ldots,K-1$ (with initial parameter $a_{f,0}^{(u)} = 0$) and $k = K-1,\ldots,0$ (with initial parameter $a_{b,K-1}^{(u)} = 0$), respectively. Then messages $a_{l,k}^{(u-1,u)}$ and $a_{r,k}^{(u+1,u)}$ are updated for $u = 2,\ldots,U$ and $u = U-1,\ldots,1$, respectively (with initial parameters $a_{l,k}^{(0,1)} = a_{r,k}^{(U+1,U)} = 0$). A few iterations are, in general, sufficient. Finally, the phase estimates are

$$\hat{\varphi}_k^{(u)} = \arg\left(a_{f,k}^{(u)} + a_{b,k}^{(u)} + a_{l,k}^{(u-1,u)} + a_{r,k}^{(u+1,u)} + \frac{z_k x_k^{(u)*}}{\Xi^2}\right).$$

2.3 Numerical results

We limit our investigation to binary CPM formats. This choice is justified by the need to illustrate the relevant concepts and by the results which show that we can design transmission schemes with a very high efficiency using simple CPMs. We consider binary CPM with $h = 1/3$, $L = 2$, and rectangular (REC) frequency pulse. This scheme turned out to be the best one among those considered in [20].

As discussed in [19] and [20], the optimal spacing depends on the considered value of E_s/N_0 (although this dependence is quite smooth). Hence, according to the operating E_s/N_0, we choose the optimal modulation format and the corresponding optimal spacing. For the REC scheme, $FT = 0.3$ is the optimal spacing at $E_s/N_0 = 10$ dB when an infinite number of users is present and the mismatched MUD considers only $U' = 5$ users, handling the remaining users as AWGN. The scheme with REC frequency pulse leads to a higher SE than the RC-based counterpart [20], even though REC and RC formats perform similarly for low values of SE [20].

The described multi-user frequency synchronization scheme results unbiased. Hence, in Fig. 2.3 we show the mean square error (MSE) of the frequency estimate for the central user versus E_s/N_0, when $P = 60$ symbols. A Wiener PN with $\sigma_\Delta = 1$ degree has been considered. As a reference curve, we show the Cramér-Rao lower bound (CRB) for a system with $U = 1$, computed according to [33]. When $U = 1$, this bound is reached by the frequency estimation algorithm in [32] for $E_s/N_0 \geq 2$ dB (curve with white circles). When $U = 5$ users are present, this algorithm gives a very poor performance (curve labeled “1 iteration” since it corresponds to the first iteration of the proposed multi-user algorithm). With 4 iterations we are able to reach, for $E_s/N_0 \geq 5$ dB, the CRB related to the presence of only one user. Hence, a very effective interference cancellation is performed. A slightly better result is obtained by using a genie-aided version of the proposed frequency synchronization algorithm in which the true values of the channel phases are employed for interference cancellation purposes.

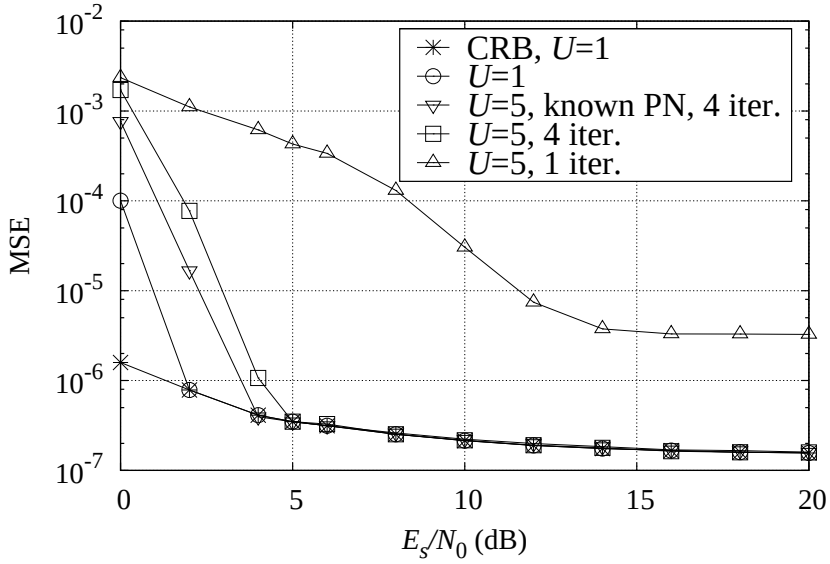

Figure 2.3: MSE of the multiuser frequency synchronization scheme in the presence of PN.

Chapter 3

Spread-spectrum CPM systems

Modern communications require modulation formats robust to nonlinearities and multiple access interference (MAI), as well as power- and spectrally efficient. Robustness to nonlinearity is mandatory in order to use strongly saturated amplifiers, and spectral efficiency is one of the most important quality figures in any communication system. For this reason the choice of using modulation formats such as continuous phase modulations (CPMs) comes quite naturally. CPMs are a family of very appealing modulation formats. Their robustness to nonlinearity stemming from the constant envelope is one of the main reasons of their popularity, along with excellent power and spectral efficiencies [19].

Code division multiple access (CDMA) is one of the most studied methods for multi-user communication systems. Based on the employed spread spectrum (SS) technique, CDMA schemes are grouped in two major classes, namely direct-sequence SS (DS-SS) and frequency-hopping SS (FH-SS).

DS-SS has been combined with CPMs in many different ways. Lane and Bush [34] proposed a SS multi-h (SSMH) CPM whose drawbacks in a multi-user scenario will be analyzed in the following. Giannetti *et al.* [35] studied a special subset of single-h binary CPMs, known as generalized minimum-shift keying (GenMSK), which can be approximately viewed as linear modulations. Hence, classical results of multi-user communications for linear modulations apply. Obviously, the main drawback

of this approach is the strict constraint on the modulation format. Hsu and Lehnert [36] considered a multi-user system where each user transmits a SS signal that is the product between a linear modulation (for the data) and a multi-h CPM (for the spreading chips), giving up to phase continuity. This problem has been solved by Yang *et al.* [37] mapping the M-ary information symbols into M binary phase spreading sequences (PSSs) modulated by a single-h CPM modulator. The main problem of this approach is the time-consuming design of a unique set of M different and orthogonal PSSs for each user. Moreover, a simple receiver structure is not available because the data and the spreading chips are not separable. The separation between data and spreading chips has been preserved in the dual-phase technique proposed by McDowell *et al.* [38]. Chips are modulated as a multi-h CPM, data are modulated as a MSK signal, and finally multiplied. The receiver, as in the linearly-modulated DS-SS systems, is composed by an analog (and therefore expensive) despreader and a detector. Müller and Lampe proposed in [39] a DS-SS system using linear modulations with constant envelope and continuous phase. To avoid phase jumps to occur at every symbol change, they pose few constraints on the information symbol alphabet, the spreading factor, and the symbol waveform. This latter must depend on the chip sequence and the chip waveform. This solution, called continuous phase chip modulation (CPCM), has nevertheless big spectral sidelobes, incompatible with spectral masks of most wireless communication standards. Therefore Müller recently proposed in [40] a linear DS-SS system where each user is assigned a set of very similar spreading sequences, which are chosen in a data-dependent fashion. These sequences are generated by an iterative algorithm ensuring their high stop-band attenuation, constant envelope and continuous phase.

To our knowledge, FH has never been studied as a multiple access technique in CPM-based systems. Nevertheless, FH has been used with the purpose of spreading the CPM power spectral density (PSD) for security issues in [41] and [42]. In this Chapter, a new multiple access technique based on multi-h CPMs is proposed. The main idea is to exploit the fact that each CPM can be viewed as a frequency modulation where the frequency deviation is strictly related to the modulation index. Since in multi-h CPMs the modulation index is replaced by a sequence of indices (with

the index varying every symbol period), the resulting effect is a sort of frequency hopping. This is *exactly* an instance of FH when applied to a continuous phase FSK (CPFSK). So, we will use multi-*h* CPM not to improve bit error rate (BER) performance (as in [34], [36], and [38]) but to spread the PSD and allow multiple access without resorting to spreading codes or to any other DS-CDMA technique. In other words, we directly construct a modulation format with a PSD extremely flat, large, and smooth at will. The corresponding single-user detector has practically the same complexity of a classical single-*h* CPM detector with the same number of phase states (which is a clear advantage if compared to the complexity of the receivers in [37] and [38]). In the CPM literature, the modulation index is hardly ever chosen bigger than one (except for [43] where satellite navigation systems have been addressed), even though this would not invalidate the CPM definition. Therefore, the most natural way to spread the CPM power spectral density is by using indices much bigger than one and varying in a wide range [44]. Moreover, using a long sequence of indices the CPM power spectral density will become smoother. Assigning to each user a different and randomly generated sequence of indices, we will obtain a new and efficient FH spread spectrum technique for CPM-based systems. With this approach, we will get rid of the constraints on the modulation formats (since we consider general *M*-ary multi-*h* partial response CPMs). Obviously the phase continuity and the constant envelope are guaranteed. The spreading factor, usually defined in DS-CDMA systems with linear modulations as the ratio between the bandwidth of the spread signal and the bandwidth of the signal before spreading, cannot be defined in the same way here because in the proposed system there is no "signal before spreading"—the spectral spreading effect is now embedded in the modulation format itself. On the other hand, the definition of spreading factor proposed in [45], as the ratio of the Fourier bandwidth of the spread signal to its Shannon bandwidth, could be used. However, it requires the computation of an orthonormal basis for the spread signal, not available here in closed form.

Since we are considering a multi-user scenario, we also address the multi-user detection (MUD) issue. Because the complexity of the optimal multi-user receiver grows exponentially with the number of users, suboptimal detection schemes are re-

quired. We consider different multi-user detectors, based on hard interference cancellation (HIC) [46], soft interference cancellation (SIC) [47], extended to frequency division multiplexed CPM-based systems in [22], and an algorithm derived in [22] by using factor graphs (FGs) and the sum-product algorithm (SPA) framework [8].

3.1 System model

3.1.1 Multi-*h* CPM signal

The complex envelope of a generic multi-*h* CPM signal is [3]

$$s(t) = \sqrt{\frac{2E_s}{T}} \exp\left\{2\pi \sum_i h_{\underline{i}} \alpha_i q(t - iT) + \theta\right\} \tag{3.1}$$

where E_s is the energy per symbol, T is the symbol period, $\{\alpha_i\}$ are the M-ary information symbols, $\{h_i\}$ is the sequence of N_h modulation indices, $\underline{i} = i \bmod N_h$, $q(t)$ is the phase-smoothing response characterizing the format, and θ is an initial phase offset. The phase-smoothing response is still a continuous function satisfying the following property:

$$q(t) = \begin{cases} 0 & \text{when } t \leq 0 \\ \frac{1}{2} & \text{when } t \geq LT \end{cases}$$

L being the correlation length of the signal. As done in Chapter 1, the frequency pulse is defined as

$$g(t) = \frac{\mathrm{d}}{\mathrm{d}t} q(t)$$

and (3.1) can be rewritten as

$$s(t) = \sqrt{\frac{2E_s}{T}} \exp\left\{\left[2\pi \int_{-\infty}^{t} \sum_i h_{\underline{i}} \alpha_i g(\tau - iT) \mathrm{d}\tau + \theta\right]\right\} \tag{3.2}$$

which is the expression of a frequency-modulated signal using a pulse amplitude modulation (PAM) with shaping pulse $g(t)$ as modulating signal. The most used frequency pulses are the rectangular pulse (L-REC to denote its duration of L symbol periods) and the raised-cosine pulse (L-RC).

CPMs are modulations with memory. In the generic symbol interval $nT \le t < (n+1)T$, the CPM signal (3.1) is completely defined by symbol α_n and state $\sigma_n = (\omega_n, \varphi_n)$, where $\omega_n = (\alpha_{n-1}, \alpha_{n-2}, \ldots, \alpha_{n-L+1})$ is the correlative state and

$$\begin{aligned} \varphi_n &= \left(\pi \sum_{i=-\infty}^{n-L} h_{\underline{i}} \alpha_i \right) \bmod 2\pi \\ &= (\varphi_{n-1} + \pi h_{\underline{n-L}} \alpha_{n-L}) \bmod 2\pi \end{aligned} \tag{3.3}$$

is the phase state [4], [48]. The correlative state can assume M^{L-1} values, whereas the phase state can assume p values, having defined $h_i = k_i/p$ where k_i and p are positive integer numbers and integer values for h_i are forbidden. Therefore, the total number of states is pM^{L-1}. A correct definition of the modulation index requires that k_i and p are relative prime to have a minimal trellis representation. As it will be clear later, the considered sequence of indices is chosen such that p is kept constant whereas k_i is chosen randomly with the only constraint that h_i cannot be integer. When k_i and p are not relative prime, we still use, for simplicity, a trellis representation with p states although it could be reduced. This allows to always use the same trellis without the need to resort to a time-varying trellis. The CPM signal in the symbol interval $nT \le t < (n+1)T$ can thus be expressed as

$$\begin{aligned} s(t) &= \sqrt{\frac{2E_s}{T}} e^{(\varphi_n + \theta)} \exp\left\{ 2\pi \sum_{i=0}^{L-1} h_{\underline{n-i}} \alpha_{n-i} q(t - nT + iT) \right\} \\ &= \sqrt{\frac{2E_s}{T}} e^{(\varphi_n + \theta)} \prod_{i=0}^{L-1} \left[\exp\left\{ \frac{2\pi}{p} q(t - nT + iT) \right\} \right]^{k_{\underline{n-i}} \alpha_{n-i}} \end{aligned} \tag{3.4}$$

3.1.2 SS-FH-CPM

In the proposed multi-user system, multiple access is guaranteed by assigning a different sequence of modulation indices to each user. We assume that each user transmits K symbols, and we denote by $\alpha_n^{(u)}$ and $\sigma_n^{(u)}$ the symbol transmitted by user u at discrete-time n and the corresponding state. We define $\boldsymbol{\alpha}^{(u)} = (\alpha_0^{(u)}, \ldots, \alpha_{K-1}^{(u)})^T$ as the vector of the K symbols transmitted by user u, and also $\boldsymbol{\alpha}_n = (\alpha_n^{(1)}, \ldots, \alpha_n^{(U)})^T$ as the vector of all symbols transmitted at discrete-time n (one symbol per user),

and $\boldsymbol{\alpha} = (\boldsymbol{\alpha}_0^T, \ldots, \boldsymbol{\alpha}_{K-1}^T)^T$, where $(.)^T$ denotes transpose. Similarly, we define $\boldsymbol{\sigma}_n = (\sigma_n^{(1)}, \ldots, \sigma_n^{(U)})^T$ and $\boldsymbol{\sigma} = (\boldsymbol{\sigma}_0^T, \ldots, \boldsymbol{\sigma}_{K-1}^T)^T$. We also define

$$s^{(u)}(\boldsymbol{\alpha}^{(u)}, t) = \sqrt{\frac{2E_s^{(u)}}{T}} \exp\left\{ 2\pi \sum_{i=0}^{K-1} h_{\underline{i}}^{(u)} \alpha_i^{(u)} q(t - iT) + \theta^{(u)} \right\} \tag{3.5}$$

the signal transmitted by user u and, without loss of generality, we assume that all users employ the same values of T, M, L, p, N_h, and $h_{\max}$, $h_{\max}$ being the maximum value taken on by the modulation index. We will also assume that all users employ the same phase smoothing response $q(t)$.

We consider an asynchronous multiple access system on an additive white Gaussian noise (AWGN) channel, so that the complex envelope of the received signal is

$$\begin{aligned} r(t) &= \sum_{u=1}^{U} s^{(u)}(\boldsymbol{\alpha}^{(u)}, t - \tau^{(u)}) + w(t) \\ &= s^{(\ell)}(\boldsymbol{\alpha}^{(\ell)}, t - \tau^{(\ell)}) + \sum_{\substack{u=1 \\ u \neq \ell}}^{U} s^{(u)}(\boldsymbol{\alpha}^{(u)}, t - \tau^{(u)}) + w(t)\,. \end{aligned} \tag{3.6}$$

Initial phase offsets $\theta^{(u)}$ and delays $\tau^{(u)}$ are random variables uniformly distributed in $[0, 2\pi)$ and $[0, T)$, respectively. For user ℓ, the reference user, without loss of generality we will assume $\theta^{(\ell)} = \tau^{(\ell)} = 0$. The thermal noise is a zero-mean circularly symmetric white Gaussian process with PSD $2N_0$.

Fixing the indices denominator p is mandatory to keep constant the number of the phase states, while fixing the maximum numerator allows every user to undergo the same spectral spreading. Each user has a different sequence of randomly-generated modulation indices. The spectral spreading depends only on the range of values assumed by the modulation index—the larger this range, the stronger the spreading effect. The number of modulation indices N_h plays a role only in the smoothness of the PSD. A CPM with high N_h will show a smooth PSD with small oscillations and no sidelobes (see the numerical results in Paragraph 3.4).

The number of users allowed in the system depends on the total number of possible indices $\nu = ph_{\max} - \lfloor h_{\max} \rfloor$ (where $\lfloor x \rfloor$ denotes the maximum integer lower than x).

If we impose the absence of overlaps, in a synchronous system the maximum number of users would coincide with the number of possible indices

$$U_{\max} = \nu .$$

3.2 Multi-user detectors

Although not necessary in the derivation of the algorithms, since it applies unmodified independently of the employed set of sufficient statistics, we will adopt, as in practical receiver implementations, an approximated set of sufficient statistics for MAP symbol detection obtained as described in [49]. We assume the useful signal component to be band-limited with bandwidth lower than $N/2T$, where N is a proper positive integer. Although this is obviously an approximation in the case of CPM signals, whose PSD has, strictly speaking, an infinite support, the choice of a proper value of N ensures that this approximation can be made good at will. The approximated statistics can be obtained by extracting N samples per symbol interval from the received signal (3.6) prefiltered by means of a low-pass filter which leaves unmodified the useful signal and has a vestigial symmetry around $N/2T$ [49]. The condition on the vestigial symmetry ensures that the noise samples are independent and identically distributed complex Gaussian random variables with independent components, each with mean zero and variance $\xi^2 = N_0 N/T$ [49]. An alternative (and not approximated) set of sufficient statistics can be obtained as described in [22]. We denote by $r_{n,m}$ the m-th received sample (with $m = 0, \ldots, N-1$) of the n-th symbol interval. It can be expressed as

$$r_{n,m} = \sum_{u=1}^{U} s_{n,m}^{(u)}(\alpha_n^{(u)}, \sigma_n^{(u)}) + w_{n,m} \tag{3.7}$$

where, as mentioned, $\{w_{n,m}\}$ are independent and identically distributed complex Gaussian noise samples and $s_{n,m}^{(u)}(\alpha_n^{(u)}, \sigma_n^{(u)})$ (whose dependence on $\alpha_n^{(u)}$ and $\sigma_n^{(u)}$ will be omitted in the following) is the contribution of user u to the useful signal component. In the following, we will denote by $\mathbf{r}_n = (r_{n,0}, r_{n,1}, \ldots, r_{n,N-1})^T$ the vector of the received samples in the n-th symbol interval, by $\mathbf{r} = (\mathbf{r}_0^T, \mathbf{r}_1^T, \ldots, \mathbf{r}_{K-1}^T)^T$ the vector of

all the received samples, and by $\mathbf{s}_n^{(u)} = (s_{n,0}^{(u)}, s_{n,1}^{(u)}, \ldots, s_{n,N-1}^{(u)})^T$ the vector collecting the samples of the signal of user u in the n-th symbol interval.

When considering coded CPM schemes where the CPM modulator is concatenated, possibly through an interleaver, with an outer encoder (as an example, see [30], [50], and references therein), the receiver is usually based on a soft-input soft-output (SISO) detector that iteratively exchanges soft information with the outer SISO decoder according to the turbo principle. Regarding single-user SISO CPM detection, little can be added to what already said in the literature (as an example, see [27] and references therein)—the adoption of multi-h CPM signals here entails only trivial modifications with respect to the case of single-h CPMs or the adoption, in case of simplified detectors, of the Laurent decomposition extended to multi-h signals [51]. As far as the optimal multi-user detector (MUD) is concerned, it has a complexity which is exponential in the number of users U and is thus infeasible. For its derivation, the reader can refer to [22, Section III.A]. In fact, although [22] deals with CPM-based frequency-division-multiplexed systems, the derivation holds unmodified in the case of SS-FH-CPM systems. Suboptimal multi-user SISO CPM detectors can also be conceived by extending those described in [22] for frequency-division-multiplexed CPM systems.

3.2.1 HIC-based receiver

The most trivial multi-user detector is that based on HIC [46]. The receiver for each user is composed by a SISO single-user detector (SUD), a SISO decoder, an encoder and a modulator. The SUD receiver for user u estimates its own information bits through a proper number of iterations of the soft detector and the soft decoder. If the estimated bits form a valid codeword, this is re-encoded and re-modulated. The resulting signal is then passed to the SUD detectors of all other users to allow the interference cancellation. Then, this process of iterative soft detection/decoding, interference estimation and cancellation is iterated until a valid codeword cannot be decoded.

3.2.2 SIC-based receivers

One of the reduced-complexity SIC algorithms with a very good performance available in the CDMA literature is that proposed in [47]. Being based on a Gaussian approximation of the MAI, the algorithm can be obtained by replacing the PMF of the interfering symbols with a complex circularly symmetric Gaussian PDF with the same mean and variance. In the following, we will denote by $P(.)$ (respectively, $p(.)$) the PMF (respectively, the PDF) of a discrete (respectively, continuous) random vector.

Users will employ a SISO SUD each, and will exchange soft information to cancel out the interference. For the sake of simplicity, let us consider U synchronous users. We assume the discrete-time equivalent channel for user ℓ to be

$$r_{n,m}^{(\ell)} = s_{n,m}^{(\ell)} + z_{n,m}^{(\ell)}$$

where $z_{n,m}^{(\ell)}$ accounts for both interference and noise, that is

$$z_{n,m}^{(\ell)} = \sum_{\substack{u=1 \\ u\neq\ell}}^{U} s_{n,m}^{(u)} + w_{n,m}\,.$$

The vector $\mathbf{z}_n^{(\ell)} = (z_{n,0}^{(\ell)},\ldots,z_{n,N-1}^{(\ell)})^T$ is assumed Gaussian with mean vector $\boldsymbol{\mu}_n^{(\ell)}$ and covariance matrix $\boldsymbol{\Phi}_n^{(\ell)}$, respectively, defined as

$$\boldsymbol{\mu}_n^{(\ell)} = \sum_{\substack{u=1 \\ u\neq\ell}}^{U} \bar{\boldsymbol{\mu}}_n^{(u)} \tag{3.8}$$

$$\bar{\boldsymbol{\mu}}_n^{(u)} = \sum_{(\alpha_n^{(u)},\sigma_n^{(u)})} \hat{P}(\alpha_n^{(u)},\sigma_n^{(u)}|\mathbf{r})\mathbf{s}_n^{(u)} \tag{3.9}$$

$$\boldsymbol{\Phi}_n^{(\ell)} = \sum_{\substack{u=1 \\ u\neq\ell}}^{U} \sum_{(\alpha_n^{(u)},\sigma_n^{(u)})} \hat{P}(\alpha_n^{(u)},\sigma_n^{(u)}|\mathbf{r})(\mathbf{s}_n^{(u)} - \bar{\boldsymbol{\mu}}_n^{(u)})(\mathbf{s}_n^{(u)} - \bar{\boldsymbol{\mu}}_n^{(u)})^H + 2\xi^2\mathbf{I} \tag{3.10}$$

where $\mathbf{I}$ is the identity matrix, $(.)^H$ denotes conjugate transpose, and $\{\hat{P}(\alpha_n^{(u)},\sigma_n^{(u)}|\mathbf{r})\}$ are the estimates of the APPs provided by the single-user SISO detector related to

the interfering user u. The SISO detector for user ℓ, in the form of a BCJR algorithm [6], will employ the following branch metric (dependencies are omitted for the sake of notational convenience)

$$G_n^{(\ell)} \propto \exp\left\{2\Re\left[\mathbf{s}_n^{(\ell)H}\mathbf{\Phi}_n^{(\ell)-1}(\mathbf{r}-\boldsymbol{\mu}_n^{(\ell)})\right] - \mathbf{s}_n^{(\ell)H}\mathbf{\Phi}_n^{(\ell)-1}\mathbf{s}_n^{(\ell)}\right\} \tag{3.11}$$

where $\Re[.]$ stands for the real part operator and $\propto$ denotes a proportionality relation. Denoting by $I_n^{(\ell)}(\sigma_{n+1}^{(\ell)}, \sigma_n^{(\ell)}, \alpha_n^{(\ell)})$ the indicator function equal to one if $\alpha_n^{(\ell)}$, $\sigma_n^{(\ell)}$, and $\sigma_{n+1}^{(\ell)}$ satisfy the trellis constraint for user ℓ, and equal to zero otherwise, we define

$$C_n^{(\ell)}(\sigma_{n+1}^{(\ell)}, \sigma_n^{(\ell)}, \alpha_n^{(\ell)}) = I_n^{(\ell)}(\sigma_{n+1}^{(\ell)}, \sigma_n^{(\ell)}, \alpha_n^{(\ell)})P(\alpha_n^{(\ell)}).$$

The outputs of the SISO detector are the estimates of the APPs needed by the other users' SISO detectors to perform soft cancellation:

$$\hat{P}(\alpha_n^{(\ell)}, \sigma_n^{(\ell)}|\mathbf{r}) \propto A_n(\sigma_n^{(\ell)})B_{n+1}(\sigma_{n+1}^{(\ell)})G_n^{(\ell)}C_n^{(\ell)} \tag{3.12}$$

where $A_n(\sigma_n^{(\ell)})$ and $B_n(\sigma_n^{(\ell)})$ are the forward and backward messages of the BCJR algorithm.

The SIC MUD is then formed by U enhanced SISO SUDs, each of which computes the mean vector $\boldsymbol{\mu}_n^{(\ell)}$ and the covariance matrix $\mathbf{\Phi}_n^{(\ell)}$ for every symbol interval through (3.8) and (3.10), inverts $\mathbf{\Phi}_n^{(\ell)}$ and then computes the branch metric in (3.11). Finally, it computes the APPs $\{\hat{P}(\alpha_n^{(\ell)}, \sigma_n^{(\ell)}|\mathbf{r})\}$ with (3.12) and passes them to all the other SISO detectors for soft cancellation. In the following, this algorithm will be referred to as SIC 1. Its complexity is quadratic in the number of users [47].

This algorithm can be simplified by neglecting the off-diagonal elements of $\mathbf{\Phi}_n^{(\ell)}$ [47]. Consequently, the matrix inversion results to be computationally less expensive at the price of a performance degradation. This simplified detector will be referred to as SIC 2 and has a complexity that linearly depends on the number of users.

3.2.3 FG-based receiver

This algorithm, proposed in [22] for FDM-CPM systems and based on the application of the FG/SPA framework, derives from a suitable factorization of the PMF $P(\boldsymbol{\alpha}, \boldsymbol{\sigma}|\mathbf{r})$:

$$P(\boldsymbol{\alpha},\boldsymbol{\sigma}|\mathbf{r}) \propto p(\mathbf{r}|\boldsymbol{\alpha},\boldsymbol{\sigma})P(\boldsymbol{\sigma}|\boldsymbol{\alpha})P(\boldsymbol{\alpha}).$$

Each term can be further factored as follows:

$$P(\boldsymbol{\alpha}) = \prod_{u=1}^{U}\prod_{n=0}^{K-1} P(\alpha_n^{(u)})$$

$$P(\boldsymbol{\sigma}|\boldsymbol{\alpha}) = \prod_{u=1}^{U} P(\sigma_0^{(u)}) \prod_{n=0}^{K-1} P(\sigma_{n+1}^{(u)}|\alpha_n^{(u)},\sigma_n^{(u)})$$

$$p(\mathbf{r}|\boldsymbol{\alpha},\boldsymbol{\sigma}) \propto \prod_{n=0}^{K-1} F_n(\boldsymbol{\alpha}_n,\boldsymbol{\sigma}_n) \prod_{u=1}^{U} H_n^{(u)}(\alpha_n^{(u)},\sigma_n^{(u)})$$

where

$$P(\sigma_{n+1}^{(u)}|\alpha_n^{(u)},\sigma_n^{(u)}) \propto I_n^{(u)}(\sigma_{n+1}^{(u)},\sigma_n^{(u)},\alpha_n^{(u)})$$

$$F_n(\boldsymbol{\alpha}_n,\boldsymbol{\sigma}_n) = \prod_{i=1}^{U-1}\prod_{j=i+1}^{U} \exp\left\{-\frac{1}{\xi^2}\Re\left[\mathbf{s}_n^{(i)H}\mathbf{s}_n^{(j)}\right]\right\}$$

$$H_n^{(u)}(\alpha_n^{(u)},\sigma_n^{(u)}) = \exp\left\{\frac{1}{\xi^2}\Re\left[\mathbf{r}_n^H\mathbf{s}_n^{(u)}\right]\right\}.$$

Hence, we finally have

$$P(\boldsymbol{\alpha},\boldsymbol{\sigma}|\mathbf{r}) \propto \left[\prod_{u=1}^{U} P(\sigma_0^{(u)})\right]\prod_{n=0}^{K-1} F_n(\boldsymbol{\alpha}_n,\boldsymbol{\sigma}_n)\cdot \cdot\prod_{u=1}^{U} H_n^{(u)}(\alpha_n^{(u)},\sigma_n^{(u)})I_n^{(u)}(\sigma_{n+1}^{(u)},\sigma_n^{(u)},\alpha_n^{(u)})P(\alpha_n^{(u)}). \quad (3.13)$$

The resulting FG has cycles of length four. As known, the application of the SPA to a FG with cycles allows an approximate (because of the presence of cycles) computation of the APPs $\{P(\alpha_n^{(u)}|\mathbf{r})\}$ required for the implementation of the MAP symbol detection strategy [8]. However, the presence of shortest cycles of length four makes the convergence of the SPA to good approximations of the APPs $\{P(\alpha_n^{(u)}|\mathbf{r})\}$ very unlikely [8]. It is possible to remove these short cycles by stretching [8] variables $\sigma_n^{(u)}$ in $(\alpha_n^{(u)},\sigma_n^{(u)})$. In other words, instead of representing variables $\alpha_n^{(u)}$ alone, we define

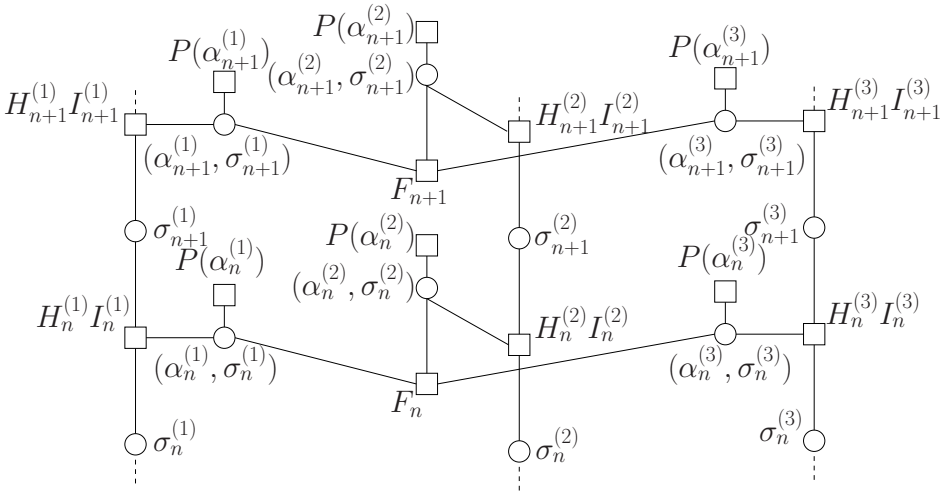

Figure 3.1: FG corresponding to (3.13) after stretching variables $\sigma_n^{(u)}$ in $(\alpha_n^{(u)}, \sigma_n^{(u)})$ and for $U = 3$. Circles and squares represent variable and function nodes, respectively.

a new variable given by the couple $(\alpha_n^{(u)}, \sigma_n^{(u)})$. This transformation does not involve approximations, since the resulting graph preserves all the information of the original graph. The resulting FG, shown in Fig. 3.1, has cycles of length twelve. Since cycles are still present, the SPA applied to this graph is iterative and still leads to an approximate computation of the APPs $\{P(\alpha_n^{(u)}|\mathbf{r})\}$ [8]. However, the absence of short cycles allows us to obtain very good approximations, as shown later. As the SIC 2, this algorithm has a complexity which is linear in the number of users [22].

3.2.4 Complexity considerations

With respect to the optimal detector for a single-h CPM signal, the SUD for a SS-FH-CPM signal has the same number of states (provided that the values of p, M, and L are the same) and the same number of trellis branches. In order to evaluate the branch metrics, we need the N samples $\mathbf{s}_n^{(u)}$ of all the possible waveforms that can be transmitted in a symbol period. These samples will be then correlated with the

received samples in a given symbol period, i.e., the product $\mathbf{r}_n^H \mathbf{s}_n^{(u)}$ has to be computed. For a single-h signal, these waveforms are M^L and can be precomputed and stored in a look-up table (LUT). On the other hand, for a SS-FH-CPM signal the number of possible waveforms also depends on the possible L-tuple of consecutive modulation indices in the sequence of N_h modulation indices adopted by the considered user, which are $\min\left\{N_h, \binom{\gamma}{L}\right\} M^L$, although not all are employed in the same trellis section. If this number is too high, it could not be convenient to store them, but could be preferable to precompute and store the samples of the L waveforms $\left\{\exp\left[\frac{2\pi}{p} q(t-iT)\right]\right\}$, $i = 0, 1, \ldots, L-1$, in (3.4) and then use them to compute the needed waveforms in each symbol period. The same waveforms are also required to be computed every symbol epoch or precomputed and stored for the implementation of all MUDs as well.

With respect to traditional DS-SS systems based on linear modulations, a much larger number of correlations has to be computed. This is the price to be paid to have signals with constant envelope (and large spectral efficiency, as shown later). However, we point out that a significant complexity reduction can be obtained by extending the technique described in [27] for single-h CPM signals to the case of multi-h signals using the decomposition in [51] that allows to express a multi-h signal as a sum of linearly-modulated components. In this case, the number of trellis states of the SUD is reduced to p and also the branch metrics computation results to be greatly simplified.

3.3 Spectral efficiency

The main quality figure we consider in this work is the overall spectral efficiency η_U of the system. Since we are considering a multiple access scenario where all users share the same bandwidth, the most intuitive way to compute η_U is to evaluate the spectral efficiency η of a reference user, and then define $\eta_U = U\eta$.

The spectral efficiency for the reference user can be computed as

$$\eta = \frac{I}{BT} \quad \text{[bit/s/Hz]} \tag{3.14}$$

where B is the bandwidth occupied by the CPM signal and I is the information rate of the user. CPM bandwidth is theoretically infinite because the PSD of a CPM signal has rigorously an infinite support. Hence, we consider the traditional definition of bandwidth based on the power concentration, that is the bandwidth that contains a given fraction of the overall power. Being this fraction a parameter, we choose to use the 99.9% of the overall power. This definition is coherent with systems where a limitation on the out-of-band power exists. To compute this bandwidth we need the CPM power spectral density, which cannot be evaluated analytically in closed form, but only numerically. The adopted algorithm is the one proposed in [52] and [53].

To compute the information rate I for the reference user, we can use the simulation-based technique described in [15], which only requires the existence of an optimal MAP symbol detector for the considered system. Unfortunately, the complexity of the optimal MUD is exponential in U, making the evaluation of I practically infeasible. Therefore, we can evaluate an achievable lower bound by resorting to the concept of mismatched detection [54]. We can consider an approximated channel model (the auxiliary channel) for which an exact MAP symbol detection with affordable complexity exists—the more similar the auxiliary channel to the actual channel, the tighter the obtained bound on the spectral efficiency.

As done in [19], we approximate the channel model at the receiver side by modeling the interference as a zero-mean circularly symmetric white Gaussian process with PSD $2N_I$, N_I being a design parameter independent of the thermal noise. This approximation is exploited only by the receiver, while in the actual channel the interference is generated as in (3.6). Hence, the considered auxiliary channel model is that for which the received signal reads

$$r(t) = s^{(\ell)}(t) + \zeta(t) \tag{3.15}$$

where $\zeta(t)$ is a zero-mean circularly symmetric white Gaussian process with PSD $2(N_0 + N_I)$. The simulation-based method described in [15] allows to evaluate the achievable information rate for the mismatched receiver, i.e.

$$I(\boldsymbol{\alpha}^{(\ell)}, \mathbf{r}) = \lim_{J\to\infty} \frac{1}{J} \mathrm{E}\left\{ \log \frac{p(\mathbf{r}^J | \boldsymbol{\alpha}^{(\ell)J})}{p(\mathbf{r}^J)} \right\} \quad \text{[bit/ch.use]} \tag{3.16}$$

where we used the superscript J to remark that a sequence is truncated to its first J elements. In (3.16) $p(\mathbf{r}^J|\boldsymbol{\alpha}^{(\ell)J})$ and $p(\mathbf{r}^J)$ are PDFs according to the auxiliary channel model (3.15), while the statistical average is with respect to the input and the output sequences evaluated according to the actual channel model (3.6). Both $p(\mathbf{r}^J|\boldsymbol{\alpha}^{(\ell)J})$ and $p(\mathbf{r}^J)$ can be evaluated recursively through the forward recursion of the MAP detection algorithm matched to the auxiliary channel model [15]. The mismatched receiver can assure communication with arbitrarily small nonzero error probability when the transmission rate at the CPM modulator input does not exceed $I(\boldsymbol{\alpha}^{(\ell)}, \mathbf{r})$ bits per channel use.

3.4 Numerical results

3.4.1 Power spectral density

In order to describe the spectral behavior of the proposed system, we consider three different binary CPM signals using the 2-RC pulse and show their PSDs in Fig. 3.2, computed by using the technique described in [52], [53]. The first signal is a single-h signal with $h = 3/8$. The remaining ones are SS-FH-CPM signals with $h < 5$ and characterized by sequences of modulation indices of different length N_h. It is possible to see that increasing the number of indices the PSD becomes smoother. Moreover, the sidelobes disappear (since there are no frequency notches) and are replaced by a small ripple. This spectral behavior is not surprising, since the PSD of a CPM signal with a long index sequence is—intuitively speaking—the average of the PSDs of all the single-h signals that use as index one of the ν possible indices.

3.4.2 Overall spectral efficiency

We consider an asynchronous SS-FH-CPM system using a 2-RC frequency pulse, $N_h = 16$, and $p = 8$. Since we are not interested in a particular sequence of indices but in the average behavior of the system, we consider a packet transmission (with 1024 symbols per packet) and, for each user, we change the sequence of indices $\{h_i^{(u)}\}_{i=0}^{N_h-1}$, the time delay $\tau^{(u)}$, and the initial phase offset $\theta^{(u)}$ every packet. We generate the

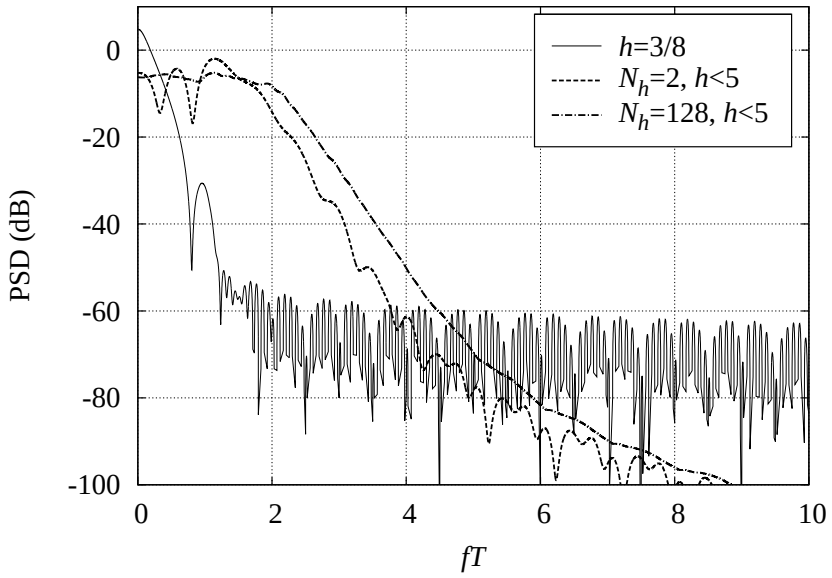

Figure 3.2: Power spectral densities for different single-*h* and SS-FH-CPM signals.

indices in a quasi-random way. For the first user we generate the index sequence randomly, while the sequences of the remaining users are shifted versions (modulus $h_{\max}$) of the sequence of the first user. The shifts are chosen in order to maximize the pairwise index distance defined as

$$d = \min_{u \neq v} \left| h_i^{(u)} - h_i^{(v)} \right|$$

between each couple of users. Obviously d remains the same for $i = 0, \ldots, N_h - 1$. Using the maximum distance, the correlations of all the possible couples of users are minimized and our system becomes more similar to an orthogonal system. Finally, to remove the correlation introduced by the shift, a random interleaver is used to scramble the simultaneous indices among the users.

In order to make some comparisons with the proposed SS-FH-CPM system, we first consider single-user systems using binary single-h CPMs with a 2-RC frequency pulse and $h < 1$, as traditionally done in literature. There is no interest in considering single-h systems with $h > 1$ because they have a larger bandwidth than those with $h < 1$ [3], resulting in a lower spectral efficiency. For the single-h systems the signal bandwidth strongly depends on h (as shown in Table 3.1), and so does the spectral efficiency.

h	1/8	3/8	1/2	5/8	7/8
BT	0.94	1.28	1.62	1.87	2.12

Table 3.1: Bandwidths of single-h 2-RC CPMs with different modulation indices.

Hence, we choose $h = 1/8$, $h = 3/8$, $h = 1/2$, $h = 5/8$, and $h = 7/8$, and compare the corresponding spectral efficiencies versus E_b/N_0, E_b being the received mean energy per information bit, with the overall spectral efficiency of the SS-FH-CPM binary system with $h_{\max} = 39/8$ and $U = 37$ asynchronous users. The number of users U has been found maximizing η_U (via numerical simulations) as a function of U and the interference variance N_I assumed at the receiver for a fixed signal-to-noise ratio (SNR) value. As it can be seen in Fig. 3.3, the SS-FH-CPM system has a better spectral efficiency than all single-user single-h systems for medium to high

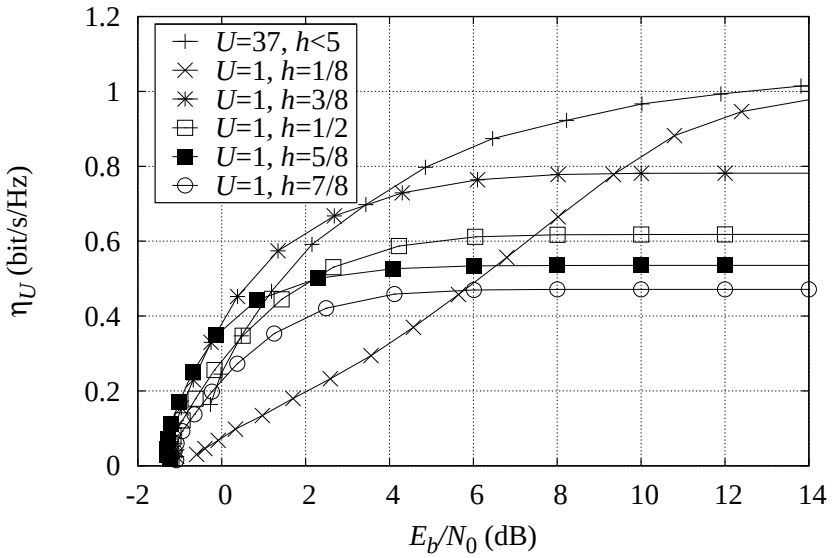

Figure 3.3: Spectral efficiencies of the considered 2-RC binary SS-FH-CPM with $N_h = 16$, $p = 8$, $h_{\max} = 39/8$, and of different single-h 2-RC CPMs with $h = 1/8$, $h = 3/8$, $h = 1/2$, $h = 5/8$, and $h = 7/8$, respectively. For the SS-FH-CPM signal, we use the (suboptimal) single-user detector.

SNR values. At low SNR, η_U is in the same range of values as the single-h spectral efficiencies. According to the well-known results in information theory, the curve in Fig. 3.3 can be approached, even with $U \gg 1$, using a SUD and a proper channel code. Then, we compare the proposed SS-FH-CPM system with two SSMH systems, described in [34]. In a multi-user scenario, the SSMH-CPM system in [34] needs the use of spreading sequences of length N_c chips per symbol period, with $N_c \geq U$ (even though some overload is possible). The normalized bandwidth of the unspread signal is then multiplied by a factor N_c, and therefore the global spectral efficiency is very low. For the considered SSMH-CPM systems, the adopted spreading sequences are random binary sequences generated every packet period together with the time delays and the initial phase offsets. We show the maximum spectral efficiencies η_U

	SS-FH-CPM	SSMH		
N_c	/	1	3	4
BT	6.04	1.75	5.26	7.01

Table 3.2: Bandwidths of the considered 2-RC binary SS-FH-CPM with $N_h = 16$, $p = 8$, $h_{\max} = 39/8$, and of the binary 2-RC SSMH schemes with $\{h_i\} = \{1/2, 5/8\}$.

achievable by the SSMH systems (obtained by the joint optimization of U and N_I) for $N_c = 3$ and $N_c = 4$ in Fig. 3.4. We chose these values of spreading factor in order to compare our SS-FH-CPM system to SSMH systems with similar bandwidths, as shown in Table 3.2. From Fig. 3.4, it is easy to see that the SSMH systems have values of η_U much lower than that of the proposed SS-FH system, for which the considered number of users U has been found jointly maximizing η_U as a function of the number of users U and the interferers noise variance N_I for a fixed SNR value. We also considered $N_c = 16$ (in analogy to the length of the indices sequences of the SS-FH system N_h), but the maximum achievable η_U fell down to zero. The same happened with $U = 37$ users. These considerations suggest that the SSMH technique is not suitable for multi-user systems.

In traditional DS-SS systems, the number of users that maximizes the global spectral efficiency linearly depends on the total occupied bandwidth. Since in the proposed system the theoretical results obtained for linear modulations cannot be used, we will show via numerical simulations that this dependence is approximately linear also for the SS-FH-CPM system. In Fig. 3.5 we show the optimized η_U of the SS-FH-CPM system considered before, and the optimized η_U of a system with the same parameters but doubled bandwidth (i.e., a higher value of $h_{\max}$). For comparison, we show the same curves also for two quaternary systems. It is clear from Table 3.3 and Fig. 3.5 that doubling the bandwidth allows (approximately) doubling the number of users. Moreover, optimized binary systems outperform optimized quaternary systems.

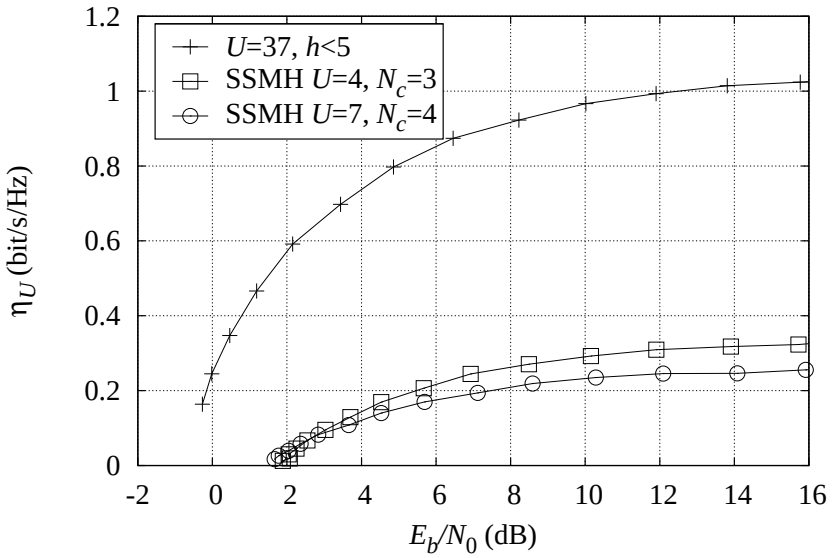

Figure 3.4: Spectral efficiencies of the proposed 2-RC binary SS-FH-CPM system with $h < 5$, $N_h = 16$, $U = 37$, and two SSMH systems with $\{h_i\} = \{1/2, 5/8\}$.

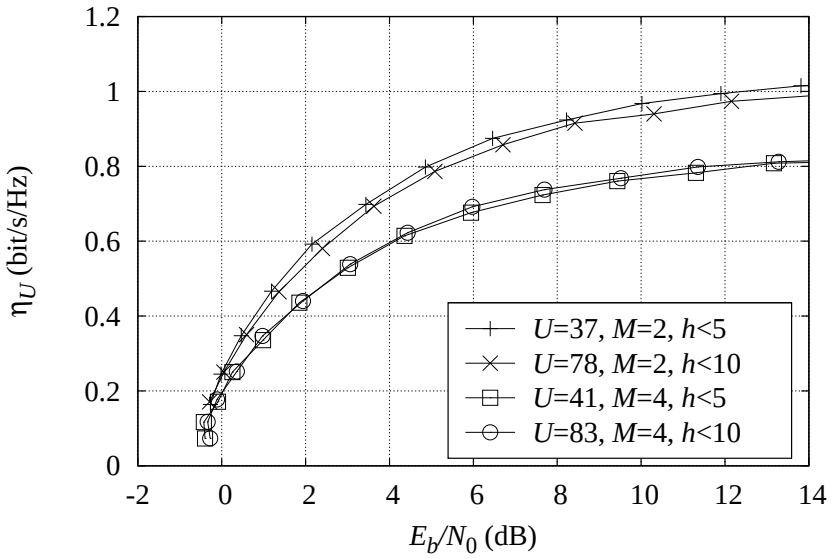

Figure 3.5: Spectral efficiencies of the considered 2-RC binary and quaternary SS-FH-CPM with $N_h = 16$, $p = 8$, $h_{\max} = 39/8$, and the same systems with double bandwidth ($h_{\max} = 79/8$). All curves have been obtained with a single-user detector.

M	2		4	
$h_{\max}$	39/8	79/8	39/8	79/8
BT	6.03	12.25	15.43	30.31

Table 3.3: Bandwidths of 2-RC CPMs with $N_h = 16$ and $p = 8$.

This last result is the reason why in the following we will discard higher order modulations and focus only on binary modulations. Therefore, a comparison among the SS-FH-CPM system and other binary systems, namely those proposed in [35], [39], and [40], named in the following GiLuRe, MuLa, and Mu, respectively, is needed. We set the total bandwidth $BT \simeq 38$ for all the four systems and chose the spreading factors of GiLuRe, MuLa, and Mu systems, and the value of $h_{\max}$ for the proposed system accordingly. The resulting parameters are shown in Table 3.4, where

γ is the spreading factor and $T_c = T/\gamma$ is the chip period.

format	$h_{\max}, \gamma$	BT_c	BT
SS-FH-CPM	311/8	⁄	38.25
GiLuRe	24	1.62	38.83
MuLa	18	2.21	39.78
Mu	44	0.88	38.63

Table 3.4: Parameters used to compare different systems with the same bandwidth $BT \simeq 38$.

The number of asynchronous users has been optimized, jointly with the interference variance N_I, for all systems in order to maximize the global spectral efficiency. For the GiLuRe system we have chosen the 2-RC format (for a fair comparison with the proposed SS-FH-CPM system) and random chips as described in [35]. For the MuLa system we have chosen a roll-off factor $\alpha = 0$ since it is the value providing the best spectral efficiency [39]. Finally, for the Mu system we used the same parameters used in [40], i.e., $p = 1/3$, 10^4 primary iterations, 10^3 secondary iterations, and random initial binary chips. The results reported in Fig. 3.6 show that our proposed system outperforms all other systems.

Finally, in order to show that it is possible to approach the performance promised by the information-theoretic analysis, we show the information rates for $U = 3$, 6, and 9 synchronous users (Fig. 3.7) and the corresponding BER curves (Fig. 3.8) obtained with rate-1/2 convolutional code with constraint length 5, generators $[2, 32]_8$ and codewords of length 64000 information bits, concatenated with the modulator through a random interleaver. It is clear that the larger the number of users, the lower the information rate of each user (see Fig. 3.7). Hence, for a high number of users the information rate of each user is very low. For this reason, in order to employ codes with a rate sufficiently high, we consider a limited number of users (at most 9). For both figures, the interference variance N_I has been optimized through numerical simulations. The interleavers (one for each user) used in the BER simulations have been generated randomly. At the receiver, iterative detection and decoding is performed

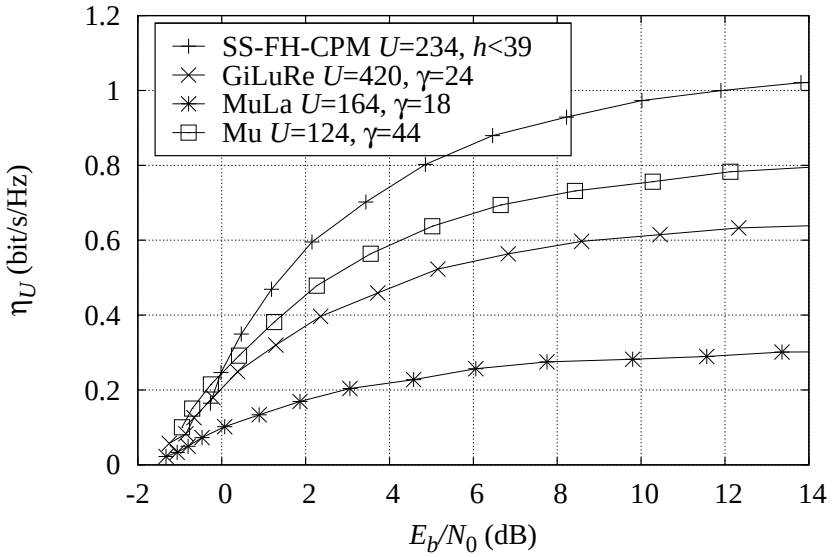

Figure 3.6: Spectral efficiencies of the proposed 2-RC binary SS-FH-CPM with N_h = 16 and $h_{\max} = 311/8$, GiLuRe 2-RC system with $\gamma = 24$, MuLa system with $\gamma = 18$ and $\alpha = 0$, and Mu system with $\gamma = 44$. All curves have been obtained with a single-user detector.

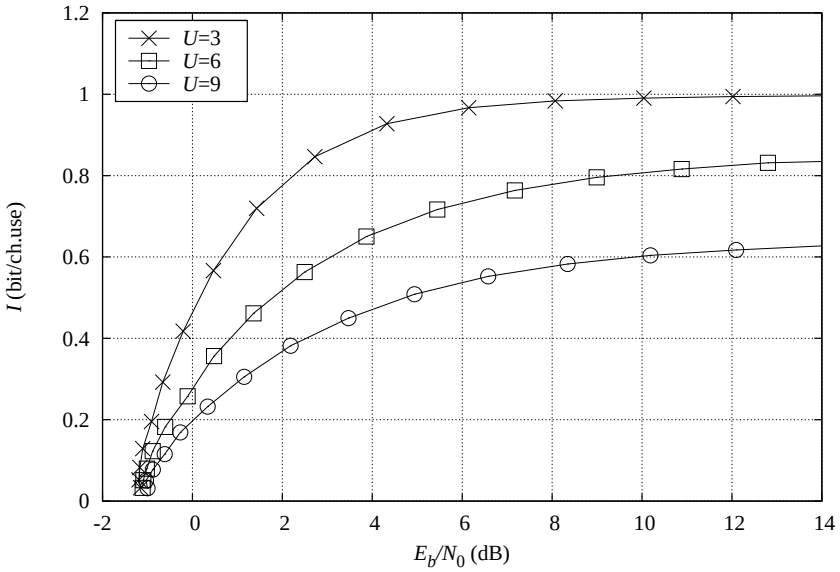

Figure 3.7: Information rates of the proposed 2-RC binary SS-FH-CPM with $N_h = 16$ and $h_{\max} = 39/8$. $U = 3$, $U = 6$, and $U = 9$ users have been considered. All curves have been obtained with a single-user detector.

for a maximum of 20 allowed iterations. As it can be observed, the loss with respect to the information rate curve is around 1 dB for $U = 3$, 2 dB for $U = 6$, and 3 dB for $U = 9$, despite the use of a very simple coding scheme [30]. An extensive search of the optimal convolutional codes for the three cases would further improve the BER performance (in particular for the system with $U = 9$).

3.4.3 BER with equal powers

In order to assess the performance of the described suboptimal MUDs, we considered a coded SS-FH-CPM system with $U = 3$ synchronous users using a binary 2-RC CPM with $p = 4$, $h_{\max} = 19/4$, and $N_h = 8$. All users have the same energy per symbol (i.e., $E_s^{(u)} = E_s$, $u = 1,2,3$) and employ the $(64,51)$ extended Bose, Ray-Chaudhuri, Hocquenghem (eBCH) code with rate $R = 0.79$ and codewords of length 1024 bits

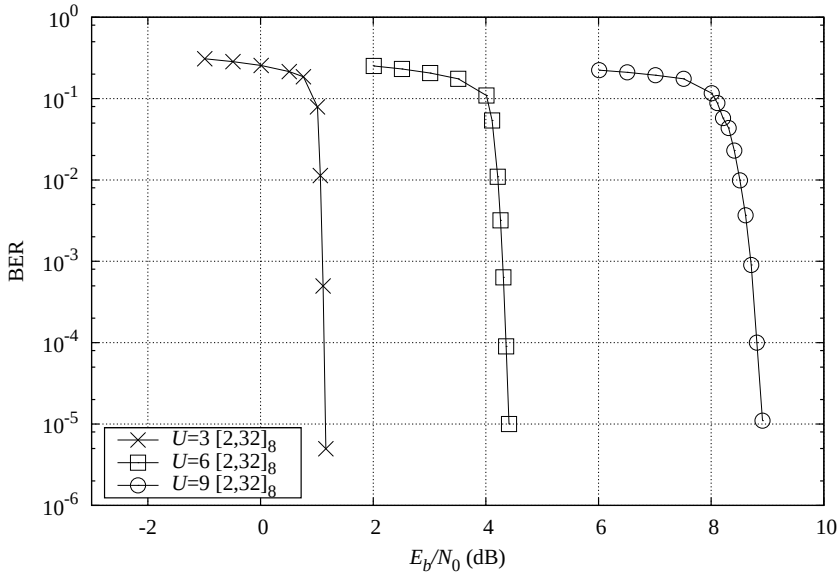

Figure 3.8: Bit error rate of the proposed 2-RC binary SS-FH-CPM with $N_h = 16$ and $h_{\max} = 39/8$. $U = 3$, $U = 6$, and $U = 9$ users have been considered.

described in [50], serially concatenated with the modulator through an S-random interleaver, with $S = 22$. As a benchmark, we consider the BER of a SUD with $U = 3$ users and the BER of a SUD in the absence of interference ($U = 1$ user). Again, we optimized the noise variance assumed by each detector and allowed 20 detection/decoding iterations.

For the suboptimal multi-user detector described in [22], the performance also depends on the adopted schedule. Serial or parallel schedules are usually considered in the literature. Since the difference in performance is practically negligible in this scenario of users transmitting at the same power, we only consider the parallel schedule. In this case, at each iteration all users are activated simultaneously. The computed soft-outputs are then provided to the other users for the next iteration and, after deinterleaving, to the decoders.

Since SIC 1 and SIC 2 detectors show the same performance when users are uncorrelated (or weakly correlated) [55], we decided to introduce a correlation to point out the different behavior of the two algorithms. Therefore, we generated the index sequence for user $u = 1$ randomly, and from that we derived all the other sequences as

$$h_i^{(u)} = h_i^{(1)} + \frac{u-1}{p}.$$

If $h_i^{(u)}$ is an integer, then we changed its value in $h_i^{(1)} + u/p$. In other words, the modulation indices of all users are close to each other as much as possible. The performance of the considered detectors is shown in Fig. 3.9. The HIC algorithm performs as the SUD because the interference prevents a correct bit estimation, which implies that (almost) no cancellation is done.

The SIC 2 algorithm performs much better than the HIC, but, as expected, even better does the SIC 1. However, the FG-based receiver has the best performance because the Gaussian approximation of the interference is not accurate with only two interferers. To see the SIC algorithms outperform the FG-based receiver, we should consider a much higher number of users.

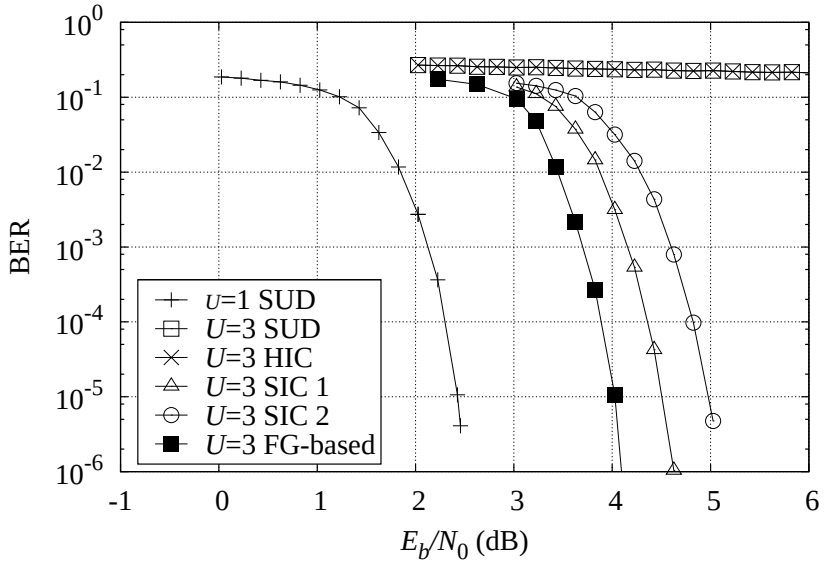

Figure 3.9: BER performance of the SUD and different MUDs in the case of a binary 2-RC system with $U = 1$ and $U = 3$, $N_h = 8$, $p = 4$, $h_{\max} = 19/4$, and a $(64, 51)$ eBCH code with rate $R = 0.79$.

3.4.4 BER with unbalanced powers

We also considered the case of unbalanced powers in a system with the same characteristics and parameters as the one described in the previous section. Without loss of generality, we chose to order users in a decreasing way according to their energy, i.e., $E_s^{(1)} \geq E_s^{(2)} \geq \ldots \geq E_s^{(U)}$. We considered as reference user the central user ℓ and fixed its power $P^{(\ell)}$, while the powers of the other users are assumed to be $P^{(u)} = P^{(\ell)} + 2(\ell - u)$ dB. We employed S-random interleavers and we adopted a serial schedule, starting the detection from the user with the highest power. The computed soft-outputs are then provided to the users with lower powers for interference cancellation and, after deinterleaving, to the decoders.

In Fig. 3.10 we show the performance of the different receivers. Again, the HIC algorithm performs as the SUD because the interference prevents a correct bit estimation. The SIC 2 has a poor performance, and again the FG-based receiver outperforms the SIC algorithms.

3.5 Optimization of the index sequences

In traditional linearly-modulated CDMA systems, the optimization of the spreading sequences (also called *signature sequences*) is a well-studied topic. Theoretical analyses have found the optimum sequences in synchronous systems, under either the condition $U \leq \gamma$ [56] or $U > \gamma$ [57], where γ is the spreading factor. In these cases, an iterative algorithm to determine the optimum sequence sets is available [58]. More recently a new approach to the optimization problem has been carried out by exploiting mathematical tools coming from game theory [59].

Nevertheless, none of these techniques can be applied to CPM-based systems because of the nonlinearity of the modulation format. In linearly-modulated CDMA systems, waveforms are independent of the information symbols and depend only on the signature sequence of each user. On the contrary, in CPM-based systems the waveforms depend in a nonlinear fashion not only on the index sequence, but also on all transmitted symbols because of the modulation memory. Therefore it is no longer possible to assume the orthogonality condition as an optimality criterion because

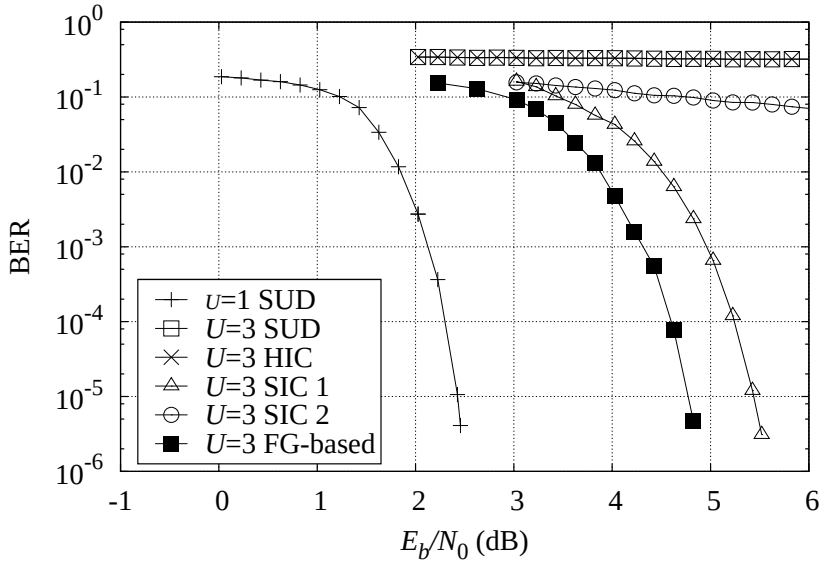

Figure 3.10: BER performance of the SUD and different MUDs in the case of an unbalanced binary 2-RC system with $U = 1$ and $U = 3$, $N_h = 8$, $p = 4$, $h_{\max} = 19/4$, and a $(64, 51)$ eBCH code with rate $R = 0.79$.

symbols and waveforms are no more separable. Therefore, even though it might be possible to further investigate this issue, there is no evidence that a simple (or, at least, a practical) solution even exists.

Chapter 4

Conditioned pilots

In modern satellite communications one of the most challenging impairments to overcome is the phase noise. A satisfactory frequency and phase synchronization is again one of the most common requirements for all kinds of practical wireless systems. Carrier synchronization is often performed through the aid of some pilot symbols periodically inserted in the transmitted data stream (e.g. DVB-S2 [1]). These topics have been studied so well during the last decades that an impressive amount of algorithms and techniques may be easily found in the literature. To gain an insight (far from being exhaustive), the reader is referred to [60]–[66] and references therein. As far as pilot symbols are concerned, their optimal position inside the data packet has been object of a thorough study in [67] where it has been shown that, under mild conditions, equally-spaced single pilots are one of the possible optimal configurations in the sense that they minimize the Cramér-Rao bound (CRB) for channel estimation. Moreover, in [62] it is shown that arranging pilots in clusters induces a substantial performance penalty on a channel with additive white Gaussian noise (AWGN) and Wiener phase noise.

For any kind of communication system, one of the merit figures that must be reckoned with during the system design process is certainly the spectral efficiency (SE). In a multi-user scenario it has been shown that for both linear [18] and continuous phase [19] modulations it is possible to increase the spectral efficiency of the

system simply giving up the orthogonality condition among users and packing them in the time and frequency domains [68]. This procedure causes known inter-symbol interference (ISI) and inter-channel interference (ICI) to arise. If the ISI, native of the channel or caused by the aforementioned technique, may be described by a high number of coefficients, the optimal detector presents an extremely high complexity since this latter grows exponentially in the size of the channel memory. In such a scenario, an effective method to reduce the complexity of the detection algorithm and maximize the information rate is the channel shortening [69]. Roughly speaking, this technique consists of optimizing the ISI coefficients assumed by the detector (and different from the actual ones) and the front-end filter with a constraint on the global complexity. The presence of ISI implies that phase and frequency synchronization must be performed through clusters of pilots. These clusters must be at least longer than the channel memory in order to force the channel state and allow the synchronization algorithm to employ at least one known observed value to perform the impairment compensation. This pilot insertion obviously induces an energy loss and a spectral efficiency degradation due to the fact that pilots do not convey information but are just necessary to properly compensate for phase and frequency impairments. Moreover, since multiple clusters distributed all over the data packet allow a more reliable estimation than concentrated pilots [67], the resulting penalties may be important.

In this Chapter, we propose a new design of the pilot symbols aiming at minimizing the overhead and guaranteeing the best performance on ISI channels. The main idea is to give up on pilot clusters and use instead equally-spaced, time-varying, data-dependent isolated pilots, allowing a dramatic reduction of the overhead and of the consequent wasted energy and bandwidth. The value assumed by each pilot is not kept constant over the whole data packet but depends on the L previous (and possibly the L following) data symbols, where L is the size of the channel memory. This dependence causes an increase in the number of possible states of the modulator and an expansion of the optimal detector trellis, but permits the receiver to observe, at sample epochs corresponding to pilots, a known value (constant over the whole transmission) that can be exploited during the synchronization for a more efficient

estimation of the carrier frequency and the phase noise. The time-variation of the trellis occurs when a pilot goes through the channel memory. Since the optimal detector for ISI channels has complexity which grows exponentially with the size of the channel memory, even when this latter is time-varying, in case of severe ISI it becomes infeasible. Reduced-complexity solutions are then to be envisaged, and in this Chapter we propose different suboptimal detectors whose definition and performance depend on the ISI model (namely those developed by Forney [70] and Ungerboeck [71]) independently adopted by the pilots and by the detector. We chose to investigate all the possible combinations of models because the classical low-complexity algorithms for ISI channels in the literature provide a satisfactory performance when the Forney observation model is adopted by the receiver (see [24] and references therein), but do not work well with the Ungerboeck model [72], [73]. On the other hand, the implementation of the whitening filter is critical in several practical scenarios [74], and for applications when the detector is designed to cope only with a portion of the existing interference, a receiver working on the matched filter output results to be more robust to the unmanaged interference [68], [69]. Therefore, the recently proposed detector based on the Ungerboeck observation model and derived in [55] and [75] is tested as well. Concerning the pilot definition, the Forney pilot model is adopted because all the estimation algorithms require samples corrupted by white noise [23]. Nevertheless, the adoption of the Forney model for pilots may entail a dangerous increase in the pilot mean squared value (MSV), which translates into an energy loss and an increase in the sensitivity to nonlinearities that cannot be avoided, as it will be shown later. Since the Ungerboeck model appears to greatly reduce this MSV increase, and since it allows to get rid of the whitening filter, we chose to develop the Ungerboeck pilot model as well. Moreover, if isolated pilots are employed, the noise samples corrupting the useful part of the sampled received signal result to be approximately uncorrelated even though the Ungerboeck pilot model is adopted, provided that the spacing between two consecutive pilots is big enough.

4.1 System model

We consider a packet transmission where each packet contains a sequence of K M-ary symbols $\{a_k\}$ and a sequence of $\lfloor K/(P-1) \rfloor$ pilots $\{b_k\}$, where $\lfloor x \rfloor$ denotes the maximum integer lower than x, which may not belong to the symbol constellation $\mathcal{A}$. A single pilot is inserted every $P-1$ information symbols. Focusing our investigation on linear modulations, the transmitted signal reads

$$s(t) = \sum_{k=-\infty}^{+\infty} (a_k + b_k)\, p(t - kT) \tag{4.1}$$

where T is the symbol period and $p(t)$ the shaping pulse (typically a root raised cosine pulse, denoted by RRC). The transmission policy is the following: when $k = mP$ with $m \in \mathbb{N}_+$, the symbol a_{mP} is fictitious and only the pilot b_{mP} is transmitted. Conversely, for all the other values of the time index k, b_k is fictitious and only the information symbol a_k is transmitted.

We consider a transmission over a channel that introduces ISI and AWGN. The ISI coefficients are assumed to be known and we also suppose that the number of these coefficients is finite. For the sake of simplicity, and in order to limit the trellis expansion (as will be explained in the following), we consider only values of P higher than the duration of the channel memory. This implies that when a pilot is transmitted, the previous pilot has already left the channel memory. In other words, two consecutive pilots never interfere on each other. In the following, we will consider different systems, differing from one another only in the ISI model adopted by pilots and by the detector.

4.1.1 Sufficient statistics

The baseband equivalent of the received signal can be viewed as

$$r(t) = \sum_{k=-\infty}^{+\infty} (a_k + b_k)\, p(t - kT) + w(t) \tag{4.2}$$

where $w(t)$ is a complex circularly-symmetric white Gaussian process with zero mean and variance $\sigma^2 = N_0$ per component. The sufficient statistics necessary for the detec-

tion can be derived simply filtering the received signal with a whitened matched filter and sampling its output at symbol periods [70]. The resulting Forney model reads

$$\begin{aligned} y_k &= x_k + w_k \\ &= \sum_{\ell=0}^{L} (a_{k-\ell} + b_{k-\ell})\, f_\ell + w_k \end{aligned} \tag{4.3}$$

where $\{f_\ell\}$ are the $L+1$ Forney ISI coefficients, $\{y_k\}$ are the Forney sufficient statistics, and $\{w_k\}$ are the uncorrelated samples of the AWGN.

A different set of sufficient statics can be obtained just replacing the whitened matched filter with a matched filter [71], and the resulting sufficient statistics $\{r_k\}$ become

$$\begin{aligned} r_k &= s_k + n_k \\ &= \sum_{\ell=-L}^{L} (a_{k-\ell} + b_{k-\ell})\, g_\ell + n_k \end{aligned} \tag{4.4}$$

where $\{n_k\}$ are samples of a complex circularly-symmetric colored Gaussian process with zero mean and autocorrelation function $R_n(m) = 2\sigma^2 g_m$. The $2L+1$ Ungerboeck ISI coefficients $\{g_\ell\}$ may be computed as

$$g_\ell = \sum_{m=0}^{L} f_m f_{m-\ell}^*$$

with $\ell \in [-L, L]$.

4.1.2 Forney pilots

If we adopt for the pilots the ISI model derived by Forney, synchronization is performed on observed samples corrupted by white noise, i.e., the sampled output of a whitened matched filter is employed. We want the useful part of the received samples to have a constant and known value $c^{(F)}$ at pilot epochs. In other words, for $k = mP$ we force the observed noiseless sample to be

$$x_{mP} = f_0 b_{mP}^{(F)} + \sum_{\ell=1}^{L} f_\ell a_{mP-\ell} = c^{(F)}$$

and therefore the pilot value may be computed by the transmitter as

$$b_{mP}^{(F)} = \frac{1}{f_0}\left(c^{(F)} - \sum_{\ell=1}^{L} f_\ell a_{mP-\ell}\right) \tag{4.5}$$

where the superscript (F or, in the next Paragraph, U) just indicates the pilot design adopted. Denoting with $\mathrm{E}\{.\}$ the expectation operator, the MSV of the information symbols is

$$\mathcal{E}_a = \mathrm{E}\left\{|a_k|^2\right\}$$

while the pilot MSV becomes

$$\mathcal{E}_b^{(F)} = \mathrm{E}\left\{\left|b_k^{(F)}\right|^2\right\} = \frac{1}{|f_0|^2}\left(\left|c^{(F)}\right|^2 + \mathcal{E}_a \sum_{\ell=1}^{L} |f_\ell|^2\right)$$

if $\mathrm{E}\{a_k\} = 0$ and the symbols are uncorrelated. The subscript F (and in the following, U) specifies the ISI representation adopted (Forney's or Ungerboeck's, respectively). In order to limit the sensitivity to amplifier nonlinearities, we choose to impose

$$\mathcal{E}_b^{(F)} = \mathcal{E}_a \tag{4.6}$$

and use $c^{(F)}$ to try to satisfy this constraint. Being the MSVs real, we have

$$\left|c^{(F)}\right|^2 = \mathcal{E}_a\left(|f_0|^2 - \sum_{\ell=1}^{L} |f_\ell|^2\right) > 0$$

which unfortunately cannot always be satisfied. In fact, it may happen that

$$|f_0|^2 < \sum_{\ell=1}^{L} |f_\ell|^2$$

especially in case of severe ISI. Moreover, it may occur that the value $|c^{(F)}|^2$ satisfying (4.6) is extremely small, namely too small to allow a correct synchronization. Hence we set a threshold—a real constant $\kappa > 0$—and impose

$$\left|c^{(F)}\right|^2 = \underset{|c^{(F)}|^2 \geq \kappa}{\arg\min} \left|\mathcal{E}_b^{(F)} - \mathcal{E}_a\right|. \tag{4.7}$$

The constant κ is chosen in order to have observed samples with enough power at pilot epoch to perform reliable estimation. Of course, a high value of κ implies that $\mathcal{E}_b^{(F)} \gg \mathcal{E}_a$, hence the peak-to-average-power ratio (PAPR) increases making the system more sensitive to the amplifier nonlinearities. Therefore, there exists a trade-off between the PAPR (or the nonlinearity sensitivity) and the synchronization accuracy.

4.1.3 Ungerboeck pilots

Adopting the Ungerboeck ISI model, synchronization is carried out by using the sampled output of a matched filter. Again we force the observed noiseless samples to be

$$s_{mP} = g_0 b_{mP}^{(U)} + \sum_{\substack{\ell=-L \\ \ell\neq 0}}^{L} g_\ell a_{mP-\ell} = c^{(U)}.$$

Hence, pilots are now defined as

$$b_{mP}^{(U)} = \frac{1}{g_0}\left(c^{(U)} - \sum_{\substack{\ell=-L \\ \ell\neq 0}}^{L} g_\ell a_{mP-\ell} \right). \tag{4.8}$$

The resulting MSV reads

$$\mathcal{E}_b^{(U)} = \frac{\mathcal{E}_a}{|g_0|^2}\left(1 + \sum_{\substack{\ell=-L \\ \ell\neq 0}}^{L} |g_\ell|^2 \right)$$

and the constraint (4.7) becomes

$$\left|c^{(U)}\right|^2 = \arg\min_{\left|c^{(U)}\right|^2 \geq \kappa} \left| \mathcal{E}_b^{(U)} - \mathcal{E}_a \right|. \tag{4.9}$$

4.1.4 Power spectral density

Since symbols and pilots are correlated, the power spectral density (PSD) of the transmitted signal is modified by this pilot design. First, we prove the cyclostationarity of

the signal (4.1) with period PT, and then we compute the PSD of a stationarized version of (4.1). In order to be cyclostationary, the signal must have periodic statistics [76]. Its mean value and a delayed version of it read

$$\eta(t) = \mathrm{E}\{s(t)\} = \sum_{k=-\infty}^{+\infty} \mathrm{E}\{a_k + b_k\}\, p(t-kT) = \sum_{k=-\infty}^{+\infty} \eta_{sp}(k) p(t-kT)$$

$$\eta(t+PT) = \mathrm{E}\{s(t+PT)\} = \sum_{k=-\infty}^{+\infty} \eta_{sp}(k+P)\, p[t-(k+P)T] \tag{4.10}$$

where

$$\eta_{sp}(k) = \begin{cases} \mathrm{E}\{a_k\} = 0 & k \neq mP \\ \mathrm{E}\{b_k\} = \dfrac{c}{h_0} & k = mP \end{cases}$$

having defined $h_0 = f_0$ if Forney pilots are used, or $h_0 = g_0$ if Ungerboeck pilots are adopted. Hence, defining $m = k + P$ and substituting it in (4.10), $\eta(t)$ results to be periodic of period PT.

The autocorrelation function of the process $s(t)$ is defined as

$$\begin{aligned} R(t,\alpha) &= \mathrm{E}\{s(t+\alpha)s^*(t)\} \\ &= \sum_{k=-\infty}^{+\infty} \sum_{m=-\infty}^{+\infty} \mathrm{E}\{(a_k + b_k)(a_m + b_m)^*\}\, p(t+\alpha-kT)\, p^*(t-mT) \\ &= \sum_{k=-\infty}^{+\infty} \sum_{\ell=-\infty}^{+\infty} R_{sp}(k,\ell)\, p(t+\alpha-kT)\, p^*(t-kT+\ell T) \end{aligned}$$

where $\ell = k - m$. Since the delayed version of the autocorrelation function reads

$$R(t+PT,\alpha) = \sum_{k,\ell=-\infty}^{+\infty} R_{sp}(k-P,\ell)\, p[t+\alpha-(k-P)T]\, p^*[t-(k-\ell-P)T]$$

defining $n = k - P$ and substituting it in the last equation, we find that also the autocorrelation function is periodic in t with period PT. Hence, the signal $s(t)$ is a cyclostationary random process and must be stationarized. To this purpose, we introduce a random delay τ uniformly distributed in $[0, PT)$ and define the delayed signal

$$\overline{s}(t) = s(t-\tau)$$

whose mean value is

$$\begin{aligned}\bar{\eta}(t) &= \mathrm{E}\{\bar{s}(t)\} = \mathrm{E}\{s(t-\tau)\} \\ &= \sum_{k=-\infty}^{+\infty} \mathrm{E}_{a,b,n}\{a_{k-n}+b_{k-n}\}\,\mathrm{E}_{\tau}\{p(t-kT-\tau)\}\end{aligned}$$

where $n = \lfloor \tau/T \rfloor$ is a discrete random variable (RV) uniformly distributed in $[0, P-1]$. We can compute the first expectation with respect to n and the second with respect to τ, obtaining

$$\bar{\eta}(t) = \sum_{k=-\infty}^{+\infty} \left(\frac{1}{P} \sum_{n=0}^{P-1} \mathrm{E}_{a,b}\{a_{k-n}+b_{k-n}\} \right) \frac{1}{PT} \int_{-PT/2}^{PT/2} p(t-kT-\tau)\,\mathrm{d}\tau .$$

Noticing that

$$\bar{\eta}_{sp} = \frac{1}{P} \sum_{n=0}^{P-1} \mathrm{E}_{a,b}\{a_{k-n}+b_{k-n}\}$$

is independent of k and decomposing the delay as $\tau = \mu T + \xi$ where μ is a discrete RV uniformly distributed in $[-\lfloor (P-1)/2 \rfloor, \lfloor (P-1)/2 \rfloor]$ and ξ is a continuous RV uniformly distributed in $[-T/2, T/2)$, it is possible to split the integral in the sum of P integrals, leading to

$$\begin{aligned}\bar{\eta}(t) &= \frac{\bar{\eta}_{sp}}{PT} \sum_{k=-\infty}^{+\infty} \sum_{\mu=-\lfloor \frac{P-1}{2} \rfloor}^{\lfloor \frac{P-1}{2} \rfloor} \int_{t-kT-2\mu T-T/2}^{t-kT-2\mu T+T/2} p(\alpha)\mathrm{d}\alpha \\ &= \frac{\bar{\eta}_{sp}}{T} \int_{-\infty}^{+\infty} p(\alpha)\mathrm{d}\alpha = \bar{\eta}\end{aligned}$$

where we exploited the fact that all the intervals of integration are disjoint and $\alpha = t - kT - \mu T - \xi$. Finally, we find that the mean value of the stationarized signal is independent of time, as expected.

A similar approach is to be considered for the autocorrelation function, yielding

$$\begin{aligned}\bar{R}(t,\alpha) &= \mathrm{E}\{s(t-\tau+\alpha)s^*(t-\tau)\} \\ &= \sum_{k,m=-\infty}^{+\infty} \mathrm{E}_{a,b,n}\{(a_{k-n}+b_{k-n})(a^*_{m-n}+b^*_{m-n})\}\mathrm{E}_\tau\{p(t-kT-\tau+\alpha)p^*(t-mT-\tau)\} \\ &= \sum_{k,\ell=-\infty}^{+\infty}\left[\frac{1}{P}\sum_{n=0}^{P-1}R_{sp}(k-n,\ell)\right]\left[\frac{1}{PT}\int_{-PT/2}^{PT/2} p(t-kT-\tau+\alpha)\,p^*(t-kT+\ell T-\tau)\,\mathrm{d}\tau\right] \\ &= \sum_{\ell=-\infty}^{+\infty}\bar{R}_{sp}(\ell)\frac{1}{PT}\sum_{k=-\infty}^{+\infty}\sum_{\mu=-\lfloor\frac{P-1}{2}\rfloor}^{\lfloor\frac{P-1}{2}\rfloor}\int_A^B p(\beta+\alpha-\ell T)p^*(\beta)\mathrm{d}\beta\end{aligned}$$

where the delay has been decomposed as $\tau = \mu T + \xi$ and we have defined

$$\begin{aligned}\beta &= t-(k+\mu-\ell)T-\xi \\ A &= t-(k+2\mu-\ell)T-\frac{T}{2} \\ B &= t-(k+2\mu-\ell)T+\frac{T}{2}\end{aligned}$$

and

$$\bar{R}_{sp}(\ell) = \frac{1}{P}\sum_{n=0}^{P-1}R_{sp}(k-n,\ell)\,. \tag{4.11}$$

Since all the intervals of integration are disjoint, it is possible to write

$$\begin{aligned}\bar{R}(t,\alpha) &= \frac{1}{T}\sum_{\ell=-\infty}^{+\infty}\bar{R}_{sp}(\ell)\int_{-\infty}^{+\infty}p(\beta+\alpha-\ell T)p^*(\beta)\mathrm{d}\beta \\ &= \bar{R}(\alpha)\end{aligned} \tag{4.12}$$

that is independent of the time epoch. Now the PSD of the signal can be easily obtained just Fourier-transforming (4.12), and the result is

$$W(f) = \frac{1}{T}|P(f)|^2 S(f)$$

that is extremely similar to the classic PSD of a pulse amplitude modulated (PAM) signal [76] (where $P(f)$ is the spectrum of the shaping pulse), the only difference being the PSD $S(f)$ defined as the discrete Fourier transform of (4.11).

Hence, for Forney pilots (4.11) becomes

$$\overline{R}_{sp}^{(F)}(\ell) = \frac{1}{P}\left(\mathcal{E}_b^{(F)} + (P-1)\mathcal{E}_a\right)\delta[\ell] - \frac{\mathcal{E}_a}{P}\sum_{k=1}^{L}\left(\frac{f_k}{f_0}\delta[k-\ell] + \frac{f_k^*}{f_0^*}\delta[k+\ell]\right)$$

where $\delta[\ell]$ denotes the Kronecker delta, and the corresponding PSD results to be

$$\begin{aligned} S^{(F)}(f) &= \mathcal{F}\left\{\overline{R}_{sp}^{(F)}(\ell)\right\} \\ &= \frac{1}{P}\left(\mathcal{E}_b^{(F)} + (P-1)\mathcal{E}_a\right) - \frac{2\mathcal{E}_a}{P}\sum_{\ell=1}^{L}\Re\left\{\frac{f_\ell}{f_0}\right\}\cos(2\pi f \ell T) \end{aligned}$$

where $\Re\{.\}$ is the real part operator. If we define

$$\mathcal{E}_P = \int_{-\infty}^{+\infty} |P(f)|^2 \,\mathrm{d}f$$

the mean energy per transmitted symbol reads

$$\begin{aligned} E_s^{(F)} &= T\int_{-\infty}^{+\infty} W(f)\mathrm{d}f \\ &= \frac{\mathcal{E}_P}{P}\left[\mathcal{E}_b^{(F)} + (P-1)\mathcal{E}_a\right] - \frac{2\mathcal{E}_a}{P}\sum_{\ell=1}^{L}\Re\left\{\frac{f_\ell}{f_0}\right\}\int_{-\infty}^{+\infty}|P(f)|^2\cos(2\pi f\ell T)\,\mathrm{d}f\,. \end{aligned}$$

In order to compute this integral, we need the analytical expression of the shaping pulse spectrum. After a few algebra, we obtain that the mean energy per symbol for the RRC pulse is

$$E_{s,RRC}^{(F)} = \frac{\mathcal{E}_P}{P}\left(\mathcal{E}_b^{(F)} + (P-1)\mathcal{E}_a\right).$$

When Ungerboeck pilots are employed, the averaged autocorrelation of symbols and pilots in (4.11) reads

$$\overline{R}_{sp}^{(U)}(\ell) = \frac{1}{P}\left(\mathcal{E}_b^{(U)} + (P-1)\mathcal{E}_a\right)\delta[\ell] - \frac{2\mathcal{E}_a}{P}\sum_{\substack{k=-L\\k\neq 0}}^{L}\Re\left\{\frac{g_k}{g_0}\right\}\delta[k-\ell]$$

and the corresponding PSD becomes

$$S^{(U)}(f) = \frac{1}{P}\left(\mathcal{E}_b^{(U)} + (P-1)\mathcal{E}_a\right) - \frac{4\mathcal{E}_a}{P}\sum_{\ell=1}^{L}\Re\left\{\frac{g_\ell}{g_0}\right\}\cos(2\pi f\ell T)\,.$$

Finally, the mean energy per transmitted symbol is

$$E_s^{(U)} = T \int_{-\infty}^{+\infty} W_s(f)\mathrm{d}f$$
$$= \frac{\mathcal{E}_P}{P}\left(\mathcal{E}_b^{(U)} + (P-1)\mathcal{E}_a\right) - \frac{4\mathcal{E}_a}{P}\sum_{\ell=1}^{L}\Re\left\{\frac{g_\ell}{g_0}\right\}\int_{-\infty}^{+\infty}|P(f)|^2\cos(2\pi f\ell T)\,\mathrm{d}f\,.$$

With the same calculations done before, we obtain the mean energy per symbol for the RRC pulse

$$E_{s,RRC}^{(U)} = \frac{\mathcal{E}_P}{P}\left(\mathcal{E}_b^{(U)} + (P-1)\mathcal{E}_a\right).$$

4.2 Optimal algorithms on expanded trellis

The optimal maximum a posteriori probability (MAP) symbol detector is the classic Bahl-Cocke-Jelinek-Raviv (BCJR) algorithm [6] whose trellis and metrics depend on the adopted type of pilots and on the ISI model assumed by the receiver. In the following, we denote by $\mathbf{a} = (a_0, \ldots, a_{K-1})^T$ the vector of the data symbols, and similarly by $\boldsymbol{\sigma}$ and $\mathbf{r}$ the vectors of states and received samples, respectively. By $p(.)$ we denote the probability density function (PDF) of a continuous random variable (RV), while by $P(.)$ we denote the probability mass function (PMF) of a discrete RV. As it will be clear later, since the state definition is not straightforward, we start this algorithm derivation with some preliminary results. The optimal MAP symbol strategy is

$$\hat{a}_k = \underset{a_k}{\operatorname{argmax}}\{P(a_k|\mathbf{r})\} \tag{4.13}$$

where $P(a_k|\mathbf{r})$ may be evaluated marginalizing the joint PMF $P(\mathbf{a}|\mathbf{r})$. This latter can be obtained as follows:

$$P(\mathbf{a}|\mathbf{r}) \propto p(\mathbf{r}|\mathbf{a})P(\mathbf{a})$$

where $\propto$ denotes a proportionality relation, and each term can be factored as

$$P(\mathbf{a}) = \prod_{k=0}^{K-1} P(a_k)$$
$$p(\mathbf{r}|\mathbf{a}) = \prod_{k=0}^{K-1} p(r_k|\mathbf{a}) \propto \prod_{k=0}^{K-1} H_k(\mathbf{a}) \,. \tag{4.14}$$

Vector $\mathbf{r}$ contains the output samples $\{r_k\}$ of the matched filter if the Ungerboeck ISI model (4.4) is adopted. Otherwise, if the ISI model employed is the Forney's one, then it contains the output samples $\{y_k\}$ of the whitened matched filter (4.3). In other words, the factorization (4.14) is independent of the ISI model adopted by the receiver.

In order to correctly define the state, we have to examine factors $\{H_k(\mathbf{a})\}$ and consider separately Forney and Ungerboeck pilots. So as to avoid misunderstandings, we define $H_k(\mathbf{a}) = H_k^{(F)}(\mathbf{a})$ if Forney pilots are used, and $H_k(\mathbf{a}) = H_k^{(U)}(\mathbf{a})$ if Ungerboeck pilots are employed. The superscript is introduced only to point out the adopted pilot design. As done in the previous Section, the subscript F (respectively, U) specifies that the ISI representation adopted by the receiver is that derived by Forney (respectively, by Ungerboeck).

4.2.1 Forney pilots

Since the expression for factors $\{H_k^{(F)}(\mathbf{a})\}$ depends on the ISI model employed by the receiver, we consider separately the two cases.

Forney pilots with Ungerboeck detection

The system with Forney pilots and Ungerboeck detection can be represented by the block diagram in Fig. 4.1. The sufficient statistics needed for the detection are extracted from the received signal by means of a matched filter [71], whose output is (4.4).

As stated before, we define $H_k(\mathbf{a}) = H_{U,k}^{(F)}(\mathbf{a})$. The general expression for factors

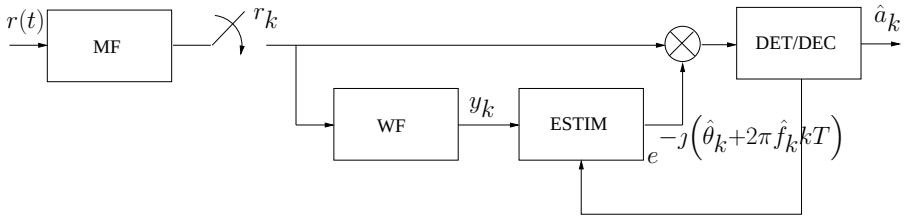

Figure 4.1: Block scheme for a system using Forney pilots and Ungerboeck detection.

$\{H_k^{(F)}(\mathbf{a})\}$ using the Ungerboeck model is [28]

$$H_{U,k}^{(F)}(\mathbf{a}) = \exp\left\{\frac{1}{\sigma^2}\Re\left[r_k\left(a_k^*+b_k^{(F)*}\right)-\frac{1}{2}g_0\left|a_k+b_k^{(F)}\right|^2-\sum_{\ell=1}^{L}g_\ell\left(a_k^*+b_k^{(F)*}\right)\left(a_{k-\ell}+b_{k-\ell}^{(F)}\right)\right]\right\}. \tag{4.15}$$

When $k = mP + j$, with $j \in [L+1, P-1]$, there are no pilots, neither transmitted nor in the channel memory. Therefore $H_{U,k}^{(F)}(\mathbf{a})$ may be reduced to the classical expression [77]

$$H_{U,k}^{(F)}(\mathbf{a}) = \exp\left\{\frac{1}{\sigma^2}\Re\left[r_k a_k^* - \frac{1}{2}g_0|a_k|^2 - \sum_{\ell=1}^{L}g_\ell a_k^* a_{k-\ell}\right]\right\}. \tag{4.16}$$

Now it is possible to correctly define the state as $\sigma_{U,k}^{(F)} = (a_{k-1}, \ldots, a_{k-L})$, i.e., the set of past symbols needed for the computation of $H_{U,k}^{(F)}(\mathbf{a})$. It is worth noting that, when $j \in [L+1, P-1]$, the factor $H_{U,k}^{(F)}(\mathbf{a})$ and the state coincide with the classical metric [77] and state [8] of the BCJR for ISI channels, and the number of possible states is M^L. When $j = 0$, a pilot is transmitted and $H_{U,mP}^{(F)}(\mathbf{a})$ may be evaluated simply by computing the pilot value as in (4.5) and by substituting this value in (4.15), obtaining

$$H_{U,mP}^{(F)}(\mathbf{a}) = \exp\left\{\frac{1}{\sigma^2}\Re\left[r_{mP}b_{mP}^{(F)*} - \frac{1}{2}g_0\left|b_{mP}^{(F)}\right|^2 - \sum_{\ell=1}^{L}g_\ell b_{mP}^{(F)*}a_{mP-\ell}\right]\right\}. \tag{4.17}$$

Again, the state is $\sigma_{U,mP}^{(F)} = (a_{mP-1}, \ldots, a_{mP-L})$ and the cardinality of the state set is still M^L, which implies that no trellis expansion occurs. Finally, when $j \in [1, L]$, a pilot is present in the channel memory and factor $H_{U,k}^{(F)}(\mathbf{a})$ may be written by substituting

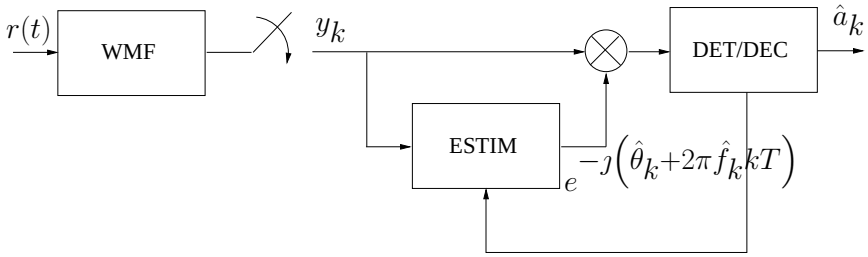

Figure 4.2: Block scheme of a system using Forney model for both pilots and detection.

(4.5) in the corresponding term in (4.15), yielding

$$H_{U,k}^{(F)}(\mathbf{a}) = \exp\left\{\frac{1}{\sigma^2}\Re\left[r_k a_k^* - \frac{1}{2}g_0|a_k|^2 - \sum_{\substack{\ell=1\\ \ell\neq j}}^{L} g_\ell a_k^* a_{k-\ell} - g_j a_k^* b_{mP}^{(F)}\right]\right\}$$
$$= \exp\left\{\frac{1}{\sigma^2}\Re\left[\left(r_k - g_j\frac{c^{(F)}}{f_0}\right)a_k^* - \frac{1}{2}g_0|a_k|^2 + \frac{g_j}{f_0}\sum_{\ell=1}^{L} f_\ell a_k^* a_{mP-\ell} - \sum_{\substack{\ell=1\\ \ell\neq j}}^{L} g_\ell a_k^* a_{k-\ell}\right]\right\}. \tag{4.18}$$

Now the state must be defined as $\sigma_{U,k}^{(F)} = (a_{k-1},\ldots,a_{mP+1},a_{mP-1},\ldots a_{mP-L})$. Since it includes a higher number of past symbols, the cardinality of the state set grows up to M^{L+j-1}, entailing a trellis expansion. □

Forney pilots with Forney detection

This system is described in Fig. 4.2. The sufficient statistics needed for detection can now be extracted by the received signal by means of a whitened matched filter (or a matched filter followed by a whitening filter), whose sampled output is (4.3). Defining $H_k(\mathbf{a}) = H_{F,k}^{(F)}(\mathbf{a})$, the general expression for factor $H_{F,k}^{(F)}(\mathbf{a})$ is

$$H_{F,k}^{(F)}(\mathbf{a}) = \exp\left\{-\frac{1}{2\sigma^2}\left|y_k - \sum_{\ell=0}^{L}\left(a_{k-\ell} + b_{k-\ell}^{(F)}\right)f_\ell\right|^2\right\}. \tag{4.19}$$

When $k = mP + j$, with $j \in [L+1, P-1]$, there are no pilots, neither transmitted nor in the channel memory, and factor $H_{F,k}^{(F)}(\mathbf{a})$ reduces to the classical expression [70]

$$H_{F,k}^{(F)}(\mathbf{a}) = \exp\left\{-\frac{1}{2\sigma^2}\left|y_k - \sum_{\ell=0}^{L} a_{k-\ell} f_\ell\right|^2\right\}. \tag{4.20}$$

As in the previous case, we can define the state as $\sigma_{F,k}^{(F)} = (a_{k-1}, \ldots, a_{k-L})$. When $j = 0$, since the noiseless observed value is $x_{mP} = c^{(F)}$, $H_{F,mP}^{(F)}(\mathbf{a})$ is constant and independent of $\mathbf{a}$

$$H_{F,mP}^{(F)}(\mathbf{a}) = \exp\left\{-\frac{1}{2\sigma^2}\left|y_{mP} - c^{(F)}\right|^2\right\}. \tag{4.21}$$

Therefore, apparently there is no need to define the state. Actually, we have to propagate the L previous symbols because they will be employed in the following L evaluations of $H_{F,k}^{(F)}(\mathbf{a})$, as will be clear later. Hence, we define the state as $\sigma_{F,mP}^{(F)} = (a_{mP-1}, \ldots, a_{mP-L})$. Finally, when $j \in [1, L]$, a pilot is present in the channel memory and therefore a trellis expansion occurs. Factor $H_{F,k}^{(F)}(\mathbf{a})$ can be obtained by combining (4.5) and (4.19), that yields

$$H_{F,k}^{(F)}(\mathbf{a}) = \exp\left\{-\frac{1}{2\sigma^2}\left|y_k - \sum_{\substack{\ell=0 \\ \ell\neq j}}^{L} a_{k-\ell} f_\ell - \frac{f_j}{f_0}\left(c^{(F)} - \sum_{i=1}^{L} f_i a_{mP-i}\right)\right|^2\right\}. \tag{4.22}$$

Therefore, we can define the state as $\sigma_{F,k}^{(F)} = (a_{k-1}, \ldots, a_{mP+1}, a_{mP-1}, \ldots, a_{mP-L})$. □

Having properly defined the state for every discrete-time k in both cases, it appears that $\sigma_{F,k}^{(F)} = \sigma_{U,k}^{(F)}$ for every k, i.e., the state definition is independent of the ISI model adopted by the receiver. Hence, we define $\sigma_k^{(F)} = \sigma_{F,k}^{(F)} = \sigma_{U,k}^{(F)}$ and we can now safely replace the vector $\mathbf{a}$ in the left hand side of (4.16), (4.17), (4.18), (4.20), (4.21), and (4.22) with the couple $(a_k, \sigma_k^{(F)})$. This can be done because not all the symbols in vector $\mathbf{a}$ are used in the computation of factors $\{H_k^{(F)}\}$. Namely, only a subset of $\mathbf{a}$ is relevant, and this subset is composed by the present symbol a_k and some past symbols (whose number depends on the discrete-time k) grouped in the state $\sigma_k^{(F)}$. Hence, factors $\{H_k^{(F)}\}$ result to be proportional to another conditional probability, equivalent to $p(r_k|\mathbf{a})$, that is

$$H_k^{(F)}(a_k, \sigma_k^{(F)}) \propto p(r_k|a_k, \sigma_k^{(F)})$$

which leads to

$$\prod_{k=0}^{K-1} H_k^{(F)}(a_k, \sigma_k^{(F)}) \propto \prod_{k=0}^{K-1} p(r_k|a_k, \sigma_k^{(F)}) = \prod_{k=0}^{K-1} p(r_k|\mathbf{a}, \boldsymbol{\sigma}^{(F)}) = p(\mathbf{r}|\mathbf{a}, \boldsymbol{\sigma}^{(F)}).$$

The usefulness of this result will be clear later. Obviously, since $\sigma_{F,k}^{(F)} = \sigma_{U,k}^{(F)}$, all the considerations done on the dimension of the state set and the trellis expansion hold unchanged also in the case of Forney detection.

4.2.2 Ungerboeck pilots

A trivial adaptation of the previous derivation to the case of Ungerboeck pilots entails the replacement of the pilot definition (4.5) with (4.8) in (4.15) and (4.19), yielding to

$$H_{U,k}^{(U)}(a_k, \sigma_k^{(F)}) = \exp\left\{\frac{1}{\sigma^2}\Re\left[r_k\left(a_k^* + b_k^{(U)*}\right) - \frac{1}{2}g_0\left|a_k + b_k^{(U)}\right|^2\right]\right\} \cdot$$

$$\cdot = \exp\left\{-\frac{1}{\sigma^2}\Re\left[\sum_{\ell=1}^{L} g_\ell\left(a_k^* + b_k^{(U)*}\right)\left(a_{k-\ell} + b_{k-\ell}^{(U)}\right)\right]\right\} \tag{4.23}$$

$$H_{F,k}^{(U)}(a_k, \sigma_k^{(F)}) = \exp\left\{-\frac{1}{2\sigma^2}\left|y_k - \sum_{\ell=0}^{L}\left(a_{k-\ell} + b_{k-\ell}^{(U)}\right) f_\ell\right|^2\right\} \tag{4.24}$$

where the state definitions obtained in the previous analysis have been kept. Unfortunately, the present symbol a_k and the present state $\sigma_k^{(F)}$ are not sufficient for the evaluation of (4.23) and (4.24). In fact, (4.8) prevents the calculation of the pilot value since the future symbols $a_{mP+1}, \ldots, a_{mP+L}$ are needed. Hence, if we straightforwardly extend the previous analysis to the case of Ungerboeck pilots, we find that the computation of factors $\{H_k^{(U)}(\mathbf{a})\}$ is impossible. This implies that the state $\sigma_k^{(F)}$ is no more correctly defined and a new derivation is needed. Fortunately, we just need to step backward and a simple trick will sort things out.

From the last term of the factorization (4.14) and the general expressions (4.15) and (4.19), we have that

$$p(\mathbf{r}|\mathbf{a}) \propto \prod_{k=0}^{K-1} H_k^{(F)}(\mathbf{a}). \tag{4.25}$$

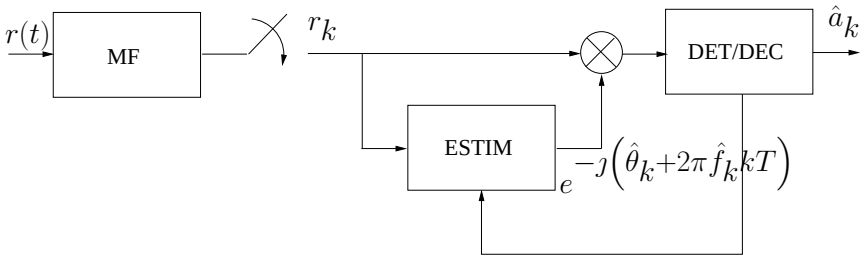

Figure 4.3: Block scheme of a system using Ungerboek model for both pilots and detection.

Since we need to know all symbols $a_{mP-L},\ldots,a_{mP+L}$ to compute the pilot value $b_{mP}^{(U)}$ according to (4.8), we just replace $b_{mP}^{(F)}$ with $b_{mP}^{(U)}$ in (4.25) (as we did in the trivial adaptation previously tried) and delay the computation of all the terms in (4.25) depending on $b_{mP}^{(U)}$. These terms, instead of being evaluated when $k = mP + j$, with $j \in [0, L]$, will be computed when all symbols $a_{mP-L},\ldots,a_{mP+L}$ are past, that is when $j = L + 1$. The total PDF $p(\mathbf{r}|\mathbf{a})$ is unchanged (except for the substitution of $b_{mP}^{(F)}$ with $b_{mP}^{(U)}$) and no approximation has been done. In other words, we rearrange the terms in (4.25) obtaining new factors $\{H_k^{(U)}(\mathbf{a})\}$ such that

$$p(\mathbf{r}|\mathbf{a}) \propto \prod_{k=0}^{K-1} H_k^{(F)}(\mathbf{a}) = \prod_{k=0}^{K-1} H_k^{(U)}(\mathbf{a})$$

where all terms depending on pilot $b_{mP}^{(U)}$ are included in factor $H_{mP+L+1}^{(U)}(\mathbf{a})$.

Now we proceed as before by analyzing separately the cases of Forney and Ungerboeck detection.

Ungerboeck pilots with Ungerboeck detection

This system is depicted in Fig. 4.3. The received samples are still in the form 4.4. Hence the MAP symbol detection strategy in (4.13) and the factorization in (4.14) hold unmodified, the only difference with respect to the previous cases being factor $H_k(\mathbf{a}) = H_{U,k}^{(U)}(\mathbf{a})$.

When $j \in [L+2, P-1]$, factor $H_{U,k}^{(U)}(\mathbf{a})$ reads

$$H_{U,k}^{(U)}(\mathbf{a}) = \exp\left\{\frac{1}{\sigma^2}\Re\left[r_k a_k^* - \frac{1}{2}|a_k|^2 g_0 - \sum_{\ell=1}^{L} a_k^* a_{k-\ell} g_\ell\right]\right\}$$

and the state can be defined as $\sigma_{U,k}^{(U)} = (a_{k-1}, \dots a_{k-L})$ as with Forney pilots. When $j \in [1, L]$, we define the new factor $H_{U,k}^{(U)}(\mathbf{a})$ as

$$H_{U,k}^{(U)}(\mathbf{a}) = \exp\left\{\frac{1}{\sigma^2}\Re\left[r_k a_k^* - \frac{1}{2}|a_k|^2 g_0 - \sum_{\substack{\ell=1 \\ \ell \neq j}}^{L} a_k^* a_{k-\ell} g_\ell\right]\right\} \tag{4.26}$$

and the state as $\sigma_{U,k}^{(U)} = (a_{k-1}, \dots, a_{mP+1}, a_{mP-1}, \dots a_{mP-L})$. It is worth noting that symbols older than a_{k-L} are not directly used in (4.26), anyway they are present in the state since they must be propagated until time $k = mP + L + 1$, when they will be properly employed to evaluate the pilot value. When $j = 0$, there is no term in (4.15) that can be computed, therefore $H_{U,mP}^{(U)}(\mathbf{a}) = 1$. However, we still need to define the state as $\sigma_{U,mP}^{(U)} = (a_{mP-1}, \dots, a_{mP-L})$ to propagate the L previous symbols. Finally, when $j = L + 1$, we can consider all previously neglected terms. Therefore, factor $H_{U,mP+L+1}^{(U)}(\mathbf{a})$ becomes

$$\begin{aligned} H_{U,mP+L+1}^{(U)}(\mathbf{a}) = &\exp\left\{\frac{1}{\sigma^2}\Re\left[r_{mP+L+1} a_{mP+L+1}^* - \frac{1}{2}|a_{mP+L+1}|^2 g_0\right]\right\} \cdot \\ &\cdot \exp\left\{-\frac{1}{\sigma^2}\Re\left[\sum_{\ell=1}^{L} a_{mP+L+1}^* a_{mP+L+1-\ell} g_\ell\right]\right\} \cdot \\ &\cdot \exp\left\{\frac{1}{\sigma^2}\Re\left[r_{mP} b_{mP}^{(U)*} - \frac{1}{2}\left|b_{mP}^{(U)}\right|^2 g_0 - \sum_{\substack{\ell=-L \\ \ell \neq 0}}^{L} b_{mP}^{(U)*} a_{mP-\ell} g_\ell\right]\right\} \end{aligned} \tag{4.27}$$

and the state may be defined as $\sigma_{U,mP+L+1}^{(U)} = (a_{mP+L}, \dots, a_{mP+1}, a_{mP-1}, \dots a_{mP-L})$. The propagation of symbols $a_{mP+j-1-L}, \dots, a_{mP-L}$ (respectively, symbols $a_{mP-1}, \dots, a_{mP-L}$) is necessary when $j \in [1, L]$ (respectively, when $j = 0$) in order to be able to compute $H_{U,mP+L+1}^{(U)}$ in (4.27). If states $\sigma_{U,k}^{(U)}$ were defined, when $j \in [0, L]$, taking in account only the symbols effectively necessary for the computation of $H_{U,k}^{(U)}(\mathbf{a})$, i.e.,

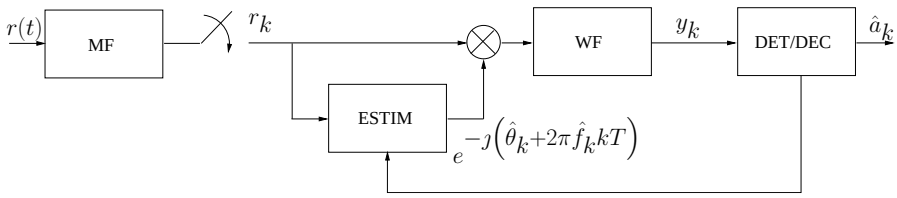

Figure 4.4: Block scheme for a system with Ungerboek pilots and Forney detection.

if they were defined as $\sigma_{U,k}^{(U)} = (a_{k-1}, \ldots, a_{mP+1}, a_{mP-1}, \ldots a_{k-L})$, when $j \in [1, L]$, and $\sigma_{U,mP}^{(U)} = 0$, when $j = 0$, then we would lose track of symbols $a_{k-L-1}, \ldots, a_{mP-L}$ (respectively, $a_{mP-1}, \ldots, a_{mP-L}$) when $j \in [1, L]$ (respectively, when $j = 0$). This loss would prevent the computation of $H_{U,mP+L+1}^{(U)}$ since we would not be able to evaluate the last factor in (4.27).

Concerning the trellis dimension, it can be easily seen that when $j = 0$ and $j \in [L+2, P-1]$ the number of possible states is still M^L, i.e., no expansion occurs. Again, when $j \in [1, L+1]$ the number of possible states is M^{L+j-1}. With respect to the case of Forney pilots, the trellis is exactly the same except for $j = L+1$, when the cardinality of the state set is M^{2L} (for Ungerboeck pilots) instead of M^L (for Forney pilots). □

Ungerboeck pilots with Forney detection

This system is represented in Fig. 4.4. The received samples are now in the form (4.3), and the MAP symbol detection strategy in (4.13) and the factorization in (4.14) still hold. The only difference, with respect to the Forney pilots case, is factor $H_k(\mathbf{a})$ that now is $H_k(\mathbf{a}) = H_{F,k}^{(U)}(\mathbf{a})$. Since

$$|x+y|^2 = |x|^2 + |y|^2 + 2\Re\{xy^*\}$$

the new factor $H_{F,k}^{(U)}(\mathbf{a})$ for symbol epoch k results to be

$$H_{F,k}^{(U)}(\mathbf{a}) = \exp\left\{-\frac{1}{2\sigma^2}\left|y_k - \sum_{\substack{\ell=0 \\ \ell \neq j}}^{L} a_{k-\ell} f_\ell\right|^2\right\}$$

for $k = mP + j$, with $j \in [0, L]$. Therefore, the state $\sigma_{F,k}^{(U)} = (a_{k-1}, \ldots, a_{mP+1}, a_{mP-1}, \ldots a_{mP-L})$ may be defined. As in the case of Ungerboeck detection, symbols older than a_{k-L} are not used in $H_{F,k}^{(U)}(\mathbf{a})$. Nevertheless, the propagation of these symbols is necessary since they will be employed at discrete-time $k = mP + L + 1$. It is worth noting that now we have a non constant factor $H_{F,k}^{(U)}(\mathbf{a})$ also when $j = 0$, since at pilot epoch a perfect ISI cancellation is no more possible. When $j \in [L+2, P-1]$ the "classic" expression holds, that is

$$H_{F,k}^{(U)}(\mathbf{a}) = \exp\left\{-\frac{1}{2\sigma^2}\left|y_k - \sum_{\ell=0}^{L} a_{k-\ell} f_\ell\right|^2\right\}$$

and the state is simply $\sigma_{F,k}^{(U)} = (a_{k-1}, \ldots, a_{k-L})$. Finally, when $j = L+1$, $H_{F,mP+L+1}^{(U)}(\mathbf{a})$ includes all terms neglected before, becoming

$$H_{F,mP+L+1}^{(U)}(\mathbf{a}) = \exp\left\{-\frac{1}{2\sigma^2}\left|y_{mP+L+1} - \sum_{\ell=0}^{L} a_{mP+L+1-\ell} f_\ell\right|^2\right\} \cdot$$
$$\cdot \exp\left\{-\frac{1}{2\sigma^2}\sum_{i=0}^{L}\left(\left|f_i b_{mP}^{(U)}\right|^2 - 2\Re\left[\left(y_{mP+i} - \sum_{\substack{\ell=0 \\ \ell\neq i}}^{L} a_{mP+i-\ell} f_\ell\right) f_i^* b_{mP}^{(U)*}\right]\right)\right\}$$

where $b_{mP}^{(U)}$ is computed according to (4.8). The state can be defined as $\sigma_{F,mP+L+1}^{(U)} = (a_{mP+L}, \ldots, a_{mP+1}, a_{mP-1}, \ldots a_{mP-L})$. □

Since the states $\sigma_{F,k}^{(U)}$ and $\sigma_{U,k}^{(U)}$ coincide for every k, we can now remove the dependence of the state on the ISI model adopted by the receiver defining $\sigma_k^{(U)} = \sigma_{F,k}^{(U)} = \sigma_{U,k}^{(U)}$. Moreover, all the considerations done on the trellis variation and the state set dimension for the system with Ungerboeck pilots and Ungerboeck detection hold unmodified also when Forney detection is used. Hence, we can now replace the symbol vector $\mathbf{a}$ in all factors $\{H_k^{(U)}(\mathbf{a})\}$ derived for Ungerboeck pilots with the couple $(a_k, \sigma_k^{(U)})$. As previously done with Forney pilots, we can introduce a conditional PDF $p(r_k|a_k, \sigma_k^{(U)})$, equivalent to $p(r_k|\mathbf{a})$, such that

$$H_k^{(U)}(a_k, \sigma_k^{(U)}) \propto p(r_k|a_k, \sigma_k^{(U)})$$

which leads to

$$\prod_{k=0}^{K-1} H_k^{(U)}(a_k, \sigma_k^{(U)}) \propto \prod_{k=0}^{K-1} p(r_k|a_k, \sigma_k^{(U)}) = \prod_{k=0}^{K-1} p(r_k|\mathbf{a}, \boldsymbol{\sigma}^{(U)}) = p(\mathbf{r}|\mathbf{a}, \boldsymbol{\sigma}^{(U)}).$$

4.2.3 Factor graph representation

We define the generic state $\sigma_k = \sigma_k^{(F)}$ if Forney pilots are used, and $\sigma_k = \sigma_k^{(U)}$ if Ungerboeck pilots are employed. Since the a posteriori probability $P(a_k|\mathbf{r})$ needed for the MAP strategy in (4.13) can be obtained also marginalizing the joint PMF $P(\mathbf{a}, \boldsymbol{\sigma}|\mathbf{r})$, we choose to use the following factorization

$$P(\mathbf{a}, \boldsymbol{\sigma}|\mathbf{r}) \propto p(\mathbf{r}|\mathbf{a}, \boldsymbol{\sigma}) P(\boldsymbol{\sigma}|\mathbf{a}) P(\mathbf{a})$$

where each term can be further factored as

$$\begin{aligned} P(\mathbf{a}) &= \prod_{k=0}^{K-1} P(a_k) \\ P(\boldsymbol{\sigma}|\mathbf{a}) &= P(\sigma_0) \prod_{k=1}^{K-1} P(\sigma_k|\sigma_{k-1}, a_{k-1}) = P(\sigma_0) \prod_{k=1}^{K-1} I(\sigma_k, \sigma_{k-1}, a_{k-1}) \\ p(\mathbf{r}|\mathbf{a}, \boldsymbol{\sigma}) &= \prod_{k=0}^{K-1} p(r_k|a_k, \sigma_k) \propto \prod_{k=0}^{K-1} H_k(a_k, \sigma_k) \end{aligned} \tag{4.28}$$

being $I(.)$ an indicator function equal to one when σ_k, σ_{k-1}, and a_{k-1} satisfy the trellis constraint, and equal to zero otherwise. From (4.28) it is possible to derive the factor graph, presented in Fig. 4.5, and almost coinciding with the Wiberg graph of the classical BCJR algorithm [8], the only difference being the absence of the variable node corresponding to the symbol transmitted at pilot epochs. Applying the SPA to the FG in Fig. 4.5, we will be able to compute the marginal APPs needed for the MAP strategy in (4.13). In Fig. 4.5 we denote

$$G_k = G_k(a_k, \sigma_k, \sigma_{k-1}) = H_k(a_k, \sigma_k) I(\sigma_k, \sigma_{k-1}, a_{k-1}).$$

The generic optimal MAP symbol detector is therefore the BCJR algorithm running on a time-varying trellis. It is worth noting that the factorization (4.28) and the corresponding FG in Fig. 4.5 are independent of the models adopted for pilots and by the

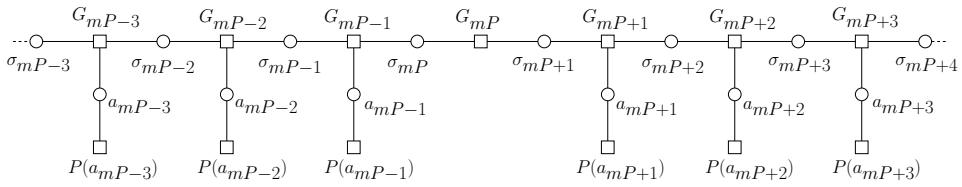

Figure 4.5: Factor graph for the optimal algorithms for $P > 3$.

detector. On the contrary, the state definition and hence the trellis structure depend on the assumed pilot model. With Forney pilots, the number of states varies from M^L (in the case of absence of trellis expansion) up to M^{2L-1} (in the case of maximum expansion), whereas with Ungerboeck pilots the cardinality increase reaches M^{2L}. Moreover, according to the adopted pilot and ISI models, factors $\{H_k(a_k, \sigma_k)\}$ have different expressions. In other words, the choice of the ISI model affects only factors $\{H_k(a_k, \sigma_k)\}$, while the choice of the pilot design impacts also on the state definition (and therefore on the trellis structure). Nevertheless, the FG is always the same.

4.3 Suboptimal algorithms on reduced trellis

Since the complexity of the optimal MAP symbol detection algorithms derived in the previous Paragraph grows exponentially with the size of the memory, reduced-complexity suboptimal algorithms are to be envisaged. For this purpose, we resort to the FG/SPA framework to obtain suboptimal algorithms on a reduced trellis. As will be shown in the following, all the proposed algorithms have the same FG and the same trellis structure independently of the ISI models adopted by pilots and by the detector.

In the following, we denote by ϱ_k a hidden variable playing a role similar to that played by state σ_k in the derivation of the optimal algorithms in the previous Paragraph. It is worth noting that ϱ_k is not a proper state since the couple (a_k, ϱ_k) is not enough to perfectly describe the system in a given discrete-time k, as will be clear later. However, the same notation used for state σ_k is adopted for ϱ_k as well, i.e., the superscript denotes the employed pilot design, while the subscript indicates the ISI

model used by the receiver.

4.3.1 Forney pilots

We follow the same approach adopted before, that is we separately analyze the cases of Forney and Ungerboeck detection.

Forney pilots with Ungerboeck detection

The trellis expansion occurs when a pilot enters in the channel memory, that is when $k = mP + j$, with $j \in [1, L]$. In this situation, the third term at the exponential of the Ungerboeck factor (4.15) becomes

$$\sum_{\ell=1}^{L} a_k^* \left(a_{k-\ell} + b_{k-\ell}^{(F)} \right) g_\ell = \sum_{\substack{\ell=1 \\ \ell \neq j}}^{L} a_{mP+j}^* a_{mP+j-\ell} g_\ell + a_{mP+j}^* b_{mP}^{(F)} g_j \,.$$

To avoid the trellis expansion we move the computation of the last term $a_{mP+j}^* b_{mP}^{(F)} g_j$, that is responsible of the expansion, from discrete-time $k = mP + j$ to $k = mP$. In other words, we define a new factorization

$$p(\mathbf{r}|\mathbf{a}) \propto \prod_{k=0}^{K-1} H_{U,k}^{(F)}(\mathbf{a}) = \prod_{k=0}^{K-1} C_{U,k}^{(F)}(\mathbf{a})$$

where all terms depending on $b_{mP}^{(F)}$ are now taken into account in factor $C_{U,mP}^{(F)}(\mathbf{a})$. We have now two types of factor. Namely, when $j \in [1, P-1]$, the new factor $C_{U,k}^{(F)}(\mathbf{a})$ is deprived of the ISI term caused by the pilot, yielding

$$C_{U,k}^{(F)}(\mathbf{a}) = \exp\left\{ \frac{1}{\sigma^2} \Re\left[r_k a_k^* - \frac{1}{2} |a_k|^2 g_0 - \sum_{\substack{\ell=1 \\ \ell \neq j}}^{L} a_k^* a_{k-\ell} g_\ell \right] \right\} \tag{4.29}$$

and when $j = 0$, $C_{U,mP}^{(F)}(\mathbf{a})$ includes all the ISI terms previously neglected, becoming

$$C_{U,mP}^{(F)}(\mathbf{a}) = \exp\left\{ \frac{1}{\sigma^2} \Re\left[r_{mP} b_{mP}^{(F)*} - \frac{1}{2} \left| b_{mP}^{(F)} \right|^2 g_0 - \sum_{\substack{\ell=-L \\ \ell \neq 0}}^{L} b_{mP}^{(F)*} a_{mP-\ell} g_\ell \right] \right\}. \tag{4.30}$$

The total PDF $p(\mathbf{r}|\mathbf{a})$ results to be unchanged, hence no approximation is introduced.

When $j \in [L+1, P-1]$, factor (4.29) depends on the L previous symbols. These latter can be grouped forming the hidden variable $\varrho_{U,k}^{(F)} = (a_{k-1}, \ldots, a_{k-L})$, taking on M^L possible values. When a pilot enters in the channel memory, that is when $j \in [1, L]$, factor $C_{U,k}^{(F)}(\mathbf{a})$ (4.29) depends only on the $L-1$ previous symbols. Therefore, the hidden variable may be reduced to $\varrho_{U,k}^{(F)} = (a_{k-1}, \ldots, a_{mP+1}, a_{mP-1}, \ldots, a_{k-L})$ and the number of possible values it can take on is only M^{L-1}. When $j = 0$, $C_{U,mP}^{(F)}(\mathbf{a})$ depends not only on the L previous symbols, grouped in the *present* hidden variable $\varrho_{U,mP}^{(F)} = (a_{mP-1}, \ldots, a_{mP-L})$, but also on the L next symbols, which may be grouped in the *future* hidden variable $\varrho_{U,mP+L+1}^{(F)} = (a_{mP+L}, \ldots, a_{mP+1})$. Both the hidden variables, the present one $\varrho_{U,mP}^{(F)}$ and the future one $\varrho_{U,mP+L+1}^{(F)}$, can take on M^L different values. The future hidden variable definition, found considering $C_{U,mP}^{(F)}(\mathbf{a})$ in (4.30), is identical to the present hidden variable definition that can be obtained considering $C_{U,mP+L+1}^{(F)}(\mathbf{a})$ in (4.29). Therefore, the hidden variable is well defined for every discrete-time k and no conflicts arise. Hence, we can safely replace the symbol vector $\mathbf{a}$ in (4.29) and (4.30) with the couple $(a_k, \varrho_{U,k}^{(F)})$ when $j \in [1, P-1]$, and with the triplet $(a_{mP}, \varrho_{U,mP}^{(F)}, \varrho_{U,mP+L+1}^{(F)})$ when $j = 0$. □

Forney pilots with Forney detection

In a similar way, it is possible to obtain the new factors $\{C_{F,k}^{(F)}(\mathbf{a})\}$ for the Forney model just moving all terms depending on $b_{mP}^{(F)}$ to factor $C_{F,mP}^{(F)}(\mathbf{a})$ computed at pilot epochs. Hence, the new factorization reads

$$p(\mathbf{r}|\mathbf{a}) \propto \prod_{k=0}^{K-1} H_{F,k}^{(F)}(\mathbf{a}) = \prod_{k=0}^{K-1} C_{F,k}^{(F)}(\mathbf{a}) \,.$$

New factor $C_{F,k}^{(F)}(\mathbf{a})$ for symbol epochs results to be

$$C_{F,k}^{(F)}(\mathbf{a}) = \exp\left\{ -\frac{1}{2\sigma^2} \left| y_k - \sum_{\substack{\ell=0 \\ \ell \neq j}}^{L} a_{k-\ell} f_\ell \right|^2 \right\} \tag{4.31}$$

for $k = mP + j$, with $j \in [1, P-1]$, while factor $C^{(F)}_{F,mP}(\mathbf{a})$ for pilot epochs becomes

$$C^{(F)}_{F,mP}(\mathbf{a}) = \exp\left\{-\frac{1}{2\sigma^2}\left|y_{mP} - \sum_{\ell=1}^{L} a_{mP-\ell} f_\ell - b^{(F)}_{mP} f_0\right|^2\right\} \cdot$$
$$\cdot \exp\left\{-\frac{1}{2\sigma^2}\sum_{i=1}^{L}\left(\left|f_i b^{(F)}_{mP}\right|^2 - 2\Re\left[\left(y_{mP+i} - \sum_{\substack{\ell=0 \\ \ell\neq i}}^{L} a_{mP+i-\ell} f_\ell\right) f_i^* b^{(F)*}_{mP}\right]\right)\right\}. \quad (4.32)$$

Again, when $j \in [1, L]$, we can define the hidden variable as $\varrho^{(F)}_{F,k} = (a_{k-1}, \ldots, a_{mP+1}, a_{mP-1}, \ldots, a_{k-L})$. As before we have trellis reduction, namely from M^{L+j-1} possible values (with the optimal MAP symbol detector) to M^{L-1}. When $j \in [L+1, P-1]$, $C^{(F)}_{F,k}(\mathbf{a})$ in (4.31) depends on the L previous symbols, hence the hidden variable can be defined once more as $\varrho^{(F)}_{F,k} = (a_{k-1}, \ldots, a_{k-L})$. Finally, when $j = 0$, $C^{(F)}_{F,mP}(\mathbf{a})$ in (4.32) depends on the present and future hidden variables, respectively defined as $\varrho^{(F)}_{F,mP} = (a_{mP-1}, \ldots, a_{mP-L})$ and $\varrho^{(F)}_{F,mP+L+1} = (a_{mP+L}, \ldots, a_{mP+1})$. As in the previous case with Ungerboeck detection, the future hidden variable is well defined and no ambiguity is present. Moreover, all the considerations on the hidden variable set dimension hold unchanged. As done before, we can replace $\mathbf{a}$ in the left hand side of expressions (4.31) and (4.32) with the couple $(a_k, \varrho^{(F)}_{F,k})$ and the triplet $(a_{mP}, \varrho^{(F)}_{F,mP}, \varrho^{(F)}_{F,mP+L+1})$, respectively. □

Since $\varrho^{(F)}_{F,k} = \varrho^{(F)}_{U,k}$ for every discrete time k, we introduce the generic hidden variable $\varrho^{(F)}_k = \varrho^{(F)}_{F,k} = \varrho^{(F)}_{U,k}$. Hence, as we previously showed in the derivation of the optimal MAP symbol detection algorithm, factors $\{C^{(F)}_k(\mathbf{a})\}$ result to be proportional to a conditional probability, equivalent to $p(\mathbf{r}|\mathbf{a})$, that is

$$p(\mathbf{r}|\mathbf{a}, \varrho^{(F)}) \propto \prod_{\substack{k=0 \\ k\neq mP}}^{K-1} C^{(F)}_k(a_k, \varrho^{(F)}_k) \prod_{m=1}^{\lfloor \frac{K-1}{P} \rfloor} C^{(F)}_{mP}(a_{mP}, \varrho^{(F)}_{mP}, \varrho^{(F)}_{mP+L+1}).$$

4.3.2 Ungerboeck pilots

Once more, we study the different combinations of models separately.

Ungerboeck pilots with Ungerboeck detection

Considering the expressions in (4.29) and (4.30), we find that they can be used also for a system based on Ungerboeck pilots with Ungerboeck detection, the only change needed being the pilot definition to employ—namely, (4.8) instead of (4.5). The substitution of the proper pilot design yields

$$C_{U,k}^{(U)}(\mathbf{a}) = C_{U,k}^{(F)}(\mathbf{a}) \tag{4.33}$$

$$C_{U,mP}^{(U)}(\mathbf{a}) = \exp\left\{\frac{1}{\sigma^2}\Re\left[r_{mP}b_{mP}^{(U)*} - \frac{1}{2}\left|b_{mP}^{(U)}\right|^2 g_0 - \sum_{\substack{\ell=-L \\ \ell\neq 0}}^{L} b_{mP}^{(U)*} a_{mP-\ell} g_\ell\right]\right\} \tag{4.34}$$

where (4.33) holds for $k = mP + j$, with $j \in [1, P-1]$, and (4.34) for $j = 0$. At symbol epochs, that is when $j \in [1, P-1]$, the pilot design is irrelevant in the factor computation. Hence, the hidden variable definitions hold unchanged. In other words, $\varrho_{U,k}^{(U)} = \varrho_k^{(F)}$ for every $k \neq mP$. At pilot epochs, when $j = 0$, it can be seen that the pilot design affects only the value of (4.34), not the set of symbols the factor depends on. Therefore, we can define the present hidden variable and the future hidden variable as done before, that is $\varrho_{U,mP}^{(U)} = \varrho_{mP}^{(F)}$ and $\varrho_{U,mP+L+1}^{(U)} = \varrho_{mP+L+1}^{(F)}$. Since we reuse the hidden variable definitions introduced for the Forney pilots case, also $\varrho_{U,k}^{(U)}$ is well defined for every discrete-time k. Hence, we can safely replace symbol vector $\mathbf{a}$ in the left hand side of (4.33) and (4.34) with the couple $(a_k, \varrho_{U,k}^{(U)})$, when $j \in [1, P-1]$, and with the triplet $(a_{mP}, \varrho_{U,mP}^{(U)}, \varrho_{U,mP+L+1}^{(U)})$, when $j = 0$. □

Ungerboeck pilots with Forney detection

Similarly, the expressions in (4.31) and (4.32) can be adopted for Ungerboeck pilots with Forney detection, calculating pilot values with (4.8) instead of (4.5). This yields

$$C_{F,k}^{(U)}(\mathbf{a}) = C_{F,k}^{(F)}(\mathbf{a}) \tag{4.35}$$

$$C_{F,mP}^{(U)}(\mathbf{a}) = \exp\left\{-\frac{1}{2\sigma^2}\left|y_{mP} - \sum_{\ell=1}^{L} a_{mP-\ell} f_\ell - b_{mP}^{(U)} f_0\right|^2\right\} \cdot \exp\left\{-\frac{1}{2\sigma^2}\sum_{i=1}^{L}\left(\left|f_i b_{mP}^{(U)}\right|^2 - 2\Re\left[\left(y_{mP+i} - \sum_{\substack{\ell=0 \\ \ell\neq i}}^{L} a_{mP+i-\ell} f_\ell\right) f_i^* b_{mP}^{(U)*}\right]\right)\right\} \tag{4.36}$$

where (4.35) holds for $k = mP + j$, with $j \in [1, P-1]$, whereas (4.36) holds when $j = 0$. As in the case of Ungerboeck detection, the pilot design modifies only the value of (4.36) but does not affect the set of symbols on which (4.35) and (4.36) depend. Therefore, we can define the hidden variable $\varrho_{F,k}^{(U)} = \varrho_k^{(F)}$ for every discrete-time k. □

As we found for the Forney pilots, we have that $\varrho_{F,k}^{(U)} = \varrho_{U,k}^{(U)}$ for every k. Hence, the generic hidden variable $\varrho_k^{(U)} = \varrho_{F,k}^{(U)} = \varrho_{U,k}^{(U)}$ may be introduced. As we showed in the previous Paragraph, factors $\{C_k^{(U)}(\mathbf{a})\}$ result again to be proportional to the conditional probability

$$p(\mathbf{r}|\mathbf{a}, \boldsymbol{\varrho}^{(U)}) \propto \prod_{\substack{k=0 \\ k\neq mP}}^{K-1} C_k^{(U)}(a_k, \varrho_k^{(U)}) \prod_{m=1}^{\lfloor \frac{K-1}{P} \rfloor} C_{mP}^{(U)}(a_{mP}, \varrho_{mP}^{(U)}, \varrho_{mP+L+1}^{(U)}).$$

4.3.3 Factor graph representation

Since in the previous Paragraphs we showed that $\varrho_k^{(U)} = \varrho_k^{(F)}$ for every discrete-time k, we can now define the general hidden variable $\varrho_k = \varrho_k^{(U)} = \varrho_k^{(F)}$. This result implies that the corresponding FG, on which the suboptimal algorithms run, is independent of the pilot design. Since the APPs $\{P(a_k|\mathbf{r})\}$ needed for the MAP symbol detection strategy in (4.13) can be obtained also marginalizing the joint PMF $P(\mathbf{a}, \boldsymbol{\varrho}|\mathbf{r})$, we choose to use the following new factorization

$$P(\mathbf{a}, \boldsymbol{\varrho}|\mathbf{r}) \propto p(\mathbf{r}|\mathbf{a}, \boldsymbol{\varrho})\, P(\boldsymbol{\varrho}|\mathbf{a})\, P(\mathbf{a})$$

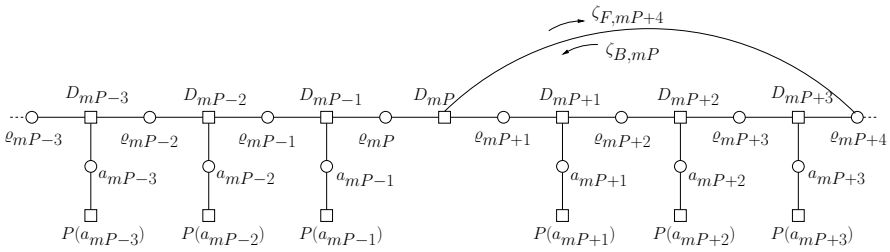

Figure 4.6: Factor graph for the suboptimal algorithm, with $L = 3$ and $P \geq 4$.

where each term can be further factored as

$$P(\mathbf{a}) = \prod_{k=0}^{K-1} P(a_k)$$

$$P(\boldsymbol{\varrho}|\mathbf{a}) = P(\varrho_0) \prod_{k=1}^{K-1} P(\varrho_k|\varrho_{k-1}, a_{k-1}) = P(\varrho_0) \prod_{k=1}^{K-1} I(\varrho_k, \varrho_{k-1}, a_{k-1})$$

$$p(\mathbf{r}|\mathbf{a}, \boldsymbol{\varrho}) = \prod_{k=0}^{K-1} p(r_k|a_k, \varrho_k) \propto \prod_{\substack{k=0 \\ k \neq mP}}^{K-1} C_k(a_k, \varrho_k) \prod_{m=1}^{\lfloor \frac{K-1}{P} \rfloor} C_{mP}(a_{mP}, \varrho_{mP}, \varrho_{mP+L+1}) \quad (4.37)$$

being $I(.)$ an indicator function equal to one when ϱ_k, ϱ_{k-1}, and a_{k-1} satisfy the new trellis constraint, and equal to zero otherwise. In (4.37) factors $\{C_k\}$ and $\{C_{mP}\}$ have different expressions according to the pilot design and the ISI model adopted by the receiver, as shown in the previous Paragraphs. From (4.37) it is possible to derive the FG of the final suboptimal algorithms, presented in Fig. 4.6, where we defined

$$D_k = \begin{cases} D_k(a_k, \varrho_k, \varrho_{k-1}) & = C_k(a_k, \varrho_k) I(\varrho_k, \varrho_{k-1}, a_{k-1}) \quad \text{if } k \neq mP \\ D_k(a_k, \varrho_k, \varrho_{k-1}, \varrho_{k+L+1}) & = C_k(a_k, \varrho_k, \varrho_{k+L+1}) I(\varrho_k, \varrho_{k-1}, a_{k-1}) \quad \text{if } k = mP. \end{cases}$$

The resulting graph has a structure similar to that of the FG of the optimal algorithms in Fig. 4.5. With respect to this latter, the new FG now presents a branch connecting factor node D_{mP} with hidden variable ϱ_{mP+L+1}, which represents the dependence of C_{mP} on the future symbols. Obviously, factors $\{C_k\}$ and $\{H_k\}$ of the two FGs are different, as well as the definitions of state σ_k and hidden variable ϱ_k. However, the

FG shown in Fig. 4.6 is the same for all the suboptimal algorithms, independently of the ISI models adopted by the pilots and by the detector. In other words, the ISI models affect only factors $\{C_k\}$ (their expression and their value), since the trellis (i.e., the hidden variable definition) and the FG are the same irrespectively of the type of pilots and the ISI representation adopted. Factors $\{C_k\}$ not only prevent the trellis expansion when a pilot enters in the channel memory, but also reduce the number of trellis states. In fact, when a pilot is in the channel memory, the number of values that ϱ_k can take on is reduced to M^{L-1} when $k = mP + j$, with $j \in [1, L]$. We want to highlight that the reduction of complexity has been obtained just by rearranging factors in a proper way.

The dependence of node D_{mP} on future hidden variable ϱ_{mP+L+1} introduces cycles in the resulting FG, as shown in Fig. 4.6. The presence of cycles yields an approximated computation of the symbol APPs, but since in the cases of practical interest (i.e., ISI channels with $L > 1$) the girth of the graph is $2(L+1) > 4$, their convergence to the exact APPs is expected [8]. Since the graph has cycles, the SPA does not have a natural termination but a proper schedule must be defined. We denote $\zeta_{F,mP+L+1}$ and $\zeta_{B,mP}$ as the messages going forward and backward (respectively) on the upper branch of the graph and connecting the function node D_{mP} to the hidden variable ϱ_{mP+L+1}. Since the main structure of the FG in Fig. 4.6 is identical to the Wiberg graph of the BCJR algorithm [8] (except for the upper branch), the SPA applied to the FG [8] will produce a slightly modified instance of the BCJR algorithm. The adopted schedule is therefore the following:

1. forward recursion of the BCJR algorithm; during the forward recursion, when $k = mP + L + 1$ the message $\zeta_{F,mP+L+1}$ is computed;

2. backward recursion of the BCJR algorithm; during the backward recursion, when $k = mP$ the message $\zeta_{B,mP}$ is computed;

3. update of the messages $\zeta_{F,mP+L+1}$;

4. completion of the BCJR algorithm considering also the contribution of messages $\zeta_{F,mP+L+1}$.

In order to correctly evaluate the message $\zeta_{F,mP+L+1}$ in step 1, the messages coming from ϱ_{mP} and ϱ_{mP+1} toward node D_{mP} are needed. However, only the message coming from ϱ_{mP} is available, since the other will be calculated in step 2 during the backward recursion. Therefore, messages $\zeta_{F,mP+L+1}$ are re-computed in step 3 when all the necessary messages are available, and this time the computation is correct. Since we consider serially concatenated schemes, we propose to perform a single detector iteration and then to pass the extrinsic information produced by the detector as a priori information to the decoder, in order to perform iterative detection and decoding.

4.4 Numerical results

We restrict our analysis to three different scenarios, as explained in the following. In all simulations concerning the bit error rate (BER), we use packets of 2000 information bits, a spread interleaver, a non-systematic non-recursive convolutional code with rate 0.5, polynomial generators $[5,7]_8$ and four states, a Gray mapper with symbol MSV $\mathcal{E}_a = 1$, a binary phase-shift keying (BPSK) modulator (i.e. $M = 2$), a RRC pulse with roll-off $\alpha = 0.2$, a maximum of 20 iterations between detector and decoder, and pilot insertion with period $P = 7$ or $P = 21$. In order to determine the ISI coefficients to be assumed, we act as follows. We compute the induced ISI coefficients of a time-packed signaling system with a RRC pulse, roll-off $\alpha = 0.2$ and $\tau = 0.9$ or $\tau = 0.5$, where τ is the time compression factor [78], defined as the ratio between the used symbol interval and symbol interval for which the Nyquist condition for ISI absence is respected. Since these coefficients would be too many (theoretically infinite) for the implementation of the optimal detectors, we keep only the first $L + 1 = 7$ taps of the Forney model. The resulting coefficients are reported in Table 4.1 for both channels. Notice that the lower the time compression factor, the heavier the ISI.

We will consider three different scenarios: in the first one we will transmit on the first channel ($\tau = 0.9$ in Table 4.1) with pilot period $P = 21$. Then we worsen the ISI considering the second channel ($\tau = 0.5$ in Table 4.1) but keeping the same spacing between pilots, in order to outline the role of the ISI coefficients in the performance

τ	ℓ	0	1	2	3	4	5	6
0.9	f_ℓ	0.98	0.15	-0.12	0.089	-0.059	0.034	-0.016
0.5		0.12	0.44	0.68	0.44	-0.094	-0.28	-0.00059

Table 4.1: Forney ISI coefficients of time-packed channels with a RRC pulse, roll-off $\alpha = 0.2$.

τ	P	$c^{(F)}$	$c^{(U)}$	$\mathcal{E}_b^{(F)}$	$\mathcal{E}_b^{(U)}$	$E_{s,RRC}^{(F)}$	$E_{s,RRC}^{(U)}$
0.9	21	0.95	0.97	1	1	1	1
0.5	21	1	1	131.29	2.026	7.204	1.049
0.5	7	1	1	131.29	2.026	19.613	1.133

Table 4.2: Pilot values, MSVs, and mean energies per symbol, for RRC pulse with roll-off $\alpha = 0.2$, relative to different pilot designs and spacings.

of the detectors. Finally, in the third scenario we keep the second channel (heavy ISI) but reduce the pilot period to $P = 7$, that is the minimum period preventing interference between two consecutive pilots. We chose to include this scenario in our work to stress the effect of the pilot MSV on the BER performance. In Table 4.2 we report the pilot values, the MSVs, and the resulting mean energies per symbol corresponding to the adopted scenarios. When the constraint (4.6) cannot be satisfied, we arbitrarily set $c = 1$. In all the suboptimal detectors we employ $\sigma^2 = N_0 + N_I$, where N_0 is the one-sided power spectral density of the AWGN and N_I is a parameter, independent of N_0, optimized via numerical simulation aiming at minimizing the BER. N_I reduces the confidence of the BCJR algorithm in the computed messages, and therefore contributes to take into account the suboptimality caused by the cycles in the FG.

In order to do some comparisons, we add in all the following BER figures also the curve corresponding to a system without pilots. Moreover, we consider two systems equivalent to the current DVB-S2 standard, which entails pilot insertion in blocks of pilots. So as to be fair, we need to make comparisons among systems having the same synchronization capability. The bottle-neck of the synchronization is the carrier estimation, and being it dependent on the spacing between pilots [32], we keep constant

τ	P	$\mathcal{E}_b^{(A)}$	$\mathcal{E}_b^{(noA)}$	$E_{s,RRC}^{(A)}$	$E_{s,RRC}^{(noA)}$
0.9	21	1	0.14	1	0.96
0.5	21	1	0.14	1	0.96
0.5	7	1	0.14	1	0.88

Table 4.3: MSVs and mean energies per symbol, for RRC pulse with roll-off $\alpha = 0.2$, relative to different block pilot designs and spacings.

the number of symbols between two consecutive pilot insertions. For the systems with pilot blocks, in order to reduce the overhead, we consider only blocks of size $N_p = L + 1$, that is the minimum size allowing to have one known observed sample to be exploited for synchronization (the previous L pilots being necessary to force the state of the channel). We will show the performance curves for random block pilots belonging to the symbol alphabet. Moreover, since our pilots are not in the same M-ary alphabet of the symbols, we decided to give this degree of freedom also to the system with block pilots, whether it be based on the Forney model or on the Ungerboeck model. Therefore, since the energy loss may be important, we choose to set the L state forcing pilots to 0, and to $\mathcal{E}_a$ the $(L+1)$-th pilot used for synchronization. The resulting MSVs and mean energy per symbol are shown in Table 4.3, where the superscript A (respectively, *noA*) denotes pilots that belong (respectively, do not belong) to the symbol alphabet.

System performance will not be evaluated only in terms of BER but also in terms of spectral efficiency. This latter can be computed as

$$\eta = \frac{I}{BT} \text{ (bits/s/Hz)}$$

where I is the information rate in bits per channel use and BT is the bandwidth normalized to the symbol period. The information rate of all systems are evaluated with the simulation-based technique described in [15] resorting to the corresponding optimal MAP symbol detector. For what concerns the bandwidth, since we are considering linear modulations employing RRC pulses with $\alpha = 0.2$, the normalized bandwidth is known and equal to $BT = \tau(1+\alpha)$ for all the systems.

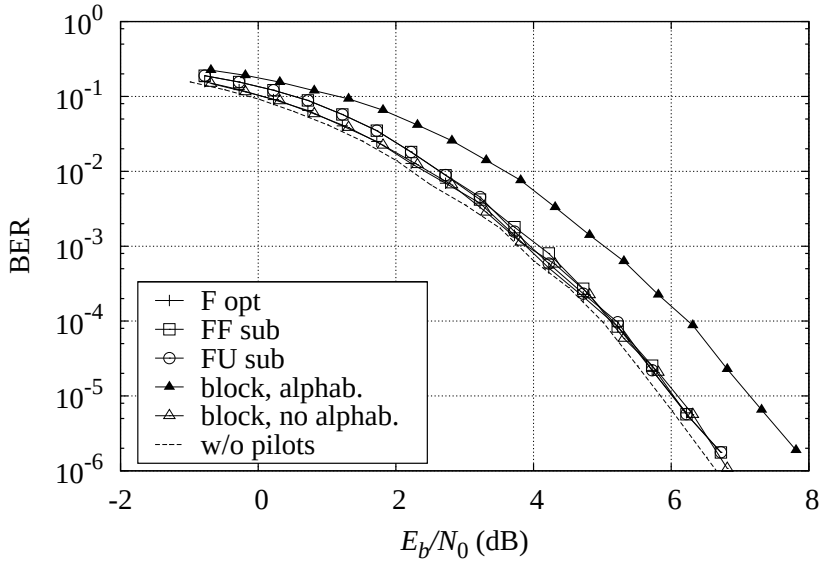

Figure 4.7: BER curves of the optimal and suboptimal detectors for Forney pilots, compared with curves of the systems with pilot blocks and without pilots, on the first ISI channel with $P = 21$.

4.4.1 First scenario

The BER performance of all the investigated systems in the first scenario are shown in Fig. 4.7 for the Forney pilots, and in Fig. 4.8 for the Ungerboeck pilots. In the legends we denote as "FU" the system using Forney pilots and Ungerboeck detection, "UU" the system completely based on the Ungerboeck model, "UF" the system with Ungerboeck pilots and Forney detection, and "FF" the system based on the Forney model. In the first scenario the ISI is very light (see Table 4.1), and all BER curves almost overlap—except the curve relative to the system with block pilots belonging to the symbol alphabet, which shows approximately a loss of 1 dB. In this case, the suboptimal algorithms have a loss of few tenth of dB if compared to the system without pilots. Moreover, at low signal-to-noise ratio (SNR) the optimal algorithm slightly outperforms the suboptimal one, but at target BER ($<10^{-4}$) the performance

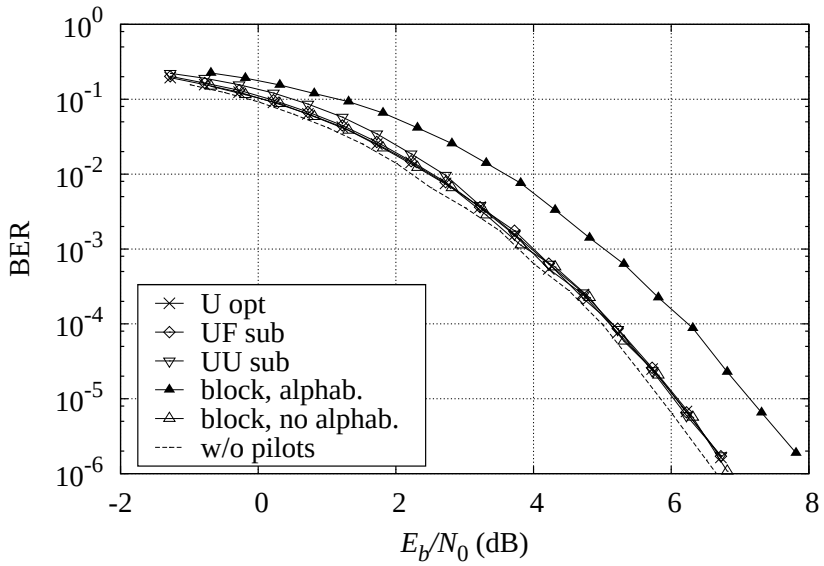

Figure 4.8: BER curves of the optimal and suboptimal detectors for Ungerboeck pilots, compared with curves of the systems with pilot blocks and without pilots, on the first ISI channel with $P = 21$.

is indistinguishable. With respect to the system without pilots, the proposed systems show an insertion loss equal to

$$I_b = \frac{\mathcal{E}_b}{(P-1)r\log_2 M} \tag{4.38}$$

while, if the pilots belong to the symbol alphabet, for the system with block pilots the energy loss increases to

$$I_b = \frac{N_p\mathcal{E}_a}{(P-1)r\log_2 M}$$

where $N_p \geq L+1$ ($N_p = L+1$ in the considered case). It can be seen that, if the pilots are 0 (when forcing the channel) or $\mathcal{E}_a$ (when used for synchronization), the performance in terms of BER is the same of the proposed systems. Nevertheless, two are the major drawbacks of block pilots which do not belong to the symbol alphabet. First, they make the PAPR increase because $\mathcal{E}_b = \mathcal{E}_a/N_p \ll \mathcal{E}_a$, and this causes detrimental effects due to the nonlinearity of the amplifiers used in the satellite link. Second, the SE is heavily reduced. At high SNR, the loss in terms of SE is the same that can be seen adopting block pilots belonging to the symbol alphabet.

The SE curves are reported in Fig. 4.9. It can be seen that the proposed systems greatly outperform systems with block pilots. If compared to the SE of the system without pilots, a loss due to the pilot insertion can be noticed. This loss may be reduced only by increasing the spacing between the consecutive pilots, which entails a reduction in the synchronization capability of the receiver. The classical trade-off between estimation accuracy and spectral efficiency is always present and cannot be avoided.

The anomalous behavior of η at low E_b/N_0 is the result of the mathematical solution of the fixed-point equation

$$I\left(\frac{E_s}{N_0}\right)\frac{E_b}{N_0} = \frac{E_s}{N_0}$$

If we plot η as a function of E_s/N_0, this behavior disappears since, for physical reasons, I is a non-decreasing function of E_s/N_0 [79].

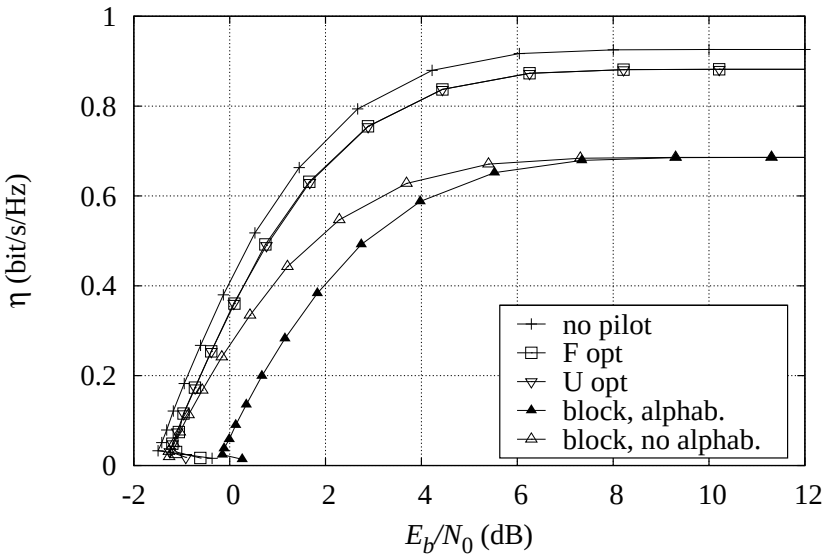

Figure 4.9: Spectral efficiencies of the systems with Forney pilots, Ungerboeck pilots, block pilots, and without pilots in the first scenario.

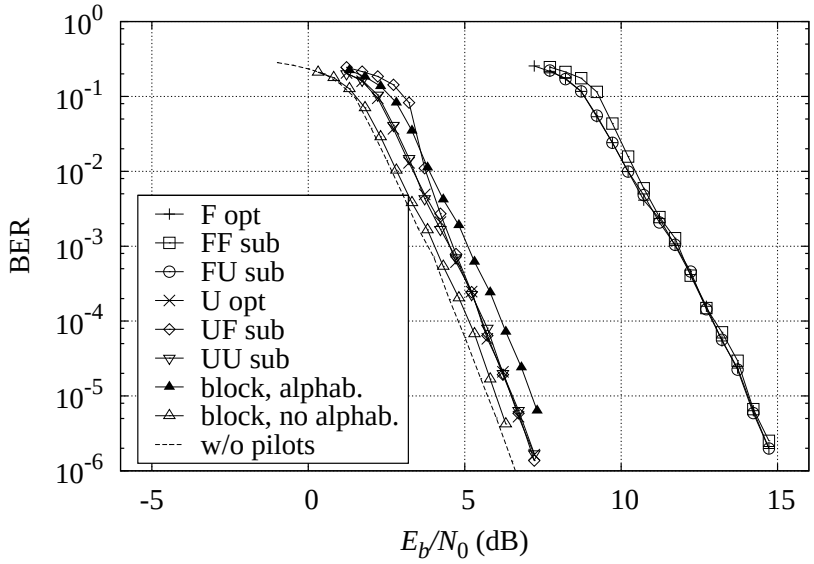

Figure 4.10: BER curves of the optimal and suboptimal detectors compared with those of the systems with block pilots and without pilots, on the second ISI channel with $P = 21$.

4.4.2 Second scenario

The BER curves of the different algorithms are shown in Fig. 4.10. For both the types of pilots, the suboptimal detector based on the Ungerboeck model (marked as FU and UU) performs as the optimal one, while the detector based on the Forney model (marked as FF and UF) shows worse performance at low SNR. This behavior may be ascribed to the higher sensitivity of Forney detection to the suboptimality of the detection algorithm, as pointed out in [68]. All the systems with Forney pilots present an impressive energy loss with respect to the system without pilots due to two different contributions. The first one is an obvious insertion loss due to the presence of pilots (4.38) (which is also present in the systems with Ungerboeck pilots), while the second and predominant is a penalty due to the difference between the symbol and pilot MSVs. Since pilots have MSV higher than the symbols, the interference they

cause to the following L symbols is much heavier than the interference caused by a symbol. Hence, from the symbol point of view, when it undergoes the interference of a previous pilot, it is as if it underwent the interference of another symbol but with stronger ISI. In other words, it is a sort of channel modification. Since for the chosen channel $\mathcal{E}_a < \mathcal{E}_b^{(U)} \ll \mathcal{E}_b^{(F)}$ as shown in Table 4.2, the transmitter has to employ a lot of energy to transmit a Forney pilot. That is why the ISI due to the pilots is much lower when the Ungerboeck pilot design (4.8) is adopted. This energy loss, caused by the difference between the MSVs, is definitely the major drawback of this technique since it is deeply rooted in the chosen pilot design and cannot be avoided. However, systems with Ungerboeck pilots still outperform the traditional system with block pilots belonging to the symbol alphabet. On the other hand, the loss with respect to the system with block pilots not belonging to the symbol alphabet is caused by the different mean energy per symbol, as can be shown in Tables 4.2 and 4.3.

In terms of SE, the performance is shown in Fig. 4.11. At high SNR the proposed systems outperform the system with block pilots, but at low SNR the systems with Forney pilots exhibit a great loss due to the much heavier ISI that the pilots induce on the information symbols.

4.4.3 Third scenario

The performance of all the investigated systems in the third scenario is shown in Fig. 4.12. Increasing the number of pilots obviously the insertion loss for both the types of system (with Forney or Ungerboeck pilots) increases. The suboptimal detectors based on the Forney ISI model always perform poorer than the detectors based on the Ungerboeck model at low SNR, while at high SNR they all perform as the optimal detectors. The systems with Forney pilots present a slope change in their BER curves because the channel modification induced by the different MSVs of symbols and pilots has become much heavier in this scenario with respect to the previous one. However, the systems with Ungerboeck pilots still outperform the system with block pilots belonging to the symbol alphabet, but the loss with respect to the system with block pilots not belonging to the symbol alphabet further increases because of the bigger difference between the mean energies per symbol (see Tables 4.2 and 4.3).

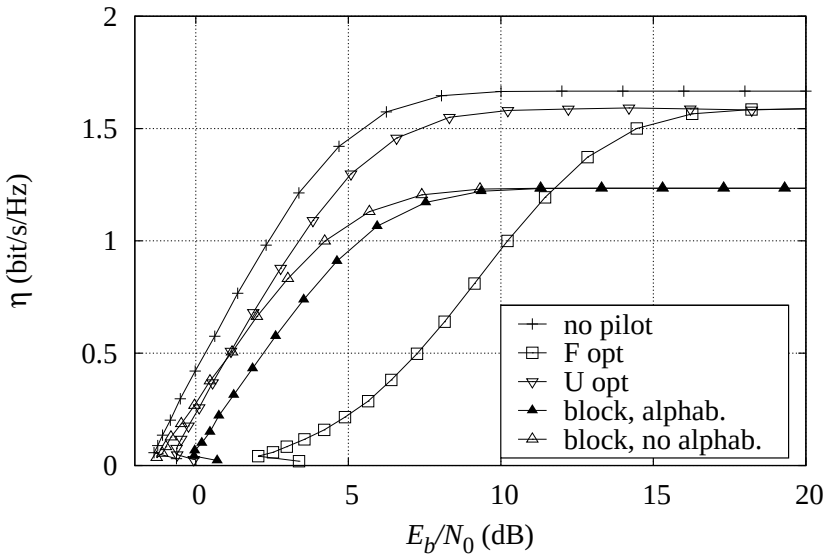

Figure 4.11: Spectral efficiencies of the systems with Forney pilots, Ungerboeck pilots, block pilots, and without pilots in the second scenario.

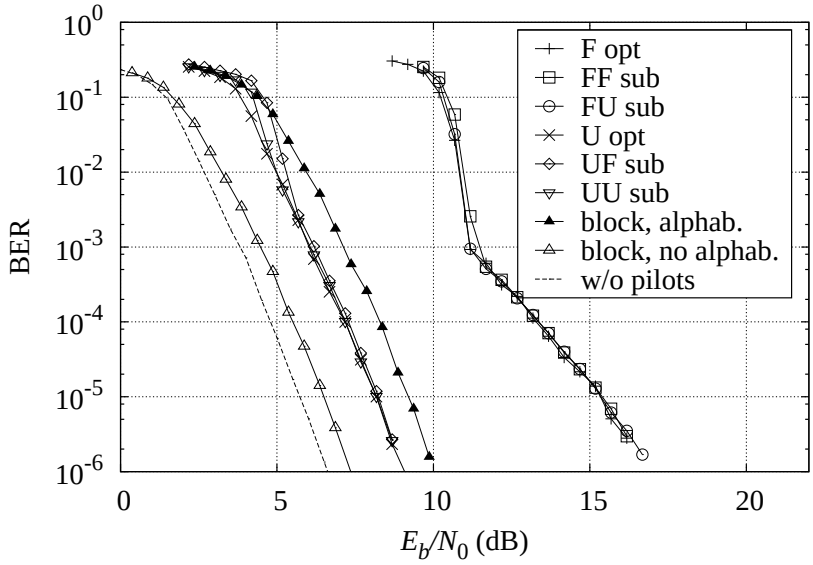

Figure 4.12: BER curves of the optimal and suboptimal detectors compared with those of the systems with block pilots and without pilots, on the second ISI channel with $P = 7$.

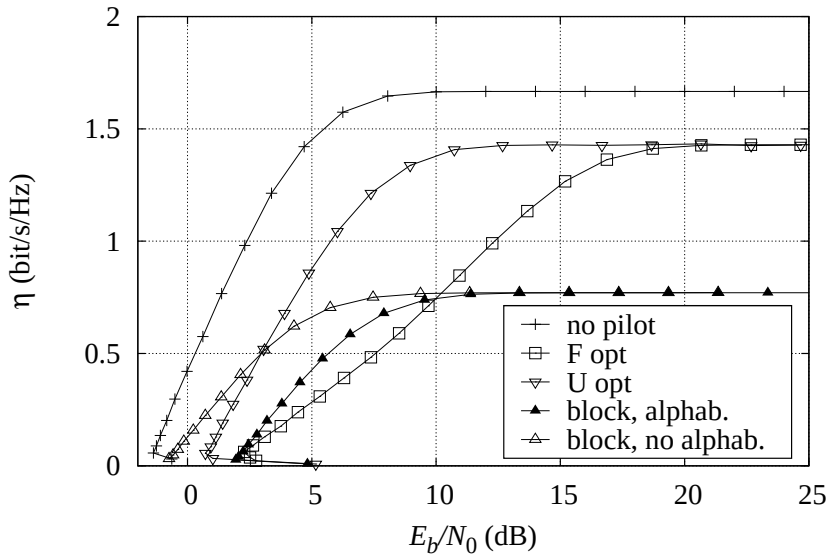

Figure 4.13: Spectral efficiencies of the systems with Forney pilots, Ungerboeck pilots, block pilots, and without pilots in the third scenario.

The corresponding SE curves are shown in Fig. 4.13. The behavior of the different systems is similar to that shown in the second scenario. Now the loss due to the pilot insertion is very high, especially for the system with block pilots. Still, the system with Ungerboeck pilots is the one with the best BER and SE performance.

Conclusions

In this Thesis we considered three satellite communication scenarios and proposed proper techniques aimed at increasing their spectral efficiency.

First, we examined frequency division multiplexed systems based on continuous phase modulations (i.e. a scenario described in the DVB-RCS standard [2]), and proposed reduced-complexity schemes for multi-user detection, possibly in the presence of phase noise, and multi-user data-aided phase and frequency synchronization schemes. We showed that it is possible to implement transmission schemes with an unprecedented spectral efficiency at a price of a limited complexity increase with respect to a receiver which neglects the interference, but in order to do so, synchronization issues have to be addressed. With this purpose, we proposed a data-aided MAP multi-user phase estimator to be used iteratively with a data-aided frequency estimator. The excellent performance of this synchronization scheme is testified by the mean squared estimation error reaching the Cramér-Rao bound at low SNR. Hence, the proposed reduced-complexity scheme for multi-user detection can be effectively employed to increase the system spectral efficiency also in the presence of phase and frequency impairments.

Then, we proposed a brand new technique allowing to use multi-h CPM in CDMA systems. We showed that it is possible to set the spectral spreading of the CPM signal tuning the highest value the modulation index can assume, and that the PSD smoothness is attainable using a long enough sequence of modulation indices. Moreover, this technique shows the same linear relation between the total occupied bandwidth and the number of allowed users that characterizes the DS-SS technique with linear

modulations. The proposed binary multi-*h* CPM-based system not only outperforms all the other alternative solutions that can be found in the literature, but outperforms also a similar quaternary system—and this is a totally unexpected result, opposite to what is known for linear modulations. Therefore, there is no need to resort to higher order modulation formats. In a multi-user scenario, the proposed SS-FH-CPM system can surpass the spectral efficiency of a single-user single-*h* system, whereas the BER performance can be improved by a suboptimal multi-user detector.

Finally, we have proposed a new design for pilot symbols to be used for synchronization over channels with known ISI. This scenario may be obtained starting from the DVB-S2 standard [1] and employing the time-packing technique to improve the spectral efficiency. Our pilots are time-varying, data-dependent, isolated, and properly defined according to the Forney model or the Ungerboeck model in order to make the detector receive, at pilot epochs, a known and constant value. For these pilots we also derived the optimal MAP symbol detection algorithms, which turned out to run over time-varying trellises with an extremely high number of states. Hence, we also proposed suboptimal algorithms based on the FG/SPA framework, whose BER performance is as good as the optimal one when Ungerboeck detection is adopted (a small penalty at low SNR may be seen when Forney detection is used). The remarkable complexity reduction has been obtained without resorting to any kind of modification of the joint PMF, but just rearranging factors in a proper way. If the ISI is light, symbol and pilot MSVs are almost the same. This implies that the PAPR is unchanged with respect to the PAPR of a system without pilots, and this is a desirable feature in presence of nonlinearities due to the amplifiers. With respect to the traditional pilots inserted in blocks, as required by the DVB-S2 standard, the proposed detectors gain in terms of BER and SE, and the choice of the design (Forney's or Ungerboeck's) is irrelevant. On the contrary, if the ISI is heavy the pilot design entails great differences in the performance of the systems. Namely, those with Ungerboeck pilots still outperform the system with block pilots both in terms of BER and SE, whereas the systems with Forney pilots show an impressive energy loss, due to the pilot MSV, degrading the BER and SE performance. Therefore, the system entirely based on the Ungerboeck model is the most performing one, and also exhibits the

appealing absence of whitening filters, often critical to design.

Once the detection algorithms with the new pilot designs are derived and tested, the extension of the phase estimation algorithm described in [23] to the Ungerboeck ISI model becomes fundamental. Hence, future works will include the extension of this algorithm to known ISI channels and its validation through numerical simulations, which are currently underway. Moreover, the whole system, highly spectrally efficient, including time-packing, the new pilot designs, ISI channels with phase noise, channel shortening, the extended phase estimation algorithm, and reduced-complexity suboptimal detection will be investigated.

Concerning the CPM-CDMA scenario analyzed in Chapter 3, the phase noise will be included and the system behavior further studied. Moreover, new criteria for the choice of the index sequences will be investigated.

Bibliography

[1] ETSI EN 301 307 Digital Video Broadcasting (DVB); V1.1.2 (2006-06), Second generation framing structure, channel coding and modulation systems for Broadcasting, Interactive Services, News Gathering and other Broadband satellite applications, 2006, Available on ETSI web site (http://www.etsi.org).

[2] Digital Video Broadcasting (DVB), "Second Generation DVB Interactive Satellite System; Part 2: Lower Layers for Satellite standard. DVB Document A155-2," Mar. 2011.

[3] J. B. Anderson, T. Aulin, and C.-E. W. Sundberg, *Digital Phase Modulation*. New York: Plenum Press, 1986.

[4] B. E. Rimoldi, "A decomposition approach to CPM," *IEEE Trans. Inform. Theory*, vol. 34, pp. 260–270, Mar. 1988.

[5] G. Ferrari, G. Colavolpe, and R. Raheli, *Detection Algorithms for Wireless Communications*. John Wiley & Sons, 2004.

[6] L. R. Bahl, J. Cocke, F. Jelinek, and J. Raviv, "Optimal decoding of linear codes for minimizing symbol error rate," *IEEE Trans. Inform. Theory*, vol. 20, pp. 284–287, Mar. 1974.

[7] P. Roberston, E. Villebrun, and P. Hoeher, "Optimal and sub-optimal maximum a posteriori algorithms suitable for turbo decoding," *European Trans. Telecommun.*, vol. 8, no. 2, pp. 119–125, March/April 1997.

[8] F. R. Kschischang, B. J. Frey, and H.-A. Loeliger, "Factor graphs and the sum-product algorithm," *IEEE Trans. Inform. Theory*, vol. 47, pp. 498–519, Feb. 2001.

[9] F. Kschischang and B. Frey, "Iterative decoding of compound codes by probability propagation in graphical models," *IEEE J. Select. Areas Commun.*, pp. 219–231, February 1998.

[10] S. Benedetto and G. Montorsi, "Design of parallel concatenated convolutional codes," *IEEE Trans. Commun.*, vol. 44, pp. 591–600, May 1996.

[11] C. Berrou, A. Glavieux, and P. Thitmajshima, "Near Shannon limit error-correcting coding and decoding: turbo-codes," in *Proc. IEEE Intern. Conf. Commun.*, Geneva, Switzerland, May 1993, pp. 1064–1070.

[12] C. Berrou and A. Glavieux, "Near optimum error correcting coding and decoding: turbo-codes," *IEEE Trans. Commun.*, vol. 44, no. 10, pp. 1261–1271, October 1996.

[13] G. Colavolpe, "Design and performance of turbo Gallager codes," *IEEE Trans. Commun.*, vol. 52, pp. 1901–1908, Nov. 2004.

[14] T. M. Cover and J. A. Thomas, *Elements of Information Theory*, 2nd ed. John Wiley & Sons, 2006.

[15] D. M. Arnold, H.-A. Loeliger, P. O. Vontobel, A. Kavčić, and W. Zeng, "Simulation-based computation of information rates for channels with memory," *IEEE Trans. Inform. Theory*, vol. 52, no. 8, pp. 3498–3508, Aug. 2006.

[16] B. F. Beidas, H. El Gamal, and S. Kay, "Iterative interference cancellation for high spectral efficiency satellite communications," *IEEE Trans. Commun.*, vol. 50, no. 1, pp. 31–36, Jan. 2002.

[17] G. Gallinaro and R. Rinaldo, "Assessment of potentiality of adjacent channel interference mitigation in a low-rate TDMA system," in *Proc. Intern. Work. on Signal Processing for Space Commun.*, Rhodes Island, Greece, October 2008.

[18] A. Barbieri, D. Fertonani, and G. Colavolpe, "Time-frequency packing for linear modulations: spectral efficiency and practical detection schemes," *IEEE Trans. Commun.*, vol. 57, pp. 2951–2959, Oct. 2009.

[19] A. Barbieri, D. Fertonani, and G. Colavolpe, "Spectrally-efficient continuous phase modulations," *IEEE Trans. Wireless Commun.*, vol. 8, pp. 1564–1572, Mar. 2009.

[20] A. Piemontese, N. Mazzali, and G. Colavolpe, "Improving the spectral efficiency of FDM-CPM systems through packing and multiuser processing," *International Journal of Satellite Communications and Networking*, vol. 30, no. 2, pp. 62 – 72, Feb. 2012.

[21] A. Piemontese, A. Graell i Amat, and G. Colavolpe, "Information-theoretic analysis and practical coding schemes for spectrally efficient FDM-CPM systems," in *Proc. Intern. Symp. on Turbo Codes & Relat. Topics*, Brest, France, Sep. 2010.

[22] A. Piemontese and G. Colavolpe, "A novel graph-based suboptimal multiuser detector for FDM-CPM transmissions," *IEEE Trans. Wireless Commun.*, vol. 9, pp. 2812–2819, Sep. 2010.

[23] G. Colavolpe, A. Barbieri, and G. Caire, "Algorithms for iterative decoding in the presence of strong phase noise," *IEEE J. Select. Areas Commun.*, vol. 23, no. 9, pp. 1748–1757, Sep. 2005.

[24] G. Colavolpe and G. Germi, "On the application of factor graphs and the sum-product algorithm to ISI channels," *IEEE Trans. Commun.*, vol. 53, pp. 818–825, May 2005.

[25] G. Colavolpe, "On LDPC codes over channels with memory," *IEEE Trans. Wireless Commun.*, vol. 5, no. 7, pp. 1757–1766, Jul. 2006.

[26] A. Barbieri and G. Colavolpe, "Soft-output decoding of rotationally invariant codes over channels with phase noise," *IEEE Trans. Commun.*, vol. 55, no. 11, pp. 2125–2133, Nov. 2007.

[27] A. Barbieri and G. Colavolpe, "Simplified soft-output detection of CPM signals over coherent and phase noise channels," *IEEE Trans. Wireless Commun.*, vol. 6, no. 7, pp. 2486–2496, Jul. 2007.

[28] G. Colavolpe and A. Barbieri, "On MAP symbol detection for ISI channels using the Ungerboeck observation model," *IEEE Commun. Letters*, vol. 9, no. 8, pp. 720–722, Aug. 2005.

[29] K. R. Narayanan and G. L. Stüber, "Performance of trellis-coded CPM with iterative demodulation and decoding," *IEEE Trans. Commun.*, vol. 49, pp. 676–687, Apr. 2001.

[30] P. Moqvist and T. M. Aulin, "Serially concatenated continuous phase modulation with iterative decoding," *IEEE Trans. Commun.*, vol. 49, pp. 1901–1915, Nov. 2001.

[31] G. Colavolpe, G. Ferrari, and R. Raheli, "Extrinsic information in iterative decoding: a unified view," *IEEE Trans. Commun.*, vol. 49, pp. 2088–2094, Dec. 2001.

[32] U. Mengali and M. Morelli, "Data-aided frequency estimation for burst digital transmission," *IEEE Trans. Commun.*, vol. 45, pp. 23–25, Jan. 1997.

[33] A. Barbieri and G. Colavolpe, "On the Cramer-Rao bound for carrier frequency estimation in the presence of phase noise," *IEEE Trans. Wireless Commun.*, vol. 6, pp. 575–582, Feb. 2007.

[34] W. Lane and A. Bush, "Spread-spectrum multi-h modulation," *Selected Areas in Communications, IEEE Journal on*, vol. 8, no. 5, pp. 728 –742, Jun. 1990.

[35] F. Giannetti, M. Luise, and R. Reggiannini, "Continuous-phase modulations for CDMA radio communications: Modem architecture and performance," *European Trans. Telecommun.*, vol. 7, no. 3, pp. 225–233, 1996.

[36] R. Hsu and J. Lehnert, "The performance of continuous-phase-coded DS/SSMA communications," *IEEE Trans. Commun.*, vol. 46, no. 4, pp. 533 –543, Apr. 1998.

[37] F. Yang, S. Leung, C. Ngan, and G. Bi, "The performance and design criterion of phase spreading sequences for DS/SSMA communications with full response CPM over Rayleigh fading channels," in *Proc. IEEE Global Telecommun. Conf.*, vol. 1B, 1999, pp. 914 –918 vol. 1b.

[38] A. McDowell, J. Lehnert, and Y. Jeong, "Dual-phase continuous phase modulation for spread-spectrum multiple-access communication," *IEEE Trans. Commun.*, vol. 52, no. 5, pp. 823 – 833, May 2004.

[39] R. R. Müller and A. Lampe, "Spectral efficiency of random CDMA with constant envelope modulation," *AEU Int. J. Electron. Commun.*, vol. 65, no. 8, pp. 701–706, Aug. 2011.

[40] R. R. Müller, "On random CDMA with constant envelope," in *Proc. IEEE International Symposium on Information Theory*, St. Petersburg, Russia, Aug. 2011, pp. 1663–1667.

[41] P. Voglewede, "Frequency hopping with multih CPM (MIL-STD-188-181B)," in *Proc. IEEE Military Comm. Conf. (MILCOM)*, vol. 2, Oct. 2003, pp. 1089 – 1094 Vol.2.

[42] C. Brown and P. Vigneron, "Spectrally efficient CPM waveforms for narrowband tactical communications in frequency hopped networks," in *Proc. IEEE Military Comm. Conf. (MILCOM)*, Oct. 2006, pp. 1 –6.

[43] F. Zanier, A. Emmanuele, G. Boccolini, and M. Luise, "Continuous phase modulated signals for satellite positioning in the C-band," in *ESA Workshop on Satellite Navigation User Equipment Technologies (NAVITEC)*, Dec. 2008.

[44] T. Maseng, "Power spectrum of small h CPM," *Wireless Personal Communications*, vol. 55, pp. 585–589, 2010.

[45] J. L. Massey, "Information theory aspects of spread spectrum communications," in *Proc. IEEE Intn'l. Conf. Spread Spectrum Tech. and Applications*, vol. 1, Oulu, Finland, Jul. 1994, pp. 16–21.

[46] T. Giallorenzi and S. Wilson, "Suboptimum multiuser receivers for convolutionally coded asynchronous DS-CDMA systems," *IEEE Trans. Commun.*, vol. 44, pp. 1183–1196, September 1996.

[47] X. Wang and H. V. Poor, "Iterative (turbo) soft interference cancellation and decoding for coded CDMA," *IEEE Trans. Commun.*, vol. 47, pp. 1046–1061, Jul. 1999.

[48] E. Perrins and M. Rice, "A new performance bound for PAM-based CPM detectors," *IEEE Trans. Commun.*, vol. 53, no. 10, pp. 1688 – 1696, Oct. 2005.

[49] H. Meyr, M. Oerder, and A. Polydoros, "On sampling rate, analog prefiltering, and sufficient statistics for digital receivers," *IEEE Trans. Commun.*, vol. 42, pp. 3208–3214, Dec. 1994.

[50] A. Graell i Amat, C. A. Nour, and C. Douillard, "Serially concatenated continuous phase modulation for satellite communications," *IEEE Trans. Wireless Commun.*, vol. 8, pp. 3260–3269, Jun. 2009.

[51] E. Perrins and M. Rice, "PAM decomposition of M-ary multi-h CPM," *IEEE Trans. Commun.*, vol. 53, no. 12, pp. 2065–2075, Dec. 2005.

[52] M. Luise, "Easy calculation of power spectra for multi-h phase-coded signals," *IEE Electronics Letters*, vol. 21, no. 14, pp. 608 –609, 4 1985.

[53] M. Luise, "Erratum: Easy calculation of power spectra for multi-h phase-coded signals," *IEE Electronics Letters*, vol. 21, no. 15, p. 661, 18 1985.

[54] N. Merhav, G. Kaplan, A. Lapidoth, and S. Shamai, "On information rates for mismatched decoders," *IEEE Trans. Inform. Theory*, vol. 40, no. 6, pp. 1953–1967, Nov. 1994.

[55] G. Colavolpe, D. Fertonani, and A. Piemontese, "SISO detection over linear channels with linear complexity in the number of interferers," *IEEE J. of Sel. Topics in Signal Proc.*, vol. 5, pp. 1475–1485, Dec. 2011.

[56] P. Viswanath and V. Anantharam, "Optimal sequences and sum capacity of synchronous CDMA systems," *IEEE Trans. Inform. Theory*, vol. 45, no. 6, pp. 1984 –1991, Sep. 1999.

[57] M. Rupf and J. Massey, "Optimum sequence multisets for synchronous code-division multiple-access channels," *IEEE Trans. Inform. Theory*, vol. 40, no. 4, pp. 1261 –1266, Jul. 1994.

[58] S. Ulukus and R. Yates, "Iterative construction of optimum signature sequence sets in synchronous CDMA systems," *IEEE Trans. Inform. Theory*, vol. 47, no. 5, pp. 1989 –1998, Jul. 2001.

[59] S. Buzzi, H. Poor, and D. Saturnino, "Noncooperative waveform adaptation games in multiuser wireless communications," *IEEE Signal Processing Mag.*, vol. 26, no. 5, pp. 64 –76, Sep. 2009.

[60] H. L. Van Trees, *Detection, Estimation, and Modulation Theory - Part I*. John Wiley & Sons, 1968.

[61] L. Barletta, M. Magarini, and A. Spalvieri, "The information rate transferred through the discrete-time Wiener's phase noise channel," *J. Lightwave Tech.*, vol. 30, no. 10, pp. 1480–1486, May 15 2012.

[62] A. Spalvieri and L. Barletta, "Pilot-aided carrier recovery in the presence of phase noise," *IEEE Trans. Commun.*, vol. 59, no. 7, pp. 1966 –1974, july 2011.

[63] N. Noels, H. Steendam, M. Moeneclaey, and H. Bruneel, "Carrier phase and frequency estimation for pilot-symbol assisted transmission: bounds and algorithms," *IEEE Trans. Signal Processing*, vol. 53, no. 12, pp. 4578–4587, Dec. 2005.

[64] A. Barbieri, D. Bolletta, and G. Colavolpe, "On the Cramer-Rao bound for carrier frequency estimation in the presence of phase noise," in *Proc. IEEE Global Telecommun. Conf.*, St. Louis, MO, U.S.A., 2005, pp. 720–724.

[65] J. A. Gansman, J. V. Krogmeier, and M. P. Fitz, "Single frequency estimation with non-uniform sampling," in *Proc. Asilomar Conf. Signals, Systems, Comp.*, Nov. 1997, pp. 399–403.

[66] A. Barbieri and G. Colavolpe, "On pilot-symbol-assisted carrier synchronization for DVB-S2 systems," *IEEE Trans. Broadcast.*, vol. 53, no. 3, pp. 685–692, Sep. 2007.

[67] M. Dong and L. Tong, "Optimal design and placement of pilot symbols for channel estimation," *IEEE Trans. Signal Processing*, vol. 50, no. 12, pp. 3055 – 3069, dec 2002.

[68] A. Modenini, G. Colavolpe, and N. Alagha, "How to significantly improve the spectral efficiency of linear modulations through time-frequency packing and advanced processing," in *Proc. IEEE Intern. Conf. Commun.*, Jun. 2012, pp. 3299–3304.

[69] F. Rusek and A. Prlja, "Optimal channel shortening for MIMO and ISI channels," *IEEE Trans. Wireless Commun.*, vol. 11, no. 2, pp. 810–818, Feb. 2012.

[70] G. D. Forney, Jr., "Maximum-likelihood sequence estimation of digital sequences in the presence of intersymbol interference," *IEEE Trans. Inform. Theory*, vol. 18, pp. 284–287, May 1972.

[71] G. Ungerboeck, "Adaptive maximum likelihood receiver for carrier-modulated data-transmission systems," *IEEE Trans. Commun.*, vol. com-22, pp. 624–636, May 1974.

[72] D. Fertonani, A. Barbieri, and G. Colavolpe, "Reduced-complexity BCJR algorithm for turbo equalization," *IEEE Trans. Commun.*, vol. 55, no. 12, pp. 2279–2287, Dec. 2007.

[73] F. Rusek, M. Loncar, and A. Prlja, "A comparison of Ungerboeck and Forney models for reduced-complexity ISI equalization," in *Proc. IEEE Global Telecommun. Conf.*, Washington, DC, U.S.A., Nov. 2007.

[74] A. Hafeez and W. E. Stark, "Decision feedback sequence estimation for unwhitened ISI channels with applications to multiuser detection," *IEEE J. Select. Areas Commun.*, vol. 16, no. 9, pp. 1785–1795, Dec. 1998.

[75] D. Fertonani, A. Barbieri, and G. Colavolpe, "A novel graph-based approach to low-complexity detection for turbo equalization," in *Turbo Codes and Related Topics, 2008 5th International Symposium on*, Sep. 2008, pp. 209 –214.

[76] J. Proakis and M. Salehi, *Digital Communications*, 5th ed., McGraw-Hill, Ed. McGraw-Hill, 2008.

[77] G. Colavolpe and A. Barbieri, "On MAP symbol detection for ISI channels using the Ungerboeck observation model," in *Proc. IEEE international Symposium on Information Theory and its Applications*, Oct. 2004, pp. 99–104.

[78] F. Rusek and J. Anderson, "Constrained capacities for faster-than-nyquist signaling," *IEEE Trans. Inform. Theory*, vol. 55, no. 2, pp. 764 –775, Feb. 2009.

[79] A. Barbieri and G. Colavolpe, "On the information rate and repeat-accumulate code design for phase noise channels," *IEEE Trans. Commun.*, vol. 59, pp. 3223–3228, Dec. 2011.

Acknowledgements

For the accomplishment of this Thesis I would like to thank several people, but most of all my supervisor, prof. Giulio Colavolpe, whose help, support, patience, and advice never missed nor failed all along these three years spent in the SPADiC Lab. A great contribution is also to be recognized to all my colleagues—Amina, Andrea, Alessandro, and Tommaso—for the friendly, collaborative, and pleasant environment we all worked in.

Moreover, I would like to express all my thankfulness to my closest friends—Giulia, Anna, Valentina, and Giulia—just for being there when I needed them. And of course to Roberto, for all what we have been through, and for what shall come.

This work is the result of three years of study and research, but also of the loving support of my family, to whom goes my deepest gratitude. For my mother's sweetest hugs, my father's true smiles, my brother's escaping advice, for the hours spent listening to me whining, and for the strength they helped me find.